DEFENCE RESEARCH ESTABLISHMENT
ATLANTIC
DARTMOUTH N.S.

D. R. E. A. TECHNICAL MEMORANDUM 82 / A

The Detection Performance of FFT Processors for Narrowband Signals

R. S. Walker

February, 1982

Approved by R. F. Brown Director / Underwater Acoustics Division

DISTRIBUTION APPROVED BY

CHIEF D. R. E. A.

RESEARCH AND DEVELOPMENT BRANCH
DEPARTMENT OF NATIONAL DEFENCE
CANADA

Abstract

The report analyses the detection performance of the Fast Fourier Transform (FFT) type signal processor for narrowband signals in white Gaussian noise. Sinusoidal and narrowband Gaussian signals are considered. The signal processor structure is based on the short-time averaged periodogram approach to spectral estimation. Processor parameters considered in the study include time-bandwidth product, data windowing, periodogram overlap, FFT zeroes extension and data normalization. A building-block approach is adopted, whereby the effects of each parameter on the detection threshold can be determined. Results are presented in graphical form. Hence, for a selected set of processor parameters, the appropriate detection threshold can be readily obtained. A thorough mathematical treatment of the problem is presented in the Appendices.

Résumé

L'auteur analyse la performance du processeur de signaux à transformée de Fourier rapide pour la détection de signaux à bande étroite en présence de bruit blanc gaussien. Il étudie le cas des signaux gaussiens à bande étroite et sinusoidaux. La structure du processeur est basée sur l'estimation spectrale par périodogrammes moyennés sur une corte période de temps. Les paramètres utilisés dans l'étude sont: le produit du temps et de la largeur de bande, le choix des fenêtres de données, le recouvrement de périodogrammes, l'addition de valeurs nulles pour la transformée de Fourier rapide et la normalization des données. Une approche par blocs fontionnels permet de déterminer les effets de chaque paramètre sur le seuil de détection. Les résultats sont présentés sous forme graphique. Il est donc possible de déterminer facilement le seuil de détection correspondant à chacune de diverses combinaisons des paramètres du processeur. Les annexes présentent un exposé mathématique détaillé de la question.

Acknowledgments

The author wishes to express his thanks to John Bird[1] for allowing use of his new results prior to their formal publication, and for providing helpful comments on several of the analyses in this report. Reid Smith[2] spent considerable time and effort in developing a mathematics capability for the document compiler that was used to prepare the report. Joe Makysm[3] performed the laborious but important task of checking the mathematics in the appendices.

[1] formerly with the Defence Research Establishment Pacific, Victoria, British Columbia, Canada, and now with the Defence Research Establishment Ottawa, Ottawa, Ontario, Canada

[2] formerly with the Defence Research Establishment Atlantic, and now with Schlumberger-Doll Research, Ridgefield, Conn., U.S.A.

[3] with the Defence Research Establishment Atlantic

Table of Contents

List of Figures

List of Tables

1 Introduction

A classical signal processing problem is the detection of a narrowband signal of unknown frequency in noise. The ability of a signal processor to detect such a signal depends on the processor structure and on the precise nature of the input waveform. This report attempts to analyze in detail the performance of the *Fast Fourier Transform* (FFT) processor in the above detection role. The name, FFT processor, comes from the fact that the processor uses the Fast Fourier Transform algorithm in estimating the power spectrum of the input process. Realistic models of the narrowband signal and noise will be used in the analysis, so that the predicted performance should correspond well with that actually realized. The FFT processor is essentially optimum for the above detection problem under a variety of practical conditions[1]. The processor also lends itself to high-speed digital implementation(cf.[2]). Hence, it is finding increasing application in areas such as passive sonar.

We shall examine in detail the detectability of a narrowband signal that is located in one of the frequency cells, or *bins*, of the FFT. Two important classes of signals will be included, namely, sinusoidal signals and narrowband Gaussian signals. The latter class is a realistic model for signals which undergo random amplitude fluctuations as they propagate through the medium. For example, continuous tonals that have undergone long range multipath propagation through the ocean have been observed at a receiver to behave like narrowband Gaussian noise[3]. We will consider various rates of signal fluctuation. The noise at the processor input will be assumed to be Gaussian, and of uniform strength over the frequency band of analysis. The noise power will be taken to be unchanging, that is,stationary over the processor integration time. The assumption of stationary Gaussian noise is often satisfied in passive sonar for processor integration times of the order of a few minutes[4], except, for example, when rapid rates of doppler frequency shift occur due to changes in the source-receiver geometry.

The report permits a reader to determine the detection threshold, DT, at the processor input that is appropriate for a selected detection probability, P_D, and false-alarm probability, P_{FA}. DT is the ratio, in decibels, of the signal power in a FFT frequency bin to the noise power in a 1 Hz frequency band that is necessary to achieve the particular P_D and P_{FA}. This convention is selected because of its historic use in the sonar equation[5]. The analysis assumes the processor input derives from the output of a single-channel receiver; however, the signal and noise models we use also permit the analysis to treat the case where the input is a linear combination of the outputs of a multichannel receiver, as would occur if the processor was preceeded by a linear beamformer.

Our analysis considers the sensitivity of the DT to various processor parameters. These include effects of integration time and FFT frequency resolution, data windowing, FFT segment overlap, extension of the FFT length with zeroes prior to Fourier transformation and data normalization. A *building-block approach* is taken, whereby each processor parameter can be isolated; this makes it possible to determine the effect on the DT of varying any individual parameter. Results of the performance analysis are presented in graphical form. For a particular processor design, the reader can readily obtain corrections to the DT due to each process parameter, and hence arrive at the final DT. Certain factors influencing the detection performance are not treated by this report. These include effects due to the display format, such as *level quantization* and *peak-picking*, effects of slow variations in the background noise level[6], and the

possibility of averaging across frequency the interpolated power estimates resulting from zeroes extension in order to reduce the display density[7]. Also, we will assume that the detection decision is made totally *in-machine*, so that variations in detection performance that arise among human operators need not be considered.

In Section 2, we present the assumptions and methods that were used in the performance evaluation. This includes a description of the properties assumed for the signal and noise, as well as a description of the FFT processor and its components. The potential corrections in DT due to these components are outlined. Section 3 contains the results of the performance analysis in graphical form. By proceeding logically through this section, the reader can select in turn the desired processor parameters, and ultimately arrive at the DT. Several examples are given in Section 4 of the use of the results in the preceeding section. For completeness, the mathematics necessary to carry out the performance analysis are developed in the Appendices. With only a few exceptions, the notation used in the report follows that presented in [8].

Parts of the analysis presented in this report have appeared previously in the literature, notably[1],[7],[9],[10],[11] and [12]. Some of the results are new, particularly those for Gaussian signals of arbitrary bandwidth. The important feature of the report is that it brings together the factors affecting the detection performance of this processor in a manner which permits ready evaluation of performance.

2 Performance Evaluation: Assumptions and Methods

This section summarizes the assumptions and methods which we have used in evaluating the processor performance. This includes a description of the processor *building-blocks*, as well as the signal and noise models to be considered. In Section 2.3 we outline the mathematical techniques used in the evaluation procedure. For the reader only interested in results, this final topic can be omitted.

2.1 The FFT Processor

The FFT processor structure is based on a power spectral estimation technique: *the method of averaged short-time periodograms*[13]. The method is well suited to digital implementation(cf. [2]). In addition, the power-law detector with integration is essentially optimum for two important classes of signal[14]: a phase-random sinusoid (at small signal-to-noise ratios) and a narrowband Gaussian signal with bandwidth matched to the processor bandwidth. The processor performance for both these types of signal will be examined in Section 3.

Figure 1 shows the basic components of the processor. The input consists of a finite record of duration, T_r, of a band-limited, stationary process, x(t). T_r is referred to as the integration time of the processor. The record is uniformly sampled at sampling frequency, f_s.[1] Hence the input sequence may be written as x(n), n=0,.....,L-1, where $L=f_sT_r$.

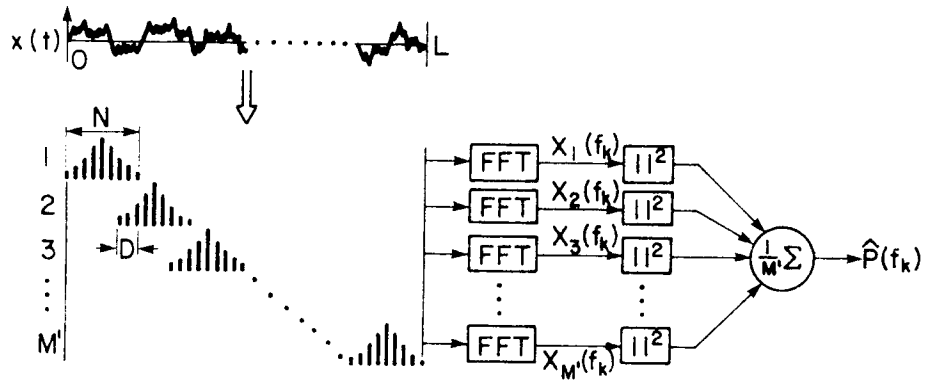

Figure 1. Schematic of the basic components of the FFT Processor

[1] The sampling frequency must be at least twice the highest frequency in the input process, in order to satisfy the Nyquist criterion[15].

The processor performs the following sequence of operations:

1) The record is subdivided into shorter segments of length T, each containing N samples. The segment length fixes the width of each FFT frequency cell, or *bin*, and hence the maximum frequency resolution[2] of the processor.[3] The FFT cell bandwidth, or FFT binwidth, will be B=1/T. The ratio of record length to FFT segment length, $M=L/N=T_r/T=BT_r$, defines the *time-bandwidth* product of the processor. M is the number of independent incoherent averages of the power estimate available in the processor integration time. A large time-bandwidth product results in a stable power estimate. However, once a record length is selected, frequency resolution and estimate stability become mutually exclusive, i.e. as resolution is increased, estimate stability is decreased, and vice-versa.

2) The segments may be overlapped by D samples. The fractional segment overlap is $\gamma=D/N$. Including overlap, we now have a total number of segments, M'. Segment overlap increases the stability of the power estimate by effectively increasing the number of independent averages in the estimate. The effective number of averages will lie between M and M'.

3) A discrete data window is applied to each segment. The shape of the data window controls two effects on the power estimate: the ability to resolve closely spaced narrowband frequency components, and the influence that high strength components at one frequency have on the estimate of components at other frequencies (*leakage*).

4) The length of the segments may be extended with zeroes to length N' prior to Fourier transformation. Zeroes extension does not affect the resolution capability of the processor since the effective bandwidth of each FFT bin is unchanged. However, it increases the density of frequency points at which the spectrum is estimated, thereby introducing a greater overlap of the effective frequency bands for adjacent FFT bins. Hence, there is less chance of *missing* the peaks of narrowband components. Note that the most commonly used *radix-2* FFT algorithm requires that the number of points in the transform be precisely a power of 2. Zeroes extension is often used simply to meet this requirement.

5) Each windowed segment is Fourier analyzed with the Discrete Fourier Transform, implemented via the Fast Fourier Transform (FFT) algorithm. The magnitude-square of the FFT is taken. The result is referred to as a (modified) *periodogram*. The periodograms obtained from each segment are then averaged to yield the power estimate. Hence, the estimation technique is referred to as the method of averaged short-time periodograms.

---

[2] Resolution in this context refers to the ability of the spectrum estimator to separate closely spaced narrowband components in the spectrum.

[3] The data window discussed in 3) will reduce the resolution from this maximum, excepting when the window is rectangular.

It is useful now to express these processor operations in mathematical form. The output of the FFT acting on the ith segment is a sequence of complex samples, $X_i(f_k)$, where $f_k=kf_s/N'$, k=0,.....N'/2, and:

$$X_i(f_k) = \sum_{n=0}^{N-1} w(n)\, x_i(n)\, e^{-j2\pi nf_k/f_s}. \qquad (1)$$

The $x_i(n)$ is the input sequence for the ith segment, i.e.:

$$x_i(n) = x[n+(i-1)(1-\gamma)N], \qquad \begin{matrix} n=0,.....,N-1 \\ i=1,.....,M' \end{matrix} \qquad (2)$$

and w(n) is the data window, n=0,.....,N-1.

The estimate, $\hat{P}(f_k)$, of the power in the frequency bin centered at f_k, is the average of the powers over the M' segments:

$$\hat{P}(f_k) = \frac{1}{M'} \sum_{i=1}^{M'} |X_i(f_k)|^2 . \qquad (3)$$

We will assume that the narrowband signal is not overresolved, i.e., the signal has a bandwidth no greater than the FFT binwidth, B. However, the results presented in this report can be extended to the case of overresolution. The approach is basically to reduce the input signal power by the ratio of the FFT binwidth to signal bandwidth and then assume the signal occupies precisely one FFT bin. This, of course, requires that the detector treat each frequency bin independently, which is a valid assumption provided a human operator does not make the detection decision.

To detect a narrowband signal in a particular frequency bin, we must choose between one of two hypotheses:

H_0: the frequency bin contains only noise;
H_1: the frequency bin contains a narrowband signal plus noise.

We can obtain a power threshold, P_T, for the FFT bin which the power estimate has a (false-alarm) probability, P_{FA}, of exceeding when noise alone is present.[4] The detector is considered optimal under the so-called Neyman-Pearson criterion**[16]** if this choice of threshold maximizes the detection probability, P_D, for each input signal to noise ratio. It can be shown that the FFT processor is essentially optimum for a narrowband signal in white Gaussian noise of known power**[1]**.

A detection will always be assumed to have occurred (with probability, P_{FA}, that

[4] For this report, we consider practical values of P_{FA} to be of the order 10^{-6} to 10^{-2}.

the decision is wrong) if the power estimate, $\hat{P}$, exceeds the power threshold, where for Gaussian noise, we choose to define P_T as:[5]

$$\begin{aligned} P_T &= P_N + rP_N \\ &= (1+r)P_N \, . \end{aligned} \tag{4}$$

P_N is the mean power in the frequency bin due to noise alone, $P_N = E(\hat{P}|H_0)$, and $E(\cdot)$ indicates expectation. Parameter, r, is a constant power ratio, in units of P_N. This notation emphasizes the fact that the power threshold is proportional to the mean noise power.[6] Hence, an increase in P_N will cause a proportional increase in P_T, and the false-alarm probability will remain unchanged. Such a detector is referred to as a constant false-alarm rate, or CFAR detector.

The power threshold is obtained by integration of the probability density function, $f(x|H_0)$, of the power estimate for the noise-only hypothesis, i.e.:

$$P_{FA} = \int_{P_T}^{\infty} f(x|H_0)\, dx \, . \tag{5}$$

In Appendix G, we discuss the problem of threshold setting for various false-alarm probabilities, and the effects of the processor on this setting.

From (4), we see that setting the power threshold for detection requires that we know *a priori* the mean noise power in the FFT bin. In practice, this is seldom the case. Then P_N must be estimated from the data available within the finite time record. One common method of estimating P_N assumes that the FFT bins adjacent to the bin of interest contain only noise, and of the same mean power. Hence P_N may be estimated by averaging the power over K adjacent bins:

$$\hat{P}_N = \frac{1}{K} \sum_{i=b_1}^{b_K} \hat{P}(f_i) \, . \tag{6}$$

where $b_1, b_2, \ldots, b_K$ are the numbers of the FFT bins to be averaged. This approach is known by a variety of names, including the moving window averager[17] or the cell-averaging CFAR[18]. When the average in (6) uses an equal number of bins on either side of f_k, it is referred to as the split window averager.

A new power estimate is obtained by normalizing the power in each bin by P_N (or $\hat{P}_N$):

---

[5] This choice of definition will become evident further in the analysis.

[6] For non-Gaussian statistics, the power threshold will likely also depend on higher moments of the noise distribution.

$$\tilde{P}(f_k) = \hat{P}(f_k)/P_N \, . \qquad (7)$$

When the spectrum is normalized as above, the new power threshold, $\tilde{P}_T = (1+r)$, becomes independent of the mean noise power.

The analysis of detection performance will require us to find that signal-to-noise power ratio, ***SNR***, in the FFT frequency bin and at the processor input which achieves a given level of correctness for the detection decision. The probability of detection, P_D, and probability of false-alarm, P_{FA}, quantify the decision confidence. Detection threshold is related to the ***SNR*** by:

$$DT = 10 \cdot \log(\mathbf{SNR} \cdot B) \, ,$$

where B is the FFT binwidth. While finding the threshold power setting as discussed above is a problem related to that of finding DT, knowledge of either DT or P_T does not directly lead to the other.

We will now summarize the procedures followed by the FFT processor. A qualitative statement of the reasoning governing parameter selection is possible. More quantitative arguments will be made in Section 3 based on the results presented there.

1) time-bandwidth product: First select the record length, L, and the number of samples, N, per segment. The ratio, M, of record length to FFT segment length defines the time-bandwidth product of the processor. It sets a lower limit on the number of segments possible. The length of the segment controls the frequency width, B, of each FFT bin and, hence, the minimum frequency resolution. The number of segments controls the stability of the final power estimate. For a fixed record length, high resolution and high stability are conflicting requirements: an increase in the number of segments reduces the individual segment length, thereby increasing the binwidth, and vice versa. The analysis in Section 3 will consider cases where the time-bandwidth product lies between 1 and 1000. The FFT binwidth will always be chosen to be no less than the signal bandwidth. These conditions are usually typical to passive sonar, except when high rates of doppler frequency shift may occur.[7]

2) overlap: select the fractional segment overlap, γ=D/N. Segment overlap increases the stability of the power estimate. Although the $X_i(f_k)$, i=1,....,M' are correlated when overlap is used (the FFT's act partially on the same input sequences), the effective number of averages is still greater than that without overlap. For overlap, γ, the number of segments, M', is:

$$M' = (M-\gamma)/(1-\gamma) \, . \qquad (8)$$

γ should be selected so that M' is an integer value. As γ approaches

[7] A common situation where high doppler rates occur is when the target passes through its closest point of approach, or CPA.

unity, the gain in stability approaches a limiting value, since adjacent FFT samples become more and more correlated with one another. The increase in signal detectability that results from use of overlap must be weighed against the increased processor load which it produces.

3) data window: select the data window to be applied to each segment. The data window fixes the ultimate frequency resolution of the power spectrum estimate. We show in Appendix C that the mean of the power estimate in the kth FFT bin is:

$$E(\hat{P}(f_k)) = \int_{-f_s/2}^{f_s/2} |W(f_k-f)|^2 \, S(f) \, df \, , \tag{9}$$

where S(f) is the power spectrum of the input sequence and W(f) is the Fourier transform of the data window. $|W(f)|^2$ is referred to as the *spectral window*.[8] Hence the mean of the spectral estimate is a convolution of the true spectrum with the spectral window. The spectral window is usually chosen to provide a reasonable trade-off between the width of its mainlobe and its sidelobe level. The mainlobe width determines the resolution capability of the window, while the sidelobe level determines the extent to which leakage of power from adjacent frequencies will affect $\hat{P}(f_k)$.

In the analysis presented in Section 3, we will consider two data windows(cf.**[19]**):

(a) rectangular window:

$$w(n) = 1 \qquad n=0,.....,N-1 \tag{10}$$

This, of course, corresponds to no weighting of the segment at all. However, we choose to refer to this as the rectangular window, and analyze its effect on the processor as we would for any other window.

(b) Hanning window(raised cosine):

$$w(n) = 0.5[1-\cos(2\pi n/N)] \qquad n=0,....., N-1 \tag{11}$$

These data windows and their corresponding spectral windows are shown in Figure 2. The shape of the spectral window has a weak dependence on N; for N greater than about 32, this dependence essentially disappears. We will always assume that N is sufficiently large that this dependence can be ignored. The rectangular window has the minimum possible mainlobe width for the class of symmetric, tapered data windows; it is also optimum when detecting a sinusoid in white noise**[20]**. However, its sidelobe level is relatively high, and consequently suffers from leakage when the spectrum contains

[8] This definition is somewhat different than that used in **[19]**, where W(f)/W(0) defines the spectral window.

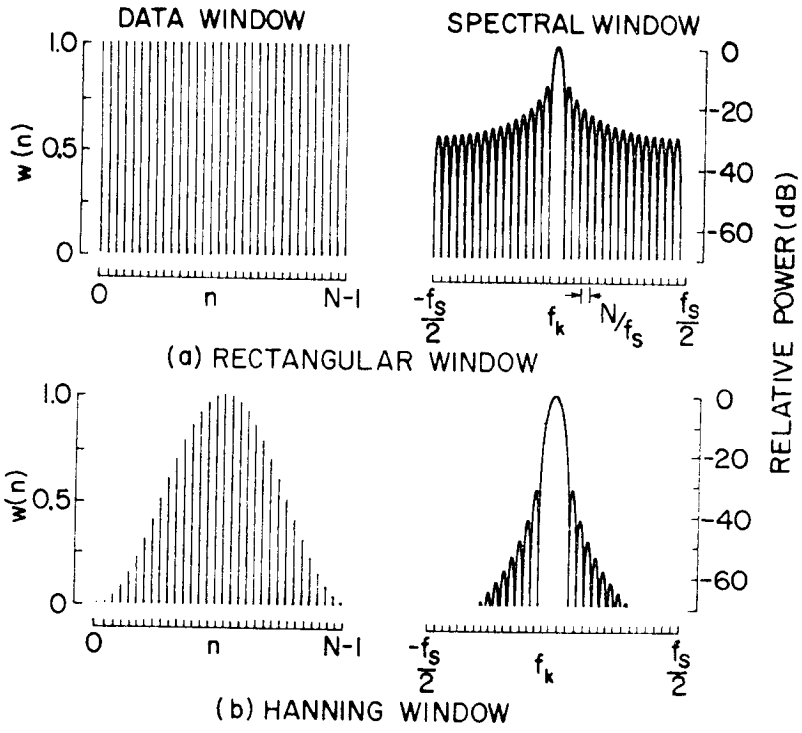

Figure 2. Data Windows and their corresponding Spectral Windows used in this report

structure. The Hanning window provides a reasonable compromise between mainlobe width and sidelobe level. Its wide use in practice is mainly due to its easy implementation. The properties of these windows are tabulated in Appendix C.

The data window influences the detectability of the signal in three ways. First the window causes leakage through its sidelobes of noise power from adjacent bins into the bin of interest. Secondly, the signal power in the bin may be less than that of the true signal power. This may result either because the spectral window does not have unity sensitivity over the signal spectrum, or because the signal is not centered on the FFT bin. The latter loss is referred to as *ripple loss*. Finally,the data window controls the correlation between the FFT samples from adjacent overlapped segments. The sharper the taper on the data window, the less will be the correlation between samples from these overlapped segments. Hence, an increase in the effective number of averages can be obtained within the integration time by increasing segment overlap, and consequently increasing the stability of the spectral estimate. All these effects are treated in Section 3 for the above two window types.

4) zeroes extension: we may extend the segment length with zeroes prior to transformation. Zeroes extension does not affect the shape of the spectral window nor the stability of the power estimate. However it does reduce the ripple loss since it increases the density of frequency bins, thereby increasing the overlap of spectral windows from adjacent bins. Hence, the maximum depth of the ripple in the sensitivity of the estimator across frequency is reduced. It is possible at this point to

average the power estimates that result from zeroes extension and that lie at frequencies between the estimates obtained with no extension. This is advantageous if only a limited number of frequency points can be displayed. Such frequency averaging[7] can be shown to result in the same detectabilty of a signal of unknown frequency as when the redundant frequency points are not averaged and all points displayed. Hence, we do not treat such frequency averaging in this report.

5) data normalization: If the noise power in the bin is unknown, the data normalizer, (6), may be applied to estimate the noise level. Hence, the number of noise-only bins to be used by the normalizer must be selected. The uncertainty in P_N will require a higher power threshold in order to achieve the same P_{FA}, than had P_N been known. We examine this increase in Section 3 as a function of the number of FFT segments and the number of bins used in the normalizer. The case where noise is stationary over a period longer than T_r and hence can be estimated with greater precision by incorporating noise estimates from prior records is not treated.

2.2 Signal and Noise Properties

Two models of the narrowband signal will be used in the analysis.

1) Sinusoidal Signal:

We assume the signal is a sinusoid, which we express as:

$$x_{SS}(n) = A\cos(2\pi n f_c/f_s + \phi)\,, \tag{12a}$$

$$= \frac{A}{2} e^{j(2\pi n f_c/f_s+\phi)} + \frac{A}{2} e^{-j(2\pi n f_c/f_s+\phi)}\,. \tag{12b}$$

A is the amplitude, ϕ is an arbitrary constant phase, and f_c is the frequency. If f_c is located within the FFT bin centered at f_k, the output of the ith FFT due to the sinusoid is obtained by substituting (12b) in (1):

$$X_{I,SS}(f_k) = \frac{A}{2} e^{j(\theta_I+\phi)} \sum_{n=0}^{N-1} w(n)\, e^{-j2\pi n(f_k-f_c)/f_s} + \frac{A}{2} e^{-j(\theta_I+\phi)} \sum_{n=0}^{N-1} w(n)\, e^{-j2\pi n(f_k+f_c)/f_s}\,, \tag{13a}$$

$$= \frac{A}{2} W(f_k-f_c)\, e^{j(\theta_I+\phi)} + \frac{A}{2} W(f_k+f_c)\, e^{-j(\theta_I+\phi)}\,. \tag{13b}$$

θ_I is the phase at the start of the ith segment, relative to the phase at the start of the record, and will be given by:

$$\theta_I = 2\pi(i-1)(1-\gamma)Nf_c/f_s\,, \tag{14}$$

where γ is the fractional segment overlap. The second term in (13b) is negligible except for f_k near zero or $\pm f_s/2$; we shall ignore this *edge effect* in the following development.

2) Gaussian Signal

We assume that the signal is a stationary, ergodic zero-mean narrowband Gaussian process, which can be expressed as:

$$x_{SG}(n) = x'_{SG}\cos(2\pi n f_c/f_s) + x''_{SG}\sin(2\pi n f_c/f_s)\,, \tag{15}$$

where $x'_{SG}(n)$ and $x''_{SG}(n)$ are stationary zero-mean Gaussian processes. The spectrum of the narrowband signal will be taken to be symmetric about center frequency, f_c, where f_c is located within the kth FFT bin; hence, $x'_{SG}(n)$ and $x''_{SG}(n)$ will be independent. The complex output, $X_{I,SG}(f_k)$, of the ith FFT and in the kth bin due to the Gaussian signal is obtained by substituting the above for x(n) in (1), in the same manner as the sinusoidal signal was treated in (13). However, since the signal is now random, we require a statistical description of the FFT output. Since we ultimately deal with the signal power output we wish to find the second-order statistics of the FFT output. The second-order statistics of the FFT samples due to the Gaussian signal are described by the M'xM' Hermitian correlation matrix, $\mathbf{K}_S$. It defines the correlation between all possible pairs of FFT samples, i.e.:

$$\mathbf{K}_S = E(\mathbf{X}_{SG}\mathbf{X}_{SG}^{\dagger})\,, \tag{16}$$

where $\mathbf{X}_{SG}$ is the M'-column vector of complex FFT samples at f_k, and † indicates complex conjugate transposition. The real and imaginary parts of $\mathbf{X}_{SG}$ represent the in-phase and quadrature components of the narrowband filter output. In Appendix C, we show that the terms in $\mathbf{K}_S$ have the form:

$$K_{pq,S} = \int_{-f_s/2}^{f_s/2} |W(f_k-f)|^2\, S_S(f)\, e^{j2\pi \tilde{n} f/f_s}\, df\,, \tag{17}$$

where: $\tilde{n} = (p-q)(1-\gamma)N$,

and $S_S(f)$ is the signal spectrum. Equation (17) may be written equivalently as (see Appendix C):

$$K_{pq,S} = \frac{1}{4}\sum_{n=-N+1}^{N-1} R_W(n)\,\bar{R}_S(n+\tilde{n})\, e^{-j2\pi n(f_k-f_c)/f_s}\,, \tag{18}$$

where we have ignored a term in $\exp[-j2\pi(f_k+f_c)/f_s]$, which is similar to the *edge effect* discussed with respect to (13b). $\bar{R}_S$ is the autocorrelation function of the signal envelope and R_W is that for the data window, i.e.:

$$R_W(n) = \sum_{i=0}^{N-|n|-1} w(i+|n|)w(i) \quad 0\le|n|\le N-1,$$
$$= 0 \qquad \text{elsewhere.} \tag{19}$$

For p=q, (18) reduces to the mean of the signal power estimate, $K_{pp,S}=P_S$.

If the signal is narrowband relative to the mainlobe of the spectral window, and if the signal is centered on the bin, (18) becomes for p=q:

$$P_S = K_{pp,S} = \frac{\bar{R}_S(0)}{4} \sum_{i=-N+1}^{N-1} R_W(n),$$
$$= \frac{\bar{R}_S(0)}{4} \left[\sum_{n=0}^{N-1} w(n)\right]^2, \tag{20}$$
$$= \frac{\sigma_S^2}{2} \left[\sum_{n=0}^{N-1} w(n)\right]^2.$$

where σ_S^2 is the two-sided power of the signal. The term in (20) dependent on the data window is referred to as the coherent power gain, P_C, of the window**[19]**, and is essentially a measure of the signal power it passes. It has a value of N^2 for the rectangular window, but only $N^2/4$ for the Hanning window, because of its taper**[19]**.

In the analysis in Section 3, we will assume that N is sufficiently large that the summation in (18) can be replaced by an integration. This is a satisfactory assumption for N greater than about 32, well below values of N typically used in practice.

In Section 3 we consider two spectral types for the Gaussian signal. These models are reasonable approximations to the measured spectra of sinusoidal signals after having undergone long-range multipath propagation in the ocean**[21]**.

(a) <u>rectangular spectrum</u>:

$$S_S(f) = \sigma_S^2/2B_S \qquad f_c-B_S/2 \le f \le f_c+B_S/2$$
$$-f_c-B_S/2 \le f \le -f_c+B_S/2$$
$$= 0 \qquad \text{elsewhere.} \tag{21}$$

B_S is the signal bandwidth, which we will assume is no greater than the FFT binwidth, B.

Frequency, f_c, locates the center of the spectrum, which lies within the FFT bin centered at f_k. One can show that the signal envelope autocorrelation is:

$$\bar{R}_S(n) = \frac{2\sigma_S^2 \sin(\pi B_S n/f_s)}{\pi B_S n/f_s} . \tag{22}$$

(b) Cauchy Spectrum:

$$S_S(f) = \frac{\sigma_S^2/B_S}{1+4\pi^2(f-f_c)^2/B_S^2} , \tag{23}$$

The Cauchy spectrum is chosen since its envelope autocorrelation is an exponential, i.e.:

$$\bar{R}_S(n) = 2\sigma_S^2 \, e^{-|n|B_S/f_s} . \tag{24}$$

and $1/B_S$ is the signal decorrelation time.

In Figure 3 we show the spectra of these two signal types and their corresponding envelope autocorrelation functions.

3) Noise

The noise will be modelled as stationary, ergodic, zero-mean Gaussian with a spectrum that is flat over the total analysis bandwidth.[9] We define $X_{i,NG}(f_k)$ as the output in the kth bin of the ith FFT acting on the noise. The correlation matrix of the FFT samples is K_N, having terms of the form:

$$\begin{aligned} K_{pq,N} &= \sigma_N^2 \int_{-f_s/2}^{f_s/2} |W(f_k-f)|^2 \, e^{j2\pi \tilde{n} f/f_s} \, df , \\ &= \sigma_N^2 f_s R_W(\tilde{n}) \, e^{j2\pi \tilde{n} f_k/f_s} , \end{aligned} \tag{25}$$

where: $\tilde{n} = (p-q)(1-\gamma)N$,

and σ_N^2 is the mean noise power per unit bandwidth (spectrum level). R_W is the autocorrelation function of the data window, as defined in (19). When the FFT segments are not overlapped, the FFT samples due to the noise become uncorrelated, since:

$$R_W(n) = 0 \qquad\qquad n \geq N . \tag{26}$$

The mean noise power in the FFT bin is obtained from (25) for p=q:

[9] This spectrum condition requires that the sampling frequency be precisely twice the Nyquist frequency. In practice, it is usually chosen higher to avoid aliasing due to imperfect anti-alias filtering.

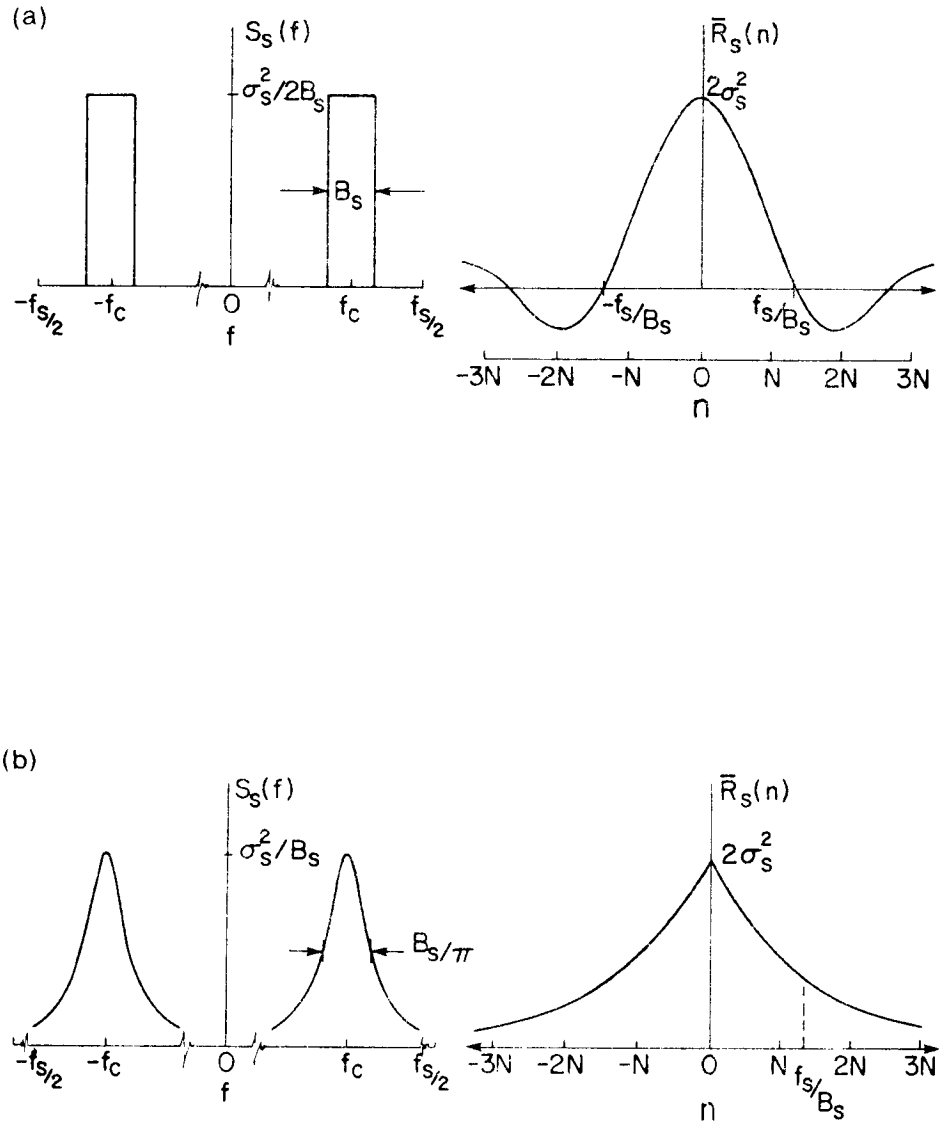

Figure 3. Spectra of the Gaussian signals used in this report, and their envelope autocorrelation functions

$$P_N = K_{pp,N} = \sigma_N^2 f_s R_W(0) ,$$
$$= \sigma_N^2 f_s \sum_{n=0}^{N-1} w^2(n) . \qquad (27)$$

Hence, it is often convenient to normalize the data window so that:

$$\int_{-f_s/2}^{f_s/2} |W(f)|^2 \, df = R_W(0) = \sum_{n=0}^{N-1} w^2(n) = \frac{1}{f_s} , \qquad (28)$$

since with this normalization, $P_N=\sigma_N^2$, i.e., the noise power is normalized to spectrum level.

Assuming the signal is narrowband relative to the spectral window, the ratio of signal power to noise power at the FFT output is (see (20) and (27)):

$$P_S/P_n = \frac{\sigma_S^2}{2\sigma_N^2 B} \left[\frac{(\Sigma w(n))^2}{N\Sigma w^2(n)}\right] ,$$
$$= \textit{SNR} \left[\frac{(\Sigma w(n))^2}{N \Sigma w^2(n)}\right] \qquad (29)$$

where ***SNR*** is the signal-to-noise ratio per FFT bin, but at the processor input. The term in [·] above is the processing gain, PG, of the data window**[19]**; it directly measures the effect of the window on the signal-to-noise ratio at the processor output. The reciprocal of PG can be used to define the bandwidth, B_{EN}, of a rectangular filter (in units of FFT binwidth) which has the same peak value as the spectral window and an equal spectrum area. For the rectangular window, B_{EN}=1, while for the Hanning window, B_{EN}=1.5. Hence, the Hanning window causes a 1.76 dB (10*log*1.5) loss in output signal-to-noise ratio compared to the rectangular window. In Section 3.3 we consider the more general problem in which the signal bandwidth is comparable to the mainlobe width of the spectral window.

In Figure 4, we show an example signal and noise power spectrum, with the spectral window centered on the kth frequency bin. The figure is intended to clarify some of the parameters we have introduced above. The example considers a rectangular signal spectrum in white noise, and the spectral window of the rectangular data window.

In the above development, the noise has been taken to be at least locally stationary over the processor integration time, T_r. The threshold power is set based on the mean noise power, P_N, (or estimate, $\hat{P}_N$) appropriate over T_r. The performance assessment of Section 3 ignores the possibility that the mean noise power in subsequent integration periods may differ. The average processor performance in noise having such a slowly fluctuating power level can be obtained by integrating the performance for fixed P_N over the distribution of possible values of P_N. Such analysis is

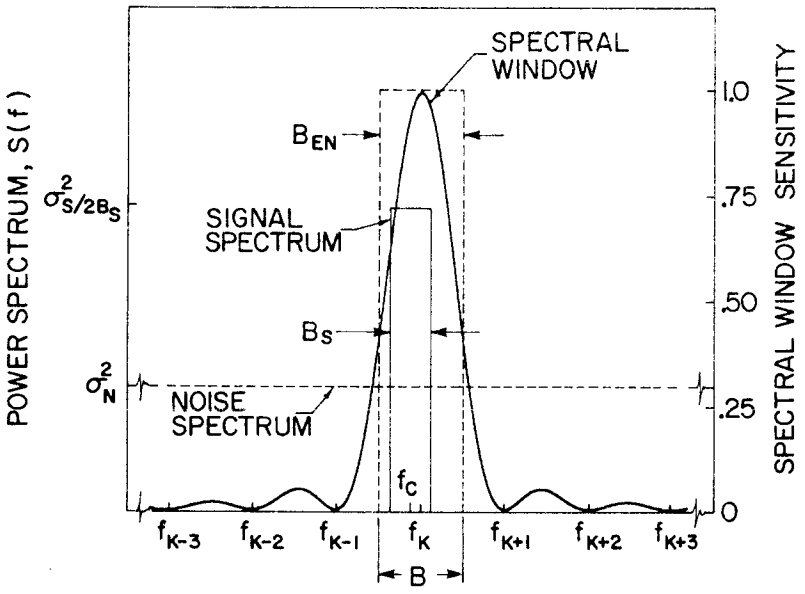

Figure 4. An example signal and noise power spectrum with spectral window

highly sensitive to the form assumed for the density function of P_N[22], and hence will not be considered in this report.

4) Signal plus noise models:

We summarize here the properties of the power estimates under the hypotheses of noise-only and of signal plus noise which are required in our analysis. These results have been derived in detail in Appendix C.

H_0: (Gaussian noise)

$$\hat{P}(f_k) = \frac{1}{M'} \sum_{i=1}^{M'} |X_{i,NG}(f_k)|^2 , \tag{30a}$$

where: $E(\hat{P}(f_k)) = \sigma_N^2 f_s R_W(0)$, (30b)

and: $$K_{pq,N} = \frac{R_W(\tilde{n})}{R_W(0)} e^{j2\pi \tilde{n} f_k/f_s} , \tag{30c}$$

$\tilde{n} = (p-q)(1-\gamma)N$.

We have chosen for convenience to normalize $K_{pq,N}$ so that $K_{pp,N}=1$. The advantage of this normalization is that the signal-to-noise ratio will appear explicitly in the correlation expressions for signal in noise (see (31c) and (34c)). Beyond this, it does not affect the analysis.

H_1: (Gaussian signal in Gaussian noise)

$$\hat{P}(f_k) = \frac{1}{M'} \sum_{i=1}^{M'} |X_{i,SG}(f_k) + X_{i,NG}(f_k)|^2 , \tag{31a}$$

where: $$E(\hat{P}(f_k)) = \int_{-f_s/2}^{f_s/2} |W(f_k-f)|^2 S_S(f)\, df + \sigma_N^2 f_s R_W(0) , \tag{31b}$$

and: $$K_{pq,SN} = \frac{SNR}{N} \sum_{n=-N+1}^{N-1} \frac{R_W(n)}{R_W(0)} \frac{\bar{R}_S(n+\tilde{n})}{2\sigma_S^2} e^{-j2\pi n(f_k-f_c)/f_s} + \frac{R_W(\tilde{n})}{R_W(0)} e^{j2\pi \tilde{n} f_k/f_s} , \tag{31c}$$

$\tilde{n} = (p-q)(1-\gamma)N$.

where ***SNR*** is the ratio of narrowband signal power to noise power per FFT bin. As in the case of noise only, the correlation expression for Gaussian signal and noise has been normalized for unity noise power in the bin, so that ***SNR*** appears explicitly. For p=q, (31c) becomes:

$$K_{pp,SN} = \frac{SNR}{N} \sum_{n=-N+1}^{N-1} \frac{R_W(n)}{R_W(0)} \frac{\bar{R}_S(n)}{2\sigma_S^2} e^{-j2\pi n(f_k-f_c)/f_s} + 1 . \qquad (32)$$

In the case where the signal is narrowband relative to the spectral window, and provided the signal is centered on the bin, (32) reduces to:

$$K_{pp,SN} = \frac{SNR}{B_{EN}} + 1 , \qquad (33)$$

where B_{EN} is the equivalent noise bandwidth of the spectral window.

H_1: (sinusoidal signal in Gaussian noise)

$$\hat{P}(f_k) = \frac{1}{M'} \sum_{l=1}^{M'} |X_{l,SS}(f_k) + X_{l,NG}(f_k)|^2 , \qquad (34a)$$

where: $$E(\hat{P}(f_k)) = \frac{A^2}{4} |W(f_k-f_c)|^2 + \sigma_N^2 f_s R_W(0) . \qquad (34b)$$

and: $$K_{pq,SN} = \frac{SNR}{N} \frac{|W(f_k-f_c)|^2}{R_W(0)} + \frac{R_W(\tilde{n})}{R_W(0)} e^{j2\pi\tilde{n}f_k/f_s} , \qquad (34c)$$

where again we have normalized $K_{pq,SN}$ for unity noise power. Note that for p=q:

$$K_{pp,SN} = \frac{SNR}{N} \frac{|W(f_k-f_c)|^2}{R_W(0)} + 1 ,$$

$$\rightarrow \frac{SNR}{B_{EN}} + 1 \quad \text{as } f_c \rightarrow f_k , \qquad (35)$$

as does (32). The performance analysis does not actually require the correlation between FFT samples for this signal and noise model (see Appendix B.3); however, we state the result here for completeness.

Finally, we comment that the above treatment does not directly apply to the frequency bins centered at $f_k=0$ or $f_k=\pm f_s/2$. In these cases, the quadrature component of the FFT filter output vanishes, with the consequence that only half the independent samples are available when compared to the power estimates for other bins. The results of Section 3 can be applied to these cases by assuming the time-bandwidth product is 1/2 its value in the other bins.

2.3 The Characteristic Function Approach to Performance Evaluation

The aim of the performance analysis of Section 3 is to obtain the signal-to-noise power ratio, ***SNR***, associated with a specified P_D and P_{FA}. These confidence measures are related to the cumulative probability distribution, F(y), of the power estimate, $\hat{P}$, conditioned on the two hypotheses, H_0 and H_1:

$$P_{FA} = 1 - F(y|H_0) = 1 - \int_0^y f(x|H_0)\,dx$$

and:

$$P_D = 1 - F(y|H_1) = 1 - \int_0^y f(x|H_1)\,dx \qquad (36)$$

where $f(x|H_1)$ is the probability density function of $\hat{P}$ conditioned on H_1, and y is the power threshold. From (4), y may be written:[10]

$$y = P_T = (1+r)P_N .$$

The approach we adopt here to solving (36) relies on the use of the characteristic function $\Phi(\xi)$ of $\hat{P}$, i.e.:

$$\Phi(\xi|H_1) = \int_0^\infty f(x|H_1)\, e^{j\xi x}\,dx . \qquad (37)$$

In general, $f(x|H_1)$ can be obtained as the inverse Fourier transform of $\Phi(\xi|H_1)$. Unfortunately, in all but a few cases, this transform does not have a ready analytic solution.[11] However, Bird**[23]** has shown that $f(x|H_1)$ can be expressed exactly out to some value Y by the Fourier series:

$$f(x|H_1) = \sum_{n=-\infty}^{\infty} \Phi_n(H_1)\, e^{-j2\pi nx/Y}, \quad 0 \le x \le Y \qquad (38a)$$

where: $$\Phi_n(H_1) = \frac{1}{Y}\int_0^Y f(x|H_1)\, e^{j2\pi nx/Y}\,dx . \qquad (38b)$$

Provided Y is chosen large enough, so that $f(x|H_1) \approx 0$, $x > Y$, it results that (see Appendix A):

[10] assuming the noise is Gaussian

[11] We look at some important cases which can be solved analytically in Appendix E.

$$F(y|H_1) \approx \frac{y}{Y} \sum_{n=-J}^{J} \Phi(\frac{2\pi n}{Y}|H_1) \left[\frac{\sin(\pi ny/Y)}{\pi ny/Y}\right] e^{-j\pi ny/Y} . \quad (39)$$

The error due to truncating the Fourier series at $J<\infty$ is negligible for moderate values of J. The technique and its error bounds are discussed in Appendix A.

To apply the above technique, we require the characteristic function of $\hat{P}$, under both hypotheses H_0 and H_1. These are obtained in Appendix B. The results are summarized below.

H_0: (Gaussian noise)

$$\Phi(\xi|H_0) = \prod_{i=1}^{M'} \left[1 - \frac{j\xi\lambda_{i,N}}{M'} \right]^{-1} , \quad (40)$$

where $\lambda_{i,N}$ is the ith eigenvalue of the correlation matrix, K_N, for the FFT noise samples (see 30c). The complex exponential in (30c) does not affect the eigenvalues of K_N and so can be ignored in their calculation.

H_1: (sinusoidal signal in Gaussian noise)

$$\Phi(\xi|H_1) = \prod_{i=1}^{M'} (1 - \frac{j\xi\lambda_{i,N}}{M'})^{-1} \exp\left[\frac{j\xi SNR \cdot C_1/M' + \xi^2 SNR \cdot C_1\lambda_{i,N}(1-K_i)/M'^2}{1 - j\xi\lambda_{i,N}/M'} \right] , \quad (41)$$

where: $$K_i = \sum_{p=1}^{M'} \sum_{q=1}^{M'} e^{j2\pi(p-q)(1-\gamma)N(f_k-f_c)/f_s} |R_{pi}||R_{qi}| ,$$

$$C_1 = |W(f_k-f_c)|^2/NR_w(0) \quad (\rightarrow 1/B_{EN} \text{ as } f_c \rightarrow f_k) ,$$

and: $$SNR = \frac{A^2}{4\sigma_N^2 B} .$$

R_{ij} is the i,jth term of an M'x M' matrix whose jth column is the orthonormal eigenvector for the jth eigenvalue of K_N. When there is no overlap, $K_i=1$, and the second term in the exponential of (41) disappears.

H_1: (Gaussian signal in Gaussian noise)

$$\Phi(\xi|H_1) = \prod_{i=1}^{M'} \left[1 - \frac{j\xi\lambda_{i,SN}}{M'}\right]^{-1} , \quad (42)$$

where $\lambda_{i,SN}$ is the ith eigenvalue of the correlation matrix, K_{SN}, for the FFT samples of

Gaussian signal plus noise (see 31c). As in the case of noise only, the complex exponential in the noise component of (31c) does not affect the $\lambda_{l,SN}$'s, and hence can be ignored in their calculation.

The performance evaluation for known noise power proceeds as follows:

1) select the processor parameters, eg. number of segments, overlap, window type, etc.;

2) select the signal type, and spectrum type (if Gaussian);

3) select a P_{FA} and iterate (39) using $\Phi(\xi|H_0)$, until the threshold, y, is obtained which yields this P_{FA};

4) using the threshold from 3), iterate (39) using $\Phi(\xi|H_1)$ until the signal-to-noise ratio, ***SNR***, is obtained corresponding to the selected P_D.

Performance evaluation for unknown noise power is treated in Appendix F.

3 Performance Evaluation Results

In this section we present results of the evaluation of the detection performance of the FFT processor for narrowband signals. The processor structure and the statistical properties of signal and noise which we have assumed are discussed in Section 2.

For a selected set of processor parameters, as well as signal and noise conditions, the detection threshold, DT, required to achieve specific P_D and P_{FA} can be defined as follows:

$$DT = G_M + 10\log B + SE + L_w + L_r - G_z - G_o + L_n \,, \tag{43}$$

where all values are in decibels. The terms in (43) are:

DT: detection threshold, or ratio of the narrowband signal power to the noise power in a 1 Hz band necessary at the processor input to achieve a specified P_D and P_{FA};

G_M: the basic DT associated with a time-bandwidth product of M, and due to averaging over M non-overlapped segments, assuming a 1 Hz FFT binwidth, P_D = 0.5 and a specified P_{FA} (see Sec. 3.1);

B : the FFT binwidth, or reciprocal of the FFT segment length, T;

SE: the signal excess, or difference in DT between that for a selected P_D and that for P_D = 0.5 (see Sec. 3.2);

L_w: the loss in DT due to data windowing, assuming the narrowband signal is centered on the FFT bin (see Sec. 3.3);

L_r: the average ripple loss, which results when the signal is not centered on the FFT bin (see Sec. 3.4);

G_z: the reduction in average ripple loss due to extension of the data segment with zeroes before the FFT is performed (see Sec. 3.5);

G_o: the gain in DT due to segment overlap (see Sec. 3.6);

L_n: the loss in DT due to data normalization, as required when the noise power is not known (see Sec. 3.7).

The first three terms in (43) define a baseline DT. They depend only on the properties of the signal and noise, and on the time-bandwidth product of the processor. The remaining terms are corrections, either losses or gains, to the basic DT due to the actual processor structure. The following sections treat each of the terms in (43) in turn. Results are presented in graphical form for convenient use by the reader. By insertion of the appropriate values for each term in (43) the detection threshold for a specific processor will result. Accuracy of the result should be of the order of ±0.2 dB.

3.1 Time-Bandwidth Product

In this section we show the basic detection threshold, G_M, associated with a given processor time-bandwidth product. The time-bandwidth product represents the number of non-overlapped segments, M, or equivalently, the ratio of the total record length to the FFT segment length. The results are presented in Figures 5-7; the figures correspond to P_{FA}'s of 10^{-2}, 10^{-4} and 10^{-6}, respectively. The detection probability is P_D = 0.5 in all cases. Values of M range from 1 to about 1000; this covers values of time-bandwidth product typically encountered in practice. For example, for a 300 second time record, and a 0.1 Hz FFT binwidth, the time-bandwidth product is 300x0.1=30. Extrapolation methods for values of M in excess of 1000 are noted below. When no segment overlap is used, then only integer values of M are permitted. However, when overlap is used, a non-integer value of M is possible, provided the total number of overlapped segments is an integer value.

Five curves appear in each of Figures 5-7. Each curve corresponds to a model of the narrowband signal. These are as follows:

1) upper solid line: narrowband Gaussian signal having a bandwidth, B_S, negligible compared to the FFT binwidth, B=1/T, i.e. B_ST=0. T is the FFT segment length. Hence, within any time record, the signal appears as a sinusoid of fixed amplitude, but with an amplitude which can fluctuate from one record to the next. Under the narrowband Gaussian assumption, these fluctuations follow a Rayleigh distribution. This type of signal has been referred to as a *Swerling I* fluctuating signal in the radar literature**[14]**.

2) lower solid line: narrowband Gaussian signal having a rectangular spectrum with a bandwidth, B_S, exactly matched to the FFT binwidth, i.e. B_ST=1. When no segment overlap is used, and ignoring effects due to the data window, the FFT output from any one segment is uncorrelated with that from any other segment (the signal envelope autocorrelation shown in Figure 3a is sampled precisely at the zeroes of the function). Such a signal has been referred to as a *Swerling II* fluctuating signal**[14]**. In general, the narrowband Gaussian signal will lie between the two limiting cases described by Swerling I and II models. These intermediate bandwidth cases are treated shortly.

3) heavy dashed line: narrowband Gaussian signal having a Cauchy spectrum with a bandwidth, B_S, matched to the FFT binwidth, i.e. B_ST=1. The results are essentially identical to those for the Swerling II signal.

4) dashed line: sinusoidal signal. The figures show that the detection threshold becomes identical to that for the two types of narrowband Gaussian signal having B_ST=1 for M greater than about 20;

5) dotted line: a frequently-used approximate solution to the problem of narrowband signal detection. It assumes that the

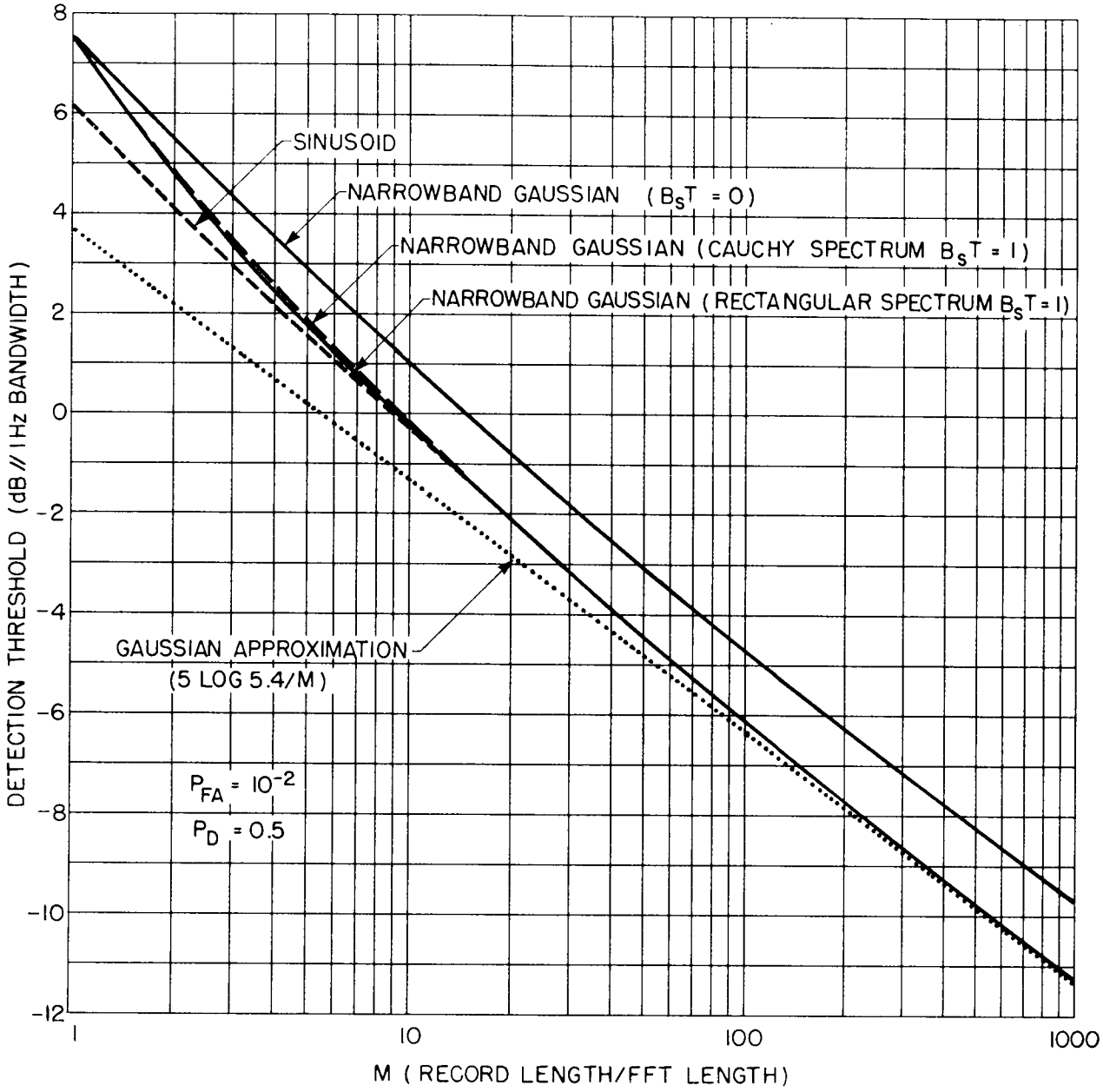

Figure 5. Basic Detection Threshold vs. time-bandwidth product, M, for P_D=0.5 and P_{FA}=10^{-2}.

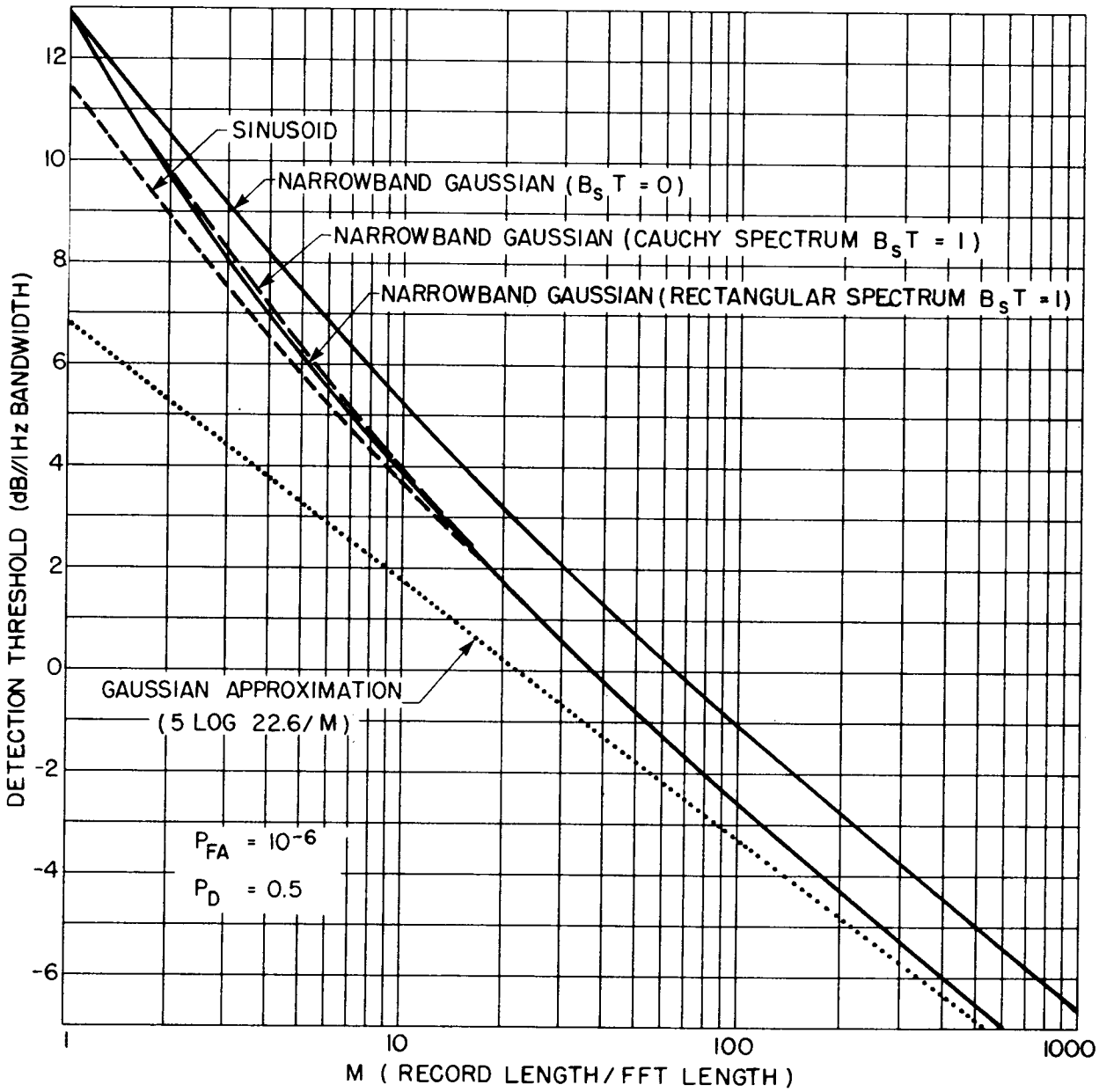

Figure 7. Basic Detection Threshold vs. time-bandwidth product, M, for P_D=0.5 and P_{FA}=10^{-6}.

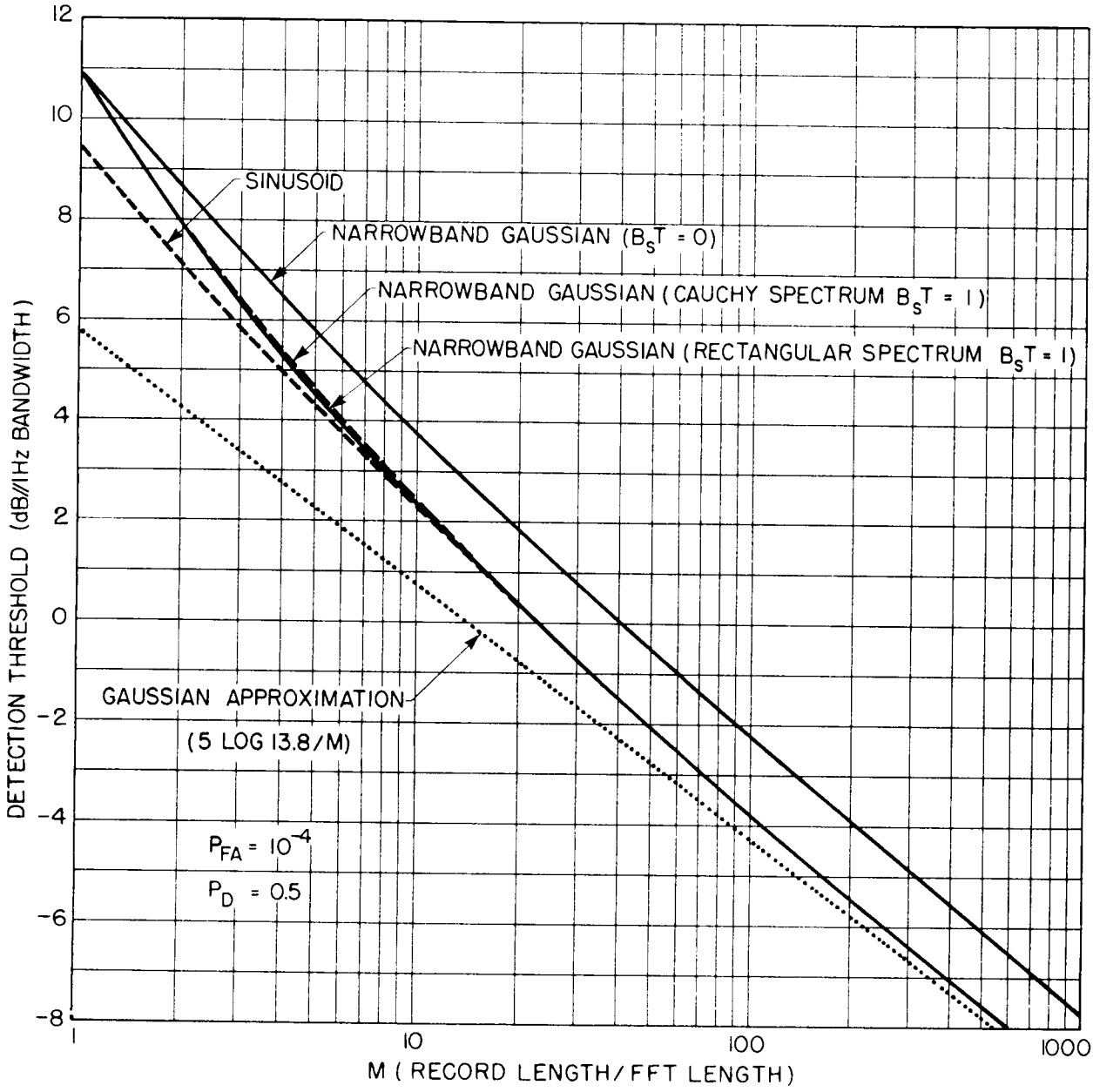

Figure 6. Basic Detection Threshold vs. time-bandwidth product, M, for P_D=0.5 and P_{FA}=10^{-4}.

probability density function of the FFT power estimates is Gaussian, both with and without signal present. In this case, the detection threshold reduces to:

$$G_M = 5\log(d/M) \qquad (44)$$

where d is referred to as the detection index[5]. It is a function of the selected P_D and P_{FA}. The above approximation is derived in Appendix D.1 and values of d are obtained for the P_D's and P_{FA}'s used in Figures 5-7. For M large, the approximation closely models the results for the sinusoidal signal and Gaussian signals having B_ST =1, since the density function of the power estimates indeed approaches a Gaussian, according to the Central Limit Theorem[8]. For M small, the error due to use of the approximation is of the order of a few dB (at least for P_D=0.5).

The above results assume that the signal-to-noise ratio is referenced to the FFT bin.[12] As we stated before, detection threshold is normalized to the equivalent noise power in a 1 Hz band (spectrum level). If the actual FFT binwidth, B, differs from 1 Hz, then the the above values must be corrected by $10\log B$, in order to preserve this normalization. This correction will cause a 3 dB decrease in DT for each halving of the FFT binwidth (or doubling of the FFT segment length). If the total record length is fixed, a decrease in the FFT binwidth results in a corresponding decrease in M, with a resulting increase in G_M. Then it is important to know at what point, if any, a decrease in the FFT binwidth (increase resolution) will gain more in DT instead of increasing the time-bandwith product, M (increase stability). From Figures 5-7, we observe that the slope of each of the curves is less than 3 dB/halving of M; hence, a decrease in the FFT binwidth should always gain more than increasing the number of FFT segments ,provided, of course, the binwidth does not become less than the signal bandwidth.

For M in excess of 1000, the Gaussian approximation, (44), provides a satisfactory estimate of G_M for the sinusoidal signal and Gaussian signals having B_ST=1. As we show in Appendix D.1, the estimate for the Swerling I signal can be obtained by adding 1.6 dB to the above value, at least when P_D=0.5.

Often the bandwidth of the Gaussian signal will lie between the limiting cases described by the Swerling I and II signals. Figures 8-13 treat G_M for such signals, and as a function of the time-bandwidth product, M. Values of M range from 1 to 100. To avoid the large decibel range of Figures 5-7, the results are presented as corrections to the thresholds for the zero bandwidth Gaussian signal (Swerling I) as given in these previous figures. Figures 8-10 consider the narrowband signal having a rectangular spectrum, while Figures 11-13 consider the signal with a Cauchy spectrum. Each Figure corresponds to one P_{FA}, either 10^{-2}, 10^{-4} or 10^{-6}, and three P_D's: 0.1, 0.5 and 0.9. For P_D=0.5, the absolute threshold is obtained as a correction to the Swerling I values in Figures 5-7. For the other P_D values, we require the transition curves which are introduced in the following section. Values of B_ST treated in Figures 8-13 are: 0.01,

[12] Alternatively, they apply to the case where the FFT binwidth is 1 Hz wide.

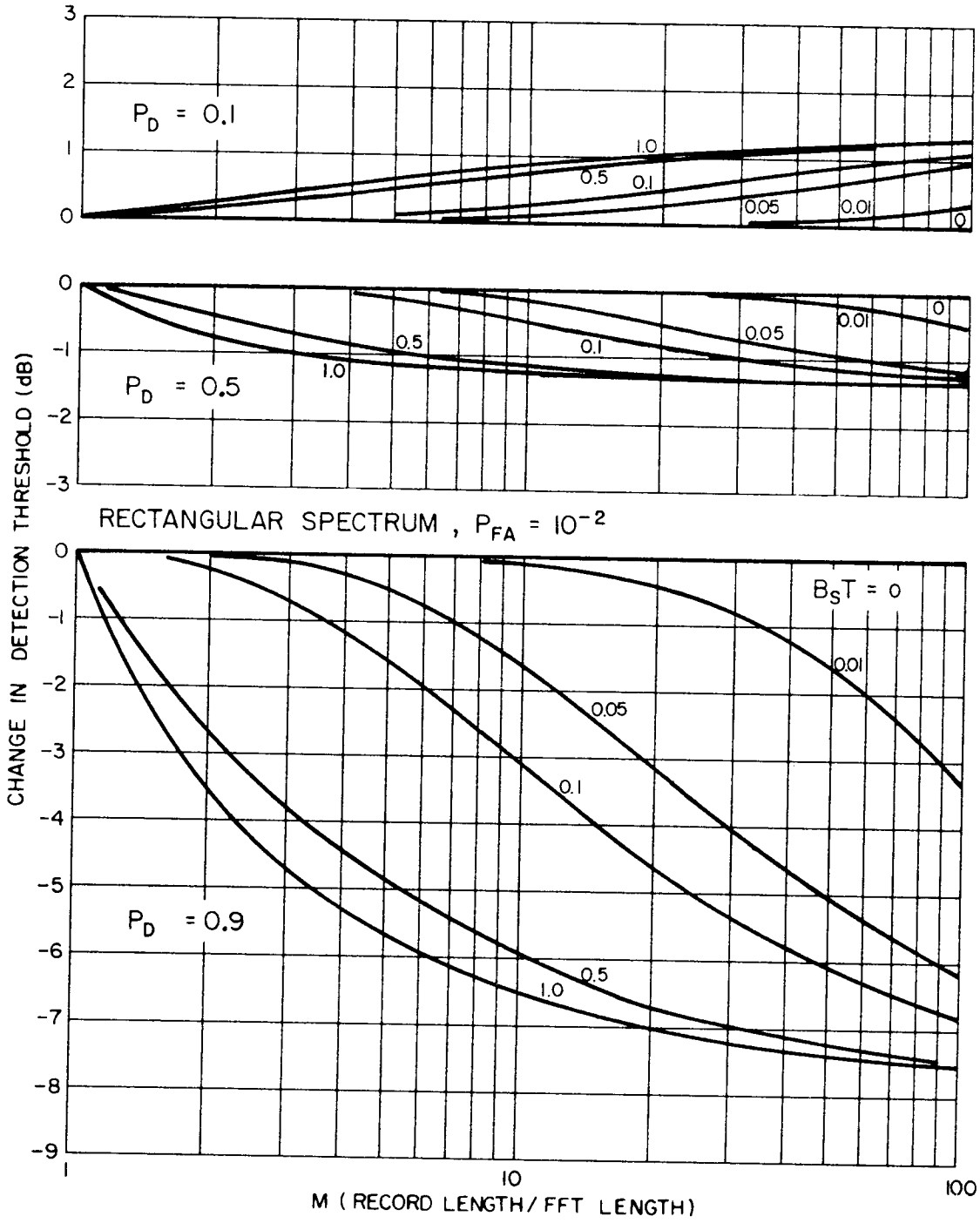

Figure 8. Change in Detection Threshold vs. M for narrowband Gaussian signal with rectangular spectrum. $P_{FA}=10^{-2}$.

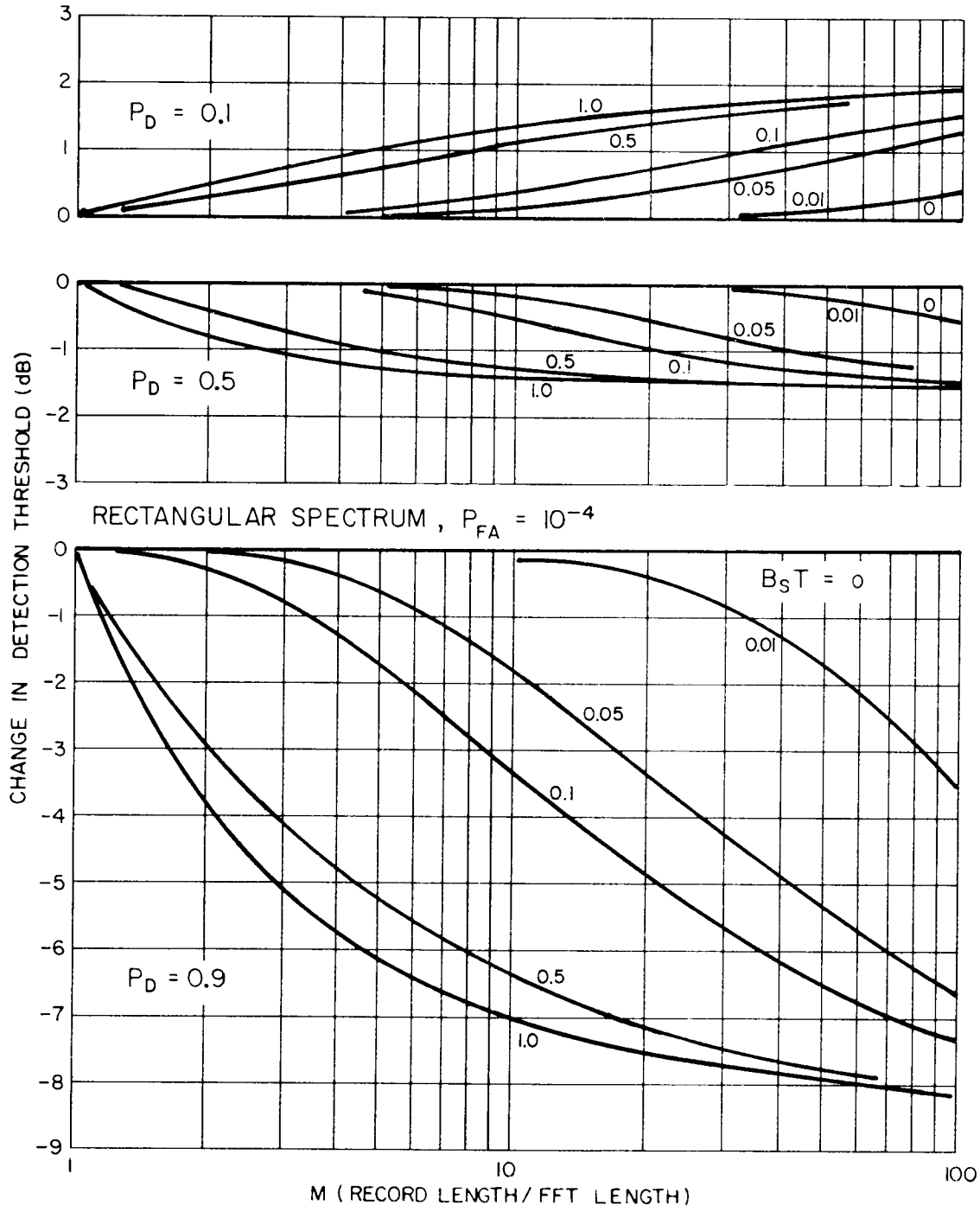

Figure 9. Change in Detection Threshold vs. M for narrowband Gaussian signal with rectangular spectrum. $P_{FA}=10^{-4}$.

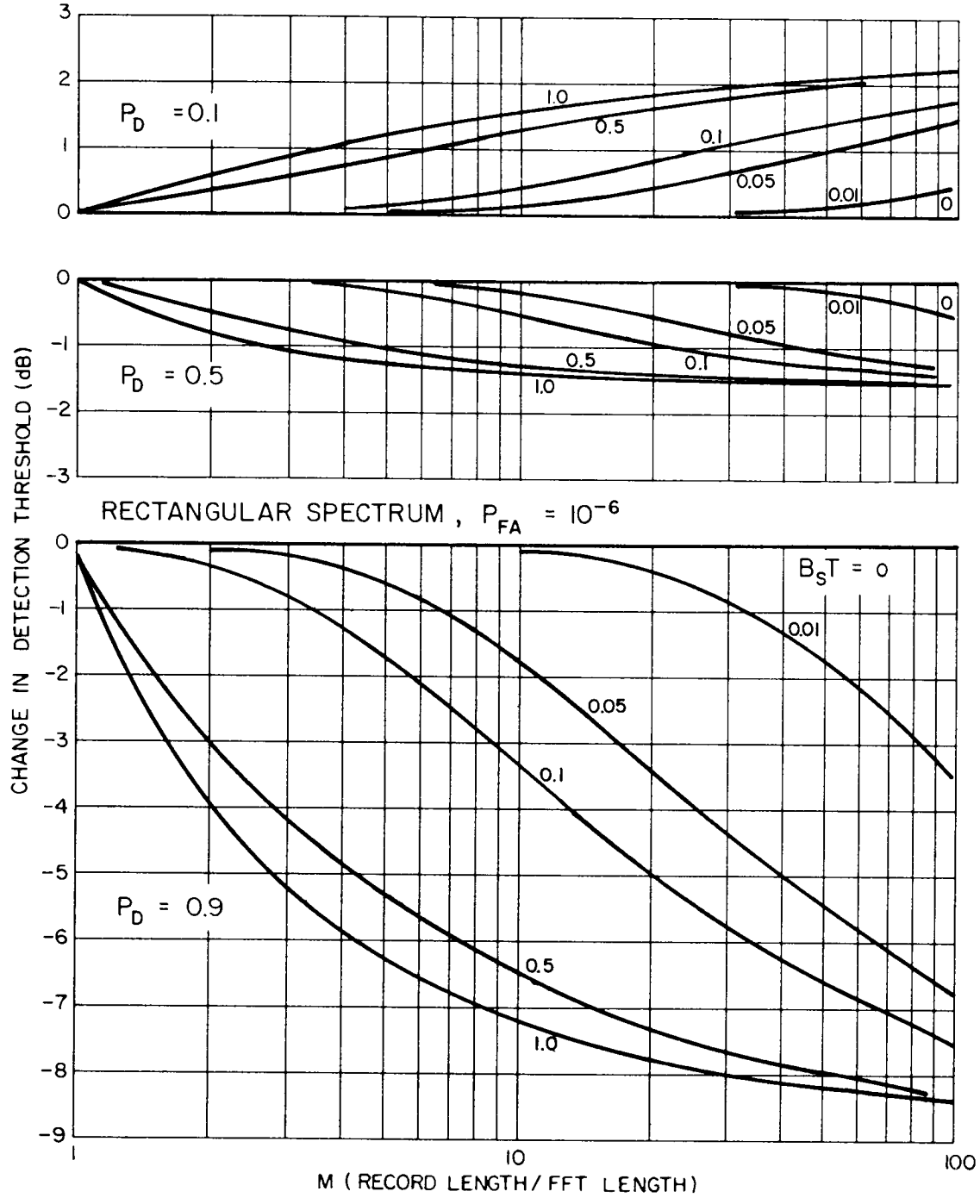

Figure 10. Change in Detection Threshold vs. M for narrowband Gaussian signal with rectangular spectrum. $P_{FA}=10^{-6}$.

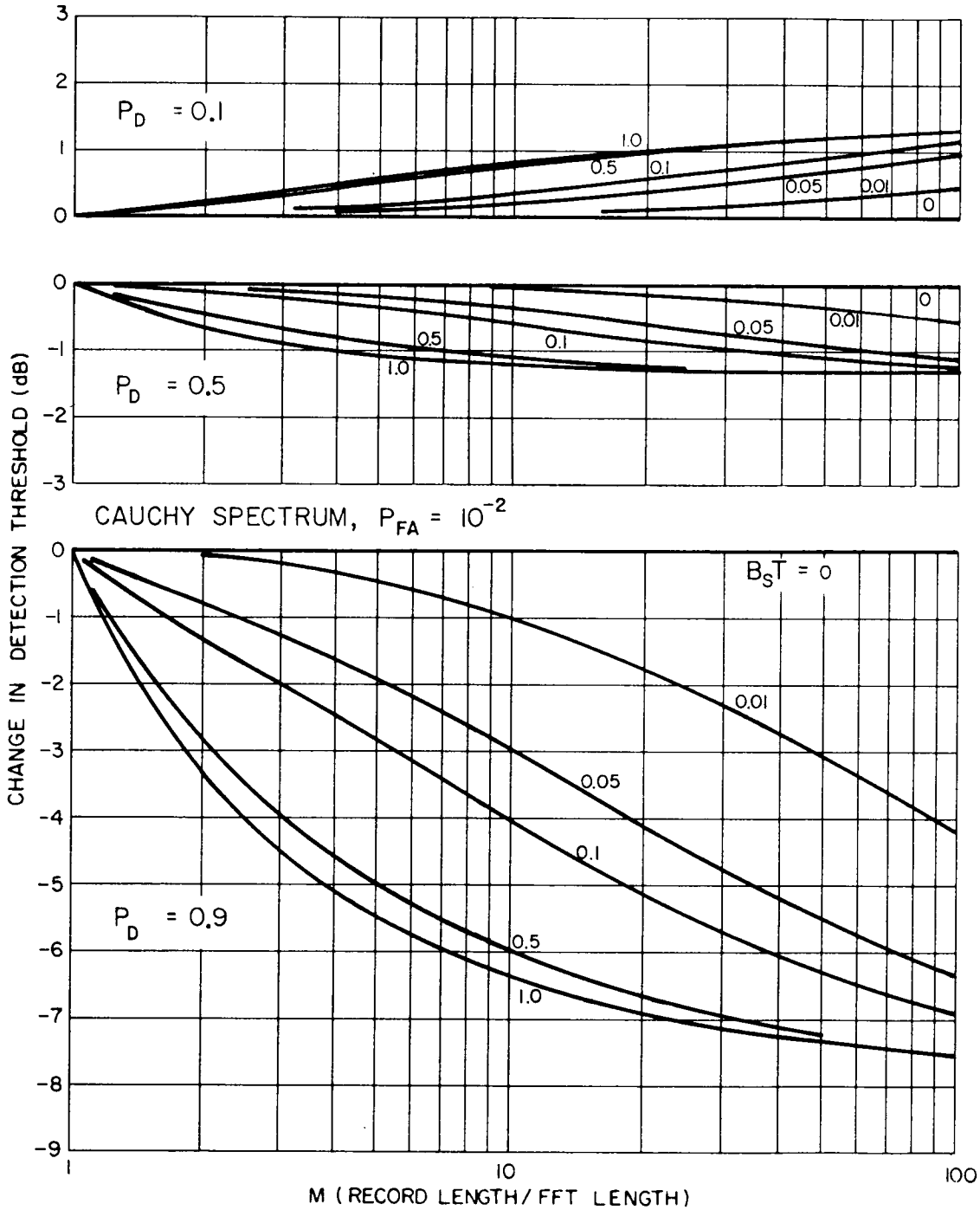

Figure 11. Change in Detection Threshold vs. M for narrowband Gaussian signal with Cauchy spectrum. $P_{FA}=10^{-2}$.

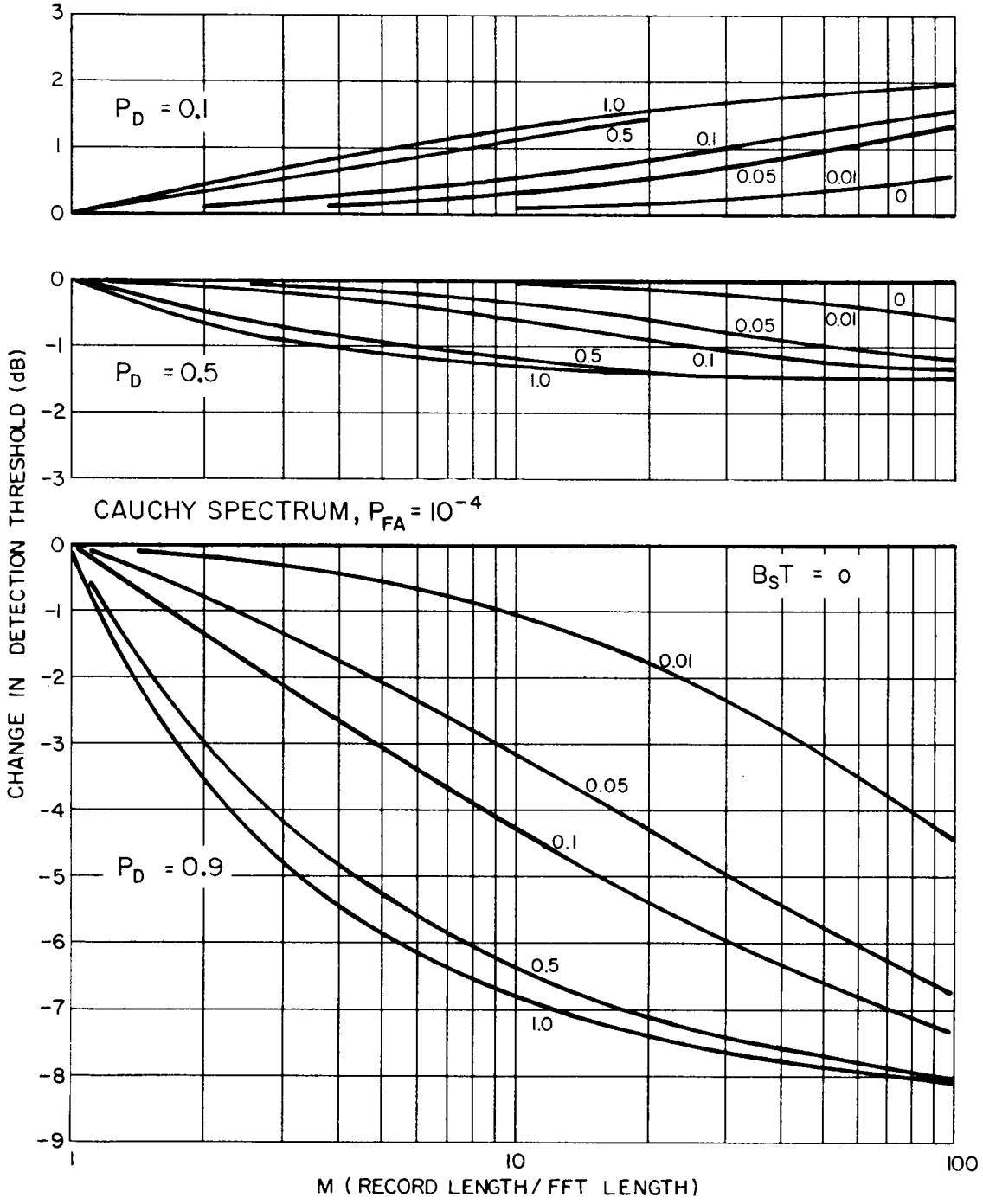

Figure 12. Change in Detection Threshold vs. M for narrowband Gaussian signal with Cauchy spectrum. $P_{FA}=10^{-4}$.

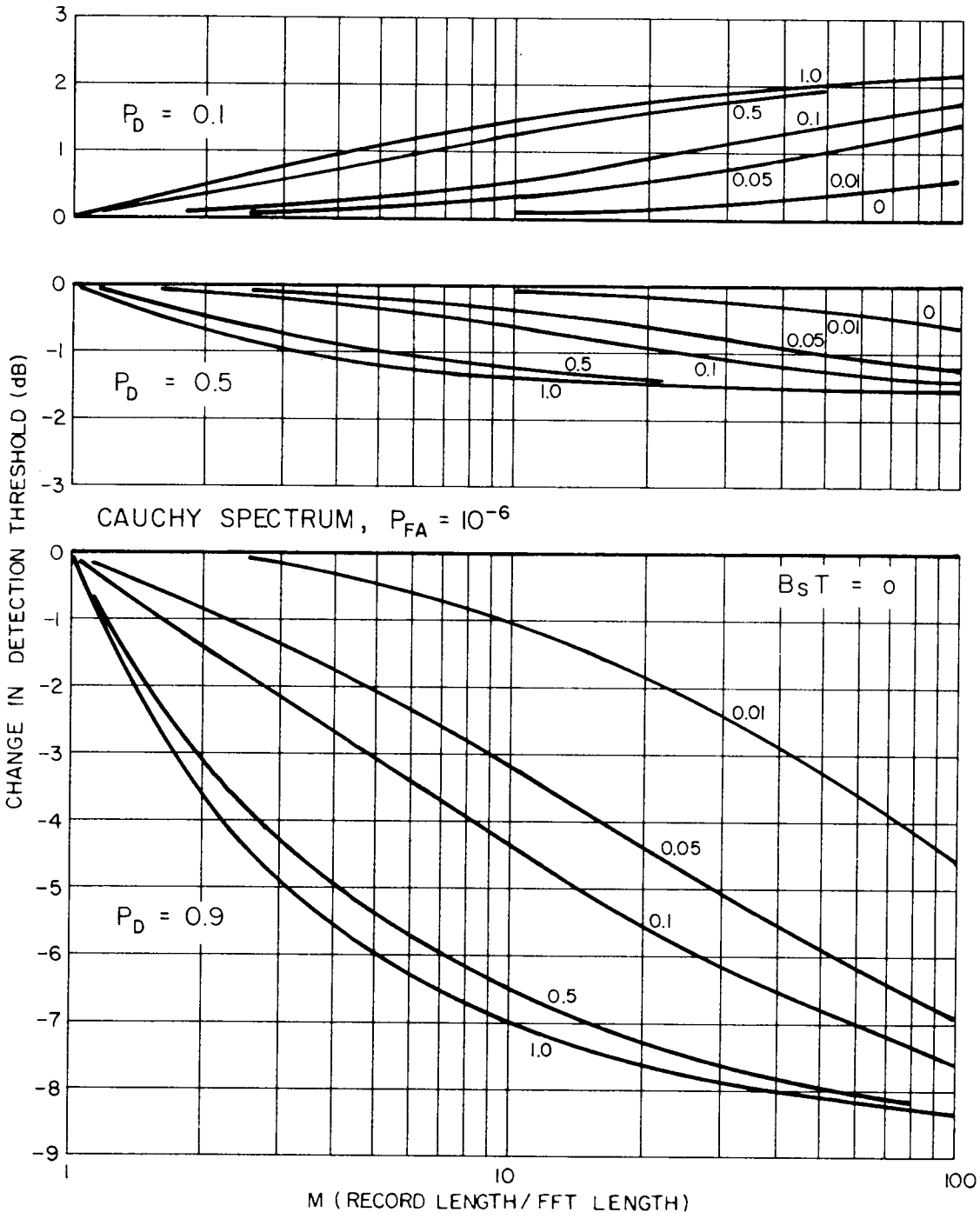

Figure 13. Change in Detection Threshold vs. M for narrowband Gaussian signal with Cauchy spectrum. $P_{FA}=10^{-6}$.

0.05, 0.1, 0.5 and 1.0. For any B_ST greater than 0, the correction in threshold approaches that for $B_ST=1$ asymptotically with increasing M. This reflects the overall decrease in correlation between the FFT samples as M increases.

3.2 Transition Curves

The detection thresholds presented in Figures 5-7 consider only one value of detection probability, namely $P_D=0.5$. Figures 14-22 allow selection of the detection threshold for other values of P_D, and for the same signal types treated in Figures 5-7. These graphs show the dependence of P_D on signal excess (SE); such a graph is commonly referred to as the transition curve. SE is defined as the difference, in dB, between the threshold required for $P_D=0.5$ and that for any other P_D. Hence, the SE is a correction to be applied to thresholds obtained from Figures 5-7. Each figure treats a single signal type and P_{FA}. Values of time-bandwidth product, M, range from 1 to 512, in powers of two. Certain values of M are omitted where the transition curves become indistinguishable from one another. The figures are grouped as follows:

Figures 14-16: Narrowband Gaussian signal, $B_ST=0$, and $P_{FA}=10^{-2}$, 10^{-4}, 10^{-6}. Labelled Swerling I.

Figures 17-19: Narrowband Gaussian signal, $B_ST=1$, and $P_{FA}=10^{-2}$, 10^{-4},10^{-6}. Signal has rectangular spectrum. Results for Cauchy spectrum are essentially identical. Labelled Swerling II.

Figures 20-22: Sinusoidal signal and $P_{FA}=10^{-2}$, 10^{-4}, 10^{-6}. Labelled Sinusoid.

Several observations can be made regarding these transition curves:

1) at a given SE, the slopes of the transition curves increase as M increases.[13] This will result in an increased detection probability at positive SE, and decreased detection probability at negative SE.

2) at large M (greater than about 100), the transition curves for the Swerling II and sinusoidal signals become identical. Similar behaviour was noted for G_M in Figures 5-7.

3) for large positive values of SE, the Swerling I transition curves are almost independent of M. Since the signal amplitude is constant within any record length for the Swerling I signal, no averaging over the distribution of signal amplitudes can occur within the processor integration time. Hence, when the signal dominates the estimate, as it does at large positive SE, there is no change in the density function of the FFT output as M increases.

As we discussed in Section 3.1, detection of Gaussian signals having bandwidths

[13] For an exception, see case 3) below.

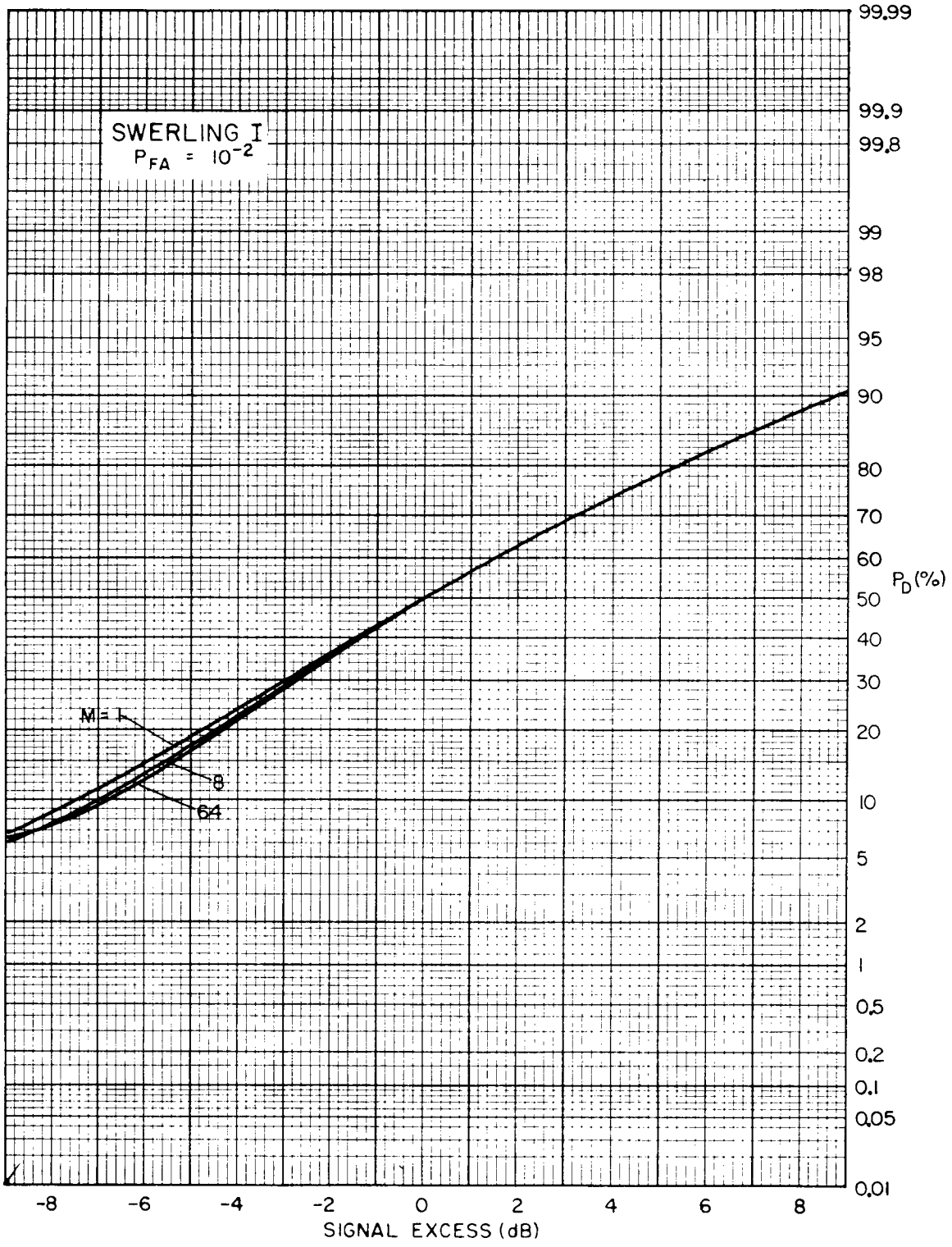

Figure 14. Transition curves for Swerling I signal and for various M. $P_{FA}=10^{-2}$.

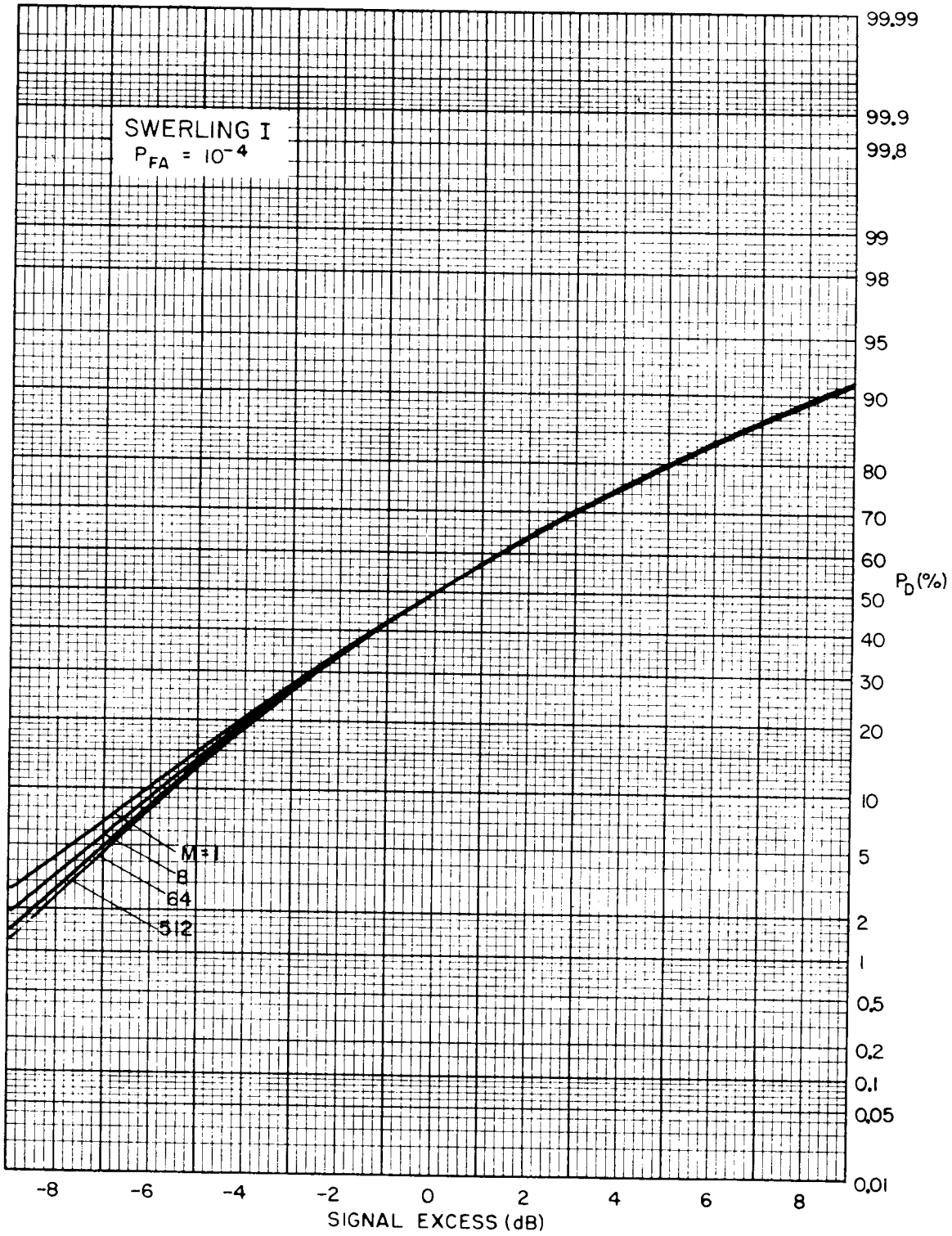

Figure 15. Transition curves for Swerling I signal and for various M. $P_{FA}=10^{-4}$.

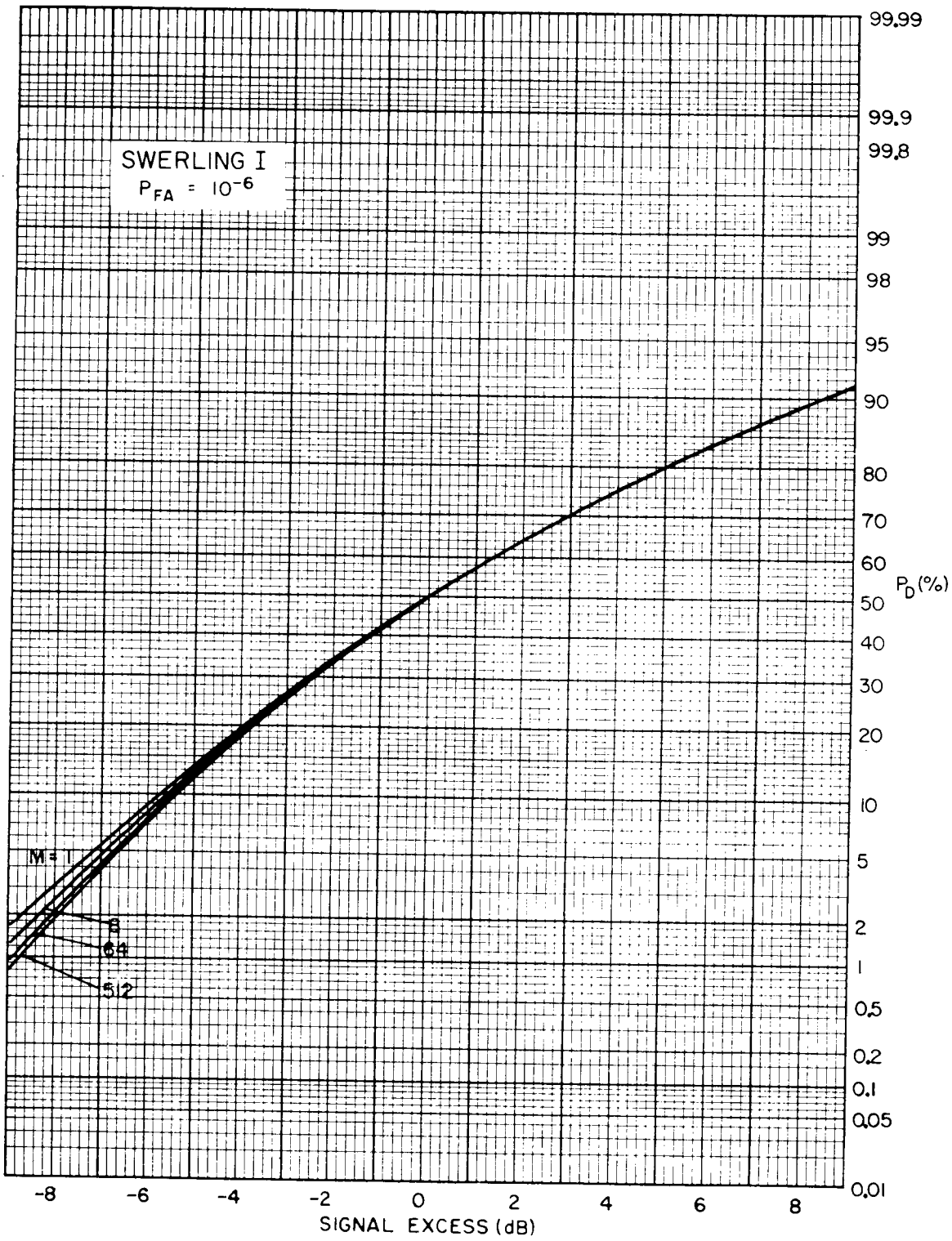

Figure 16. Transition curves for Swerling I signal and for various M. $P_{FA}=10^{-6}$.

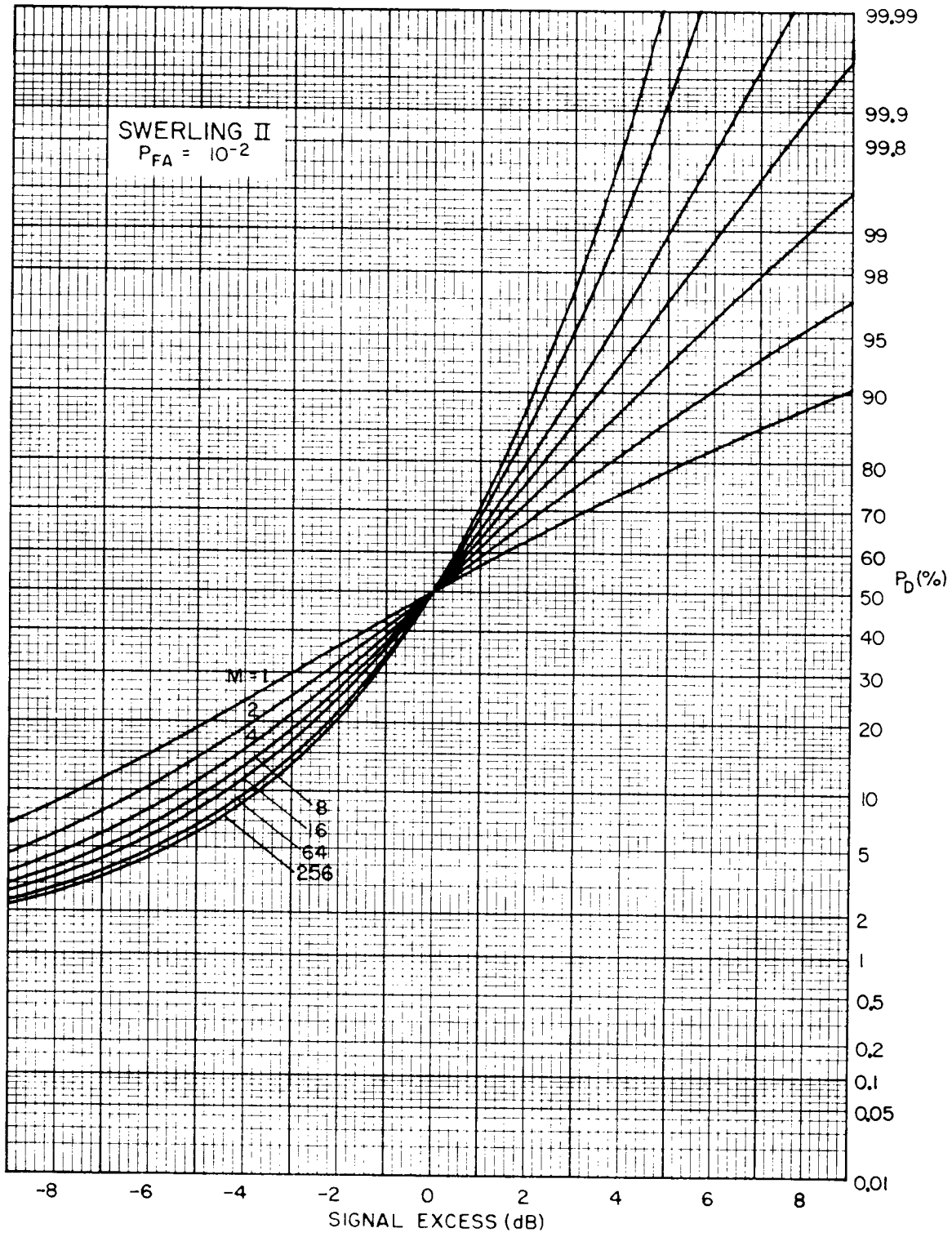

Figure 17. Transition curves for Swerling II signal and for various M. $P_{FA}=10^{-2}$.

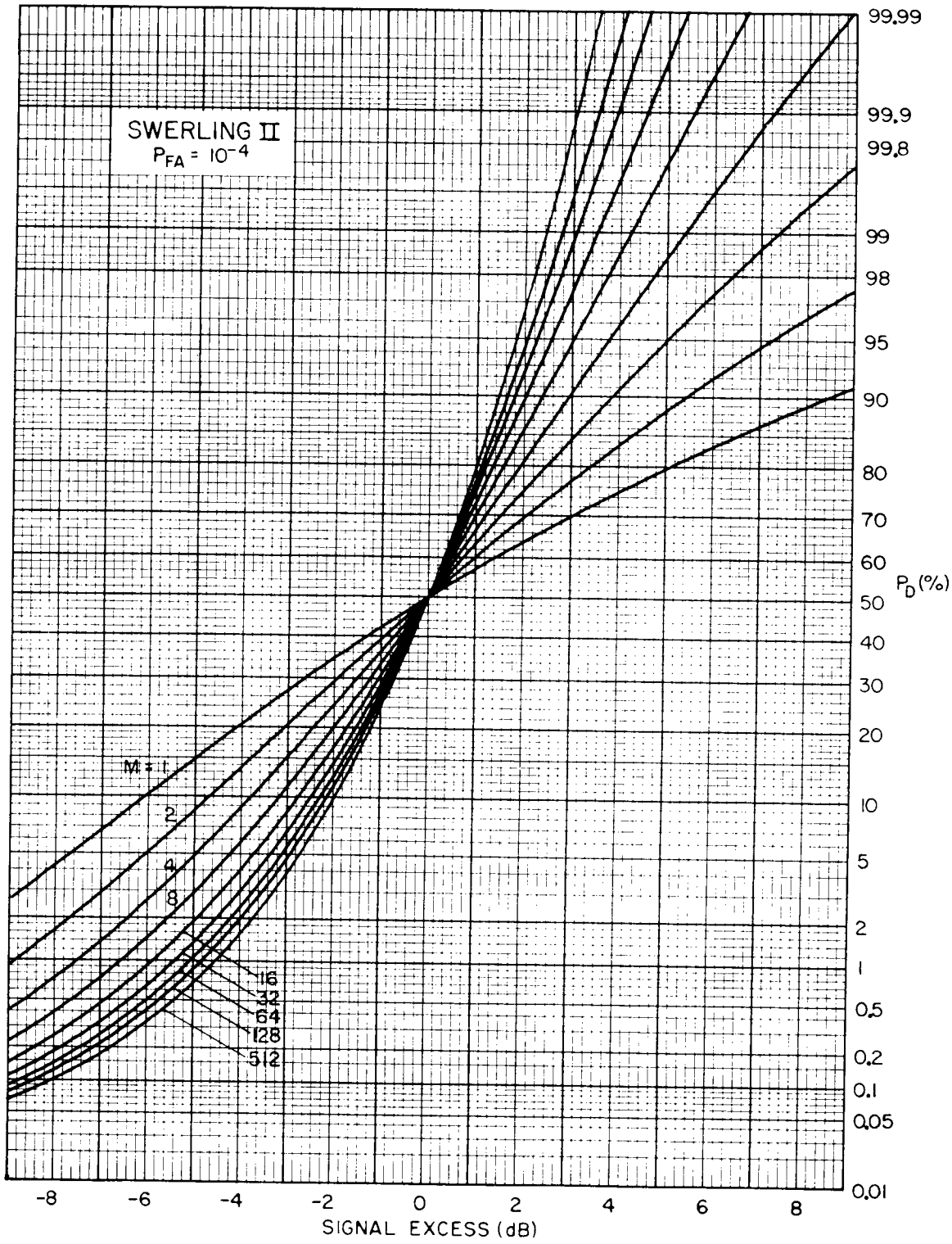

Figure 18. Transition curves for Swerling II signal and for various M. $P_{FA}=10^{-4}$.

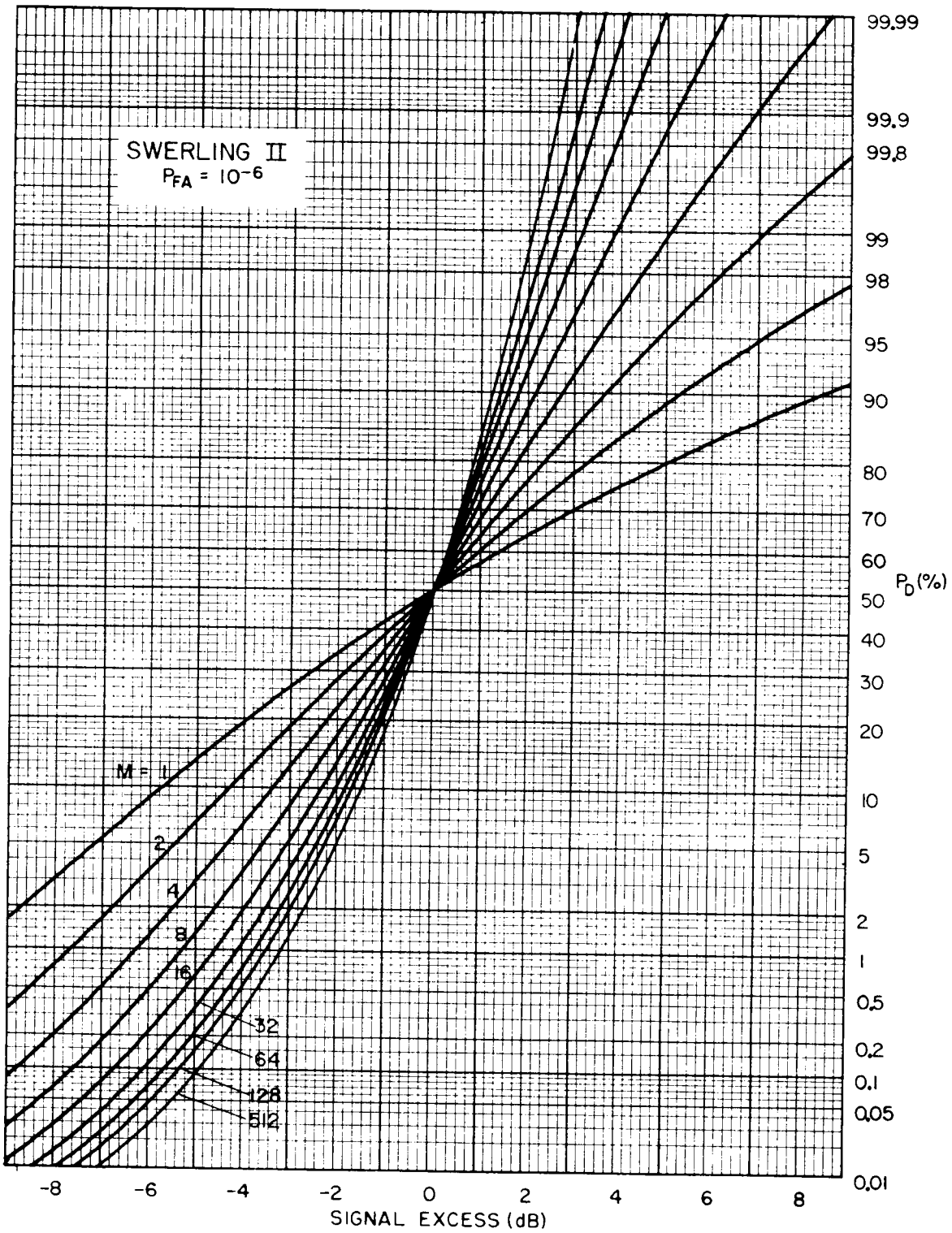

Figure 19. Transition curves for Swerling II signal and for various M. $P_{FA}=10^{-6}$.

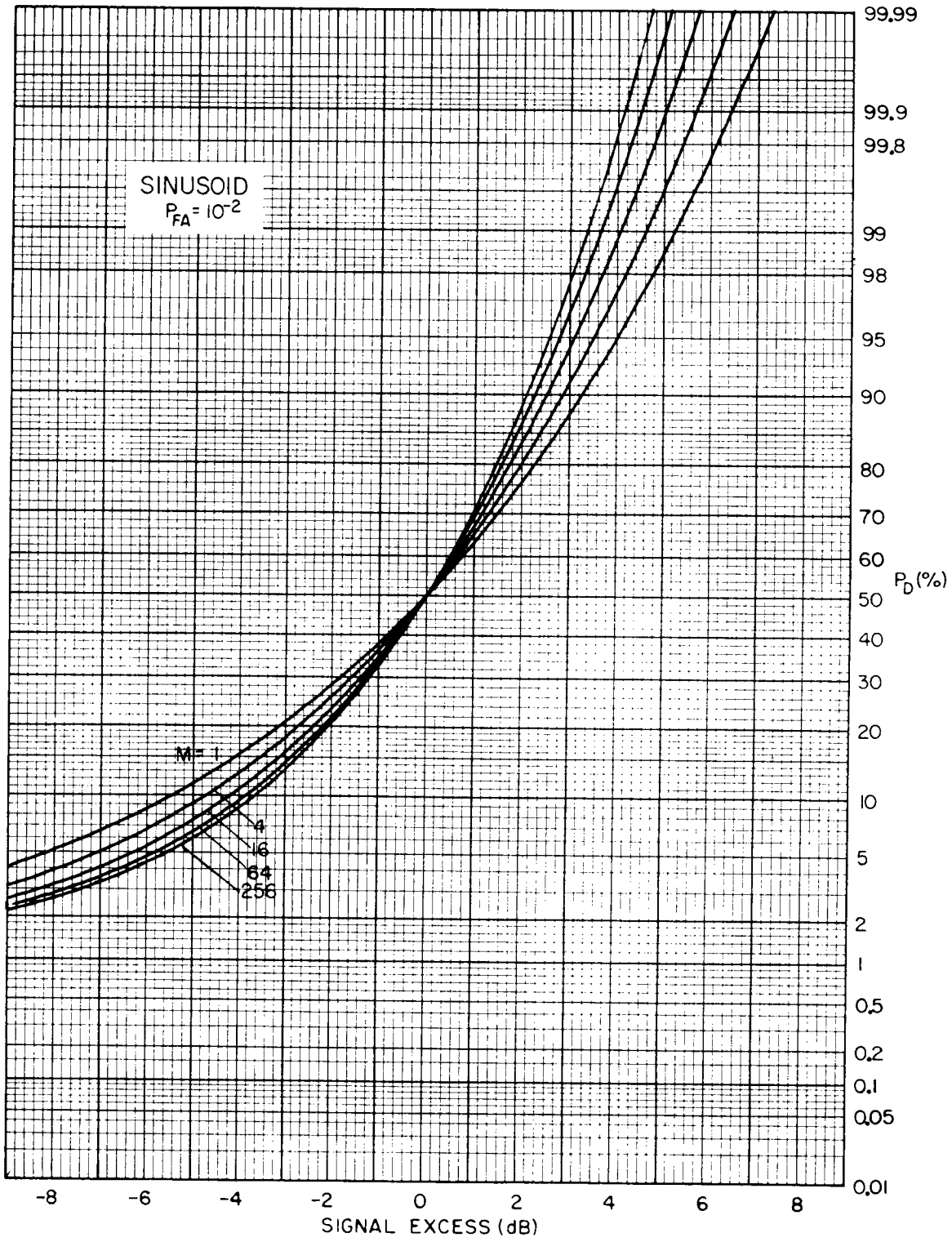

Figure 20. Transition curves for sinusoidal signal and for various M. $P_{FA}=10^{-2}$.

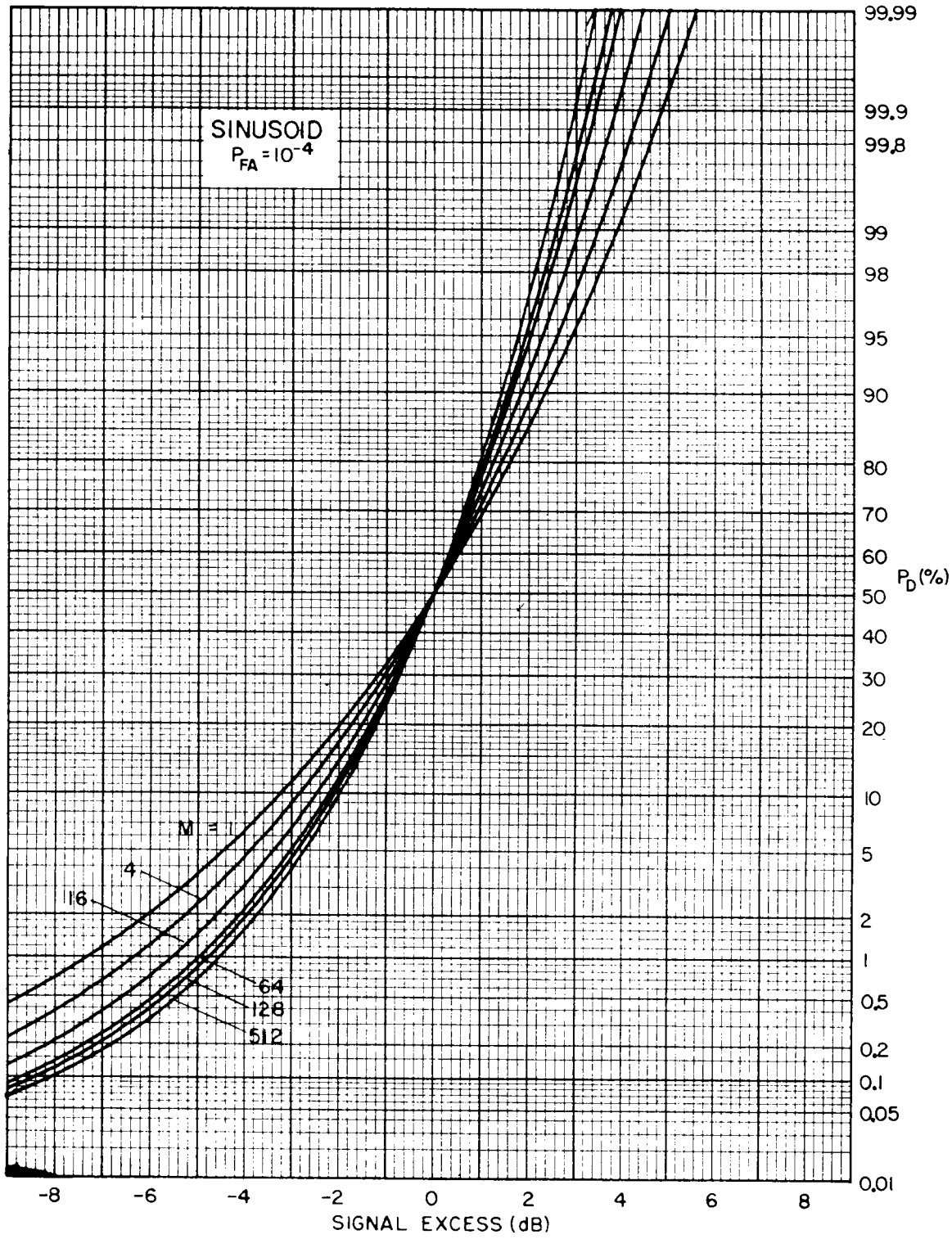

Figure 21. Transition curves for sinusoidal signal and for various M. $P_{FA}=10^{-4}$.

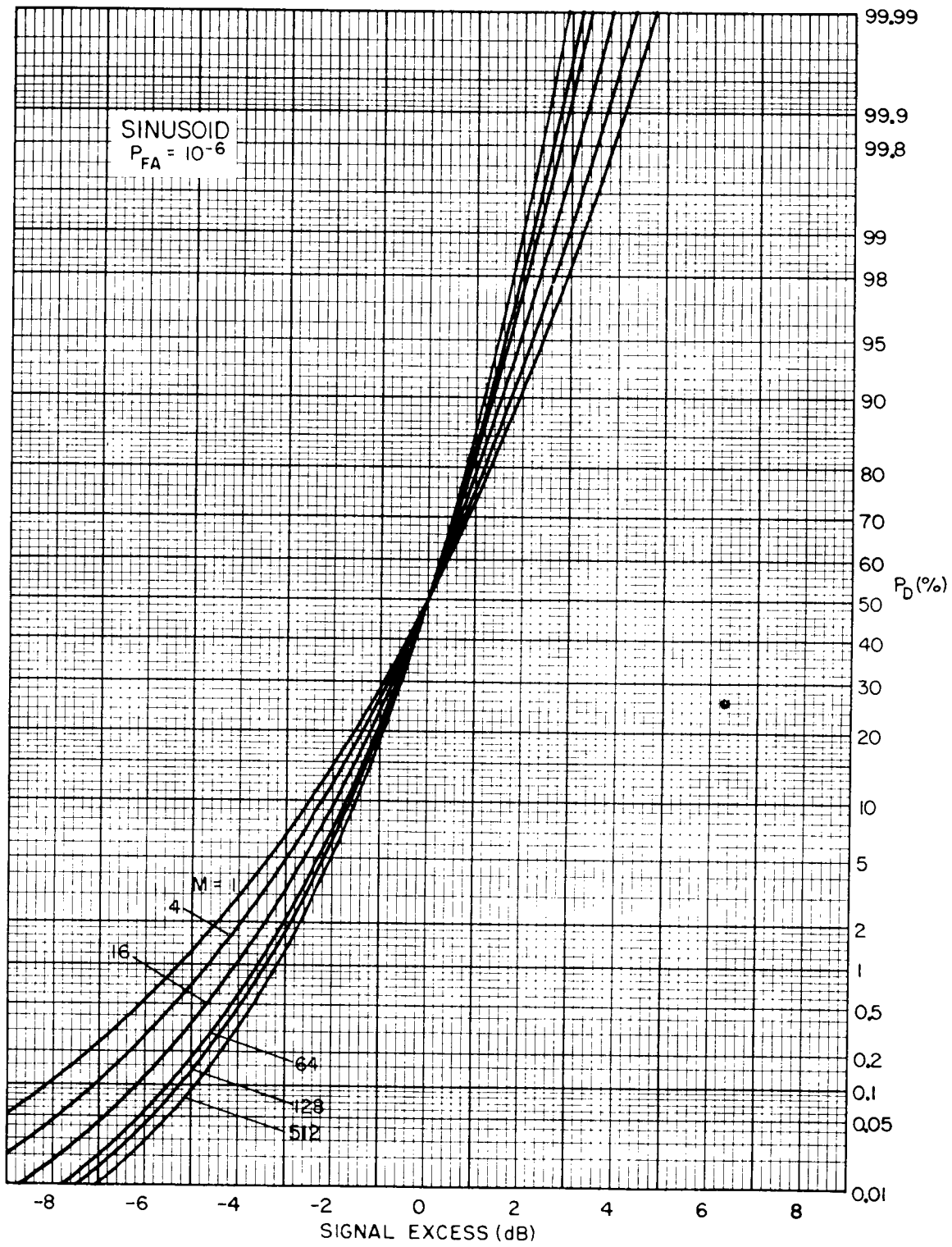

Figure 22. Transition curves for sinusoidal signal and for various M. $P_{FA}=10^{-6}$.

intermediate to the Swerling I and II models, and at values of P_D other than 0.5, is treated in Figures 8-13.

3.3 Data Windowing

Because of the data window, the narrowband signal power measured in any FFT bin may be reduced relative to its true power. This results for three reasons, all of which are best understood in terms of the spectral window, i.e. the magnitude-square of the Fourier transform of the data window.[14] The first reason that the power in the bin is reduced arises because the spectral window is not flat over the signal spectrum. Secondly, a processing gain is associated with the window [15] which may reduce the sensitivity to the narrowband signal relative to the noise. Finally the signal spectrum may not be centered on the FFT bin. These first two losses are treated in this subsection; the last is treated in Section 3.4.

Figure 23 shows the processing loss, L_W, associated with both the rectangular and Hanning windows, as a function of the relative bandwidth, B_ST, of the signal spectrum. Gaussian signals of either rectangular spectrum or Cauchy spectrum are considered. Losses for a sinusoidal signal correspond to those at $B_ST=0$. The signal spectrum is centered on the FFT bin. At $B_ST=0$, the loss is due to the processing gain we noted above. This gain is unity (0 dB) for the rectangular window, and 1/1.5 (-1.76 dB) for the Hanning window. As B_ST increases from 0, the loss associated with the droop of the spectral window is introduced. This loss is greater for the rectangular window, since its spectral window is narrower; it can cause more than a 1 dB loss for $B_ST=1$.

3.4 Ripple Loss

If the narrowband signal is not centered on the FFT bin, the signal power will be reduced because of the curvature of the spectral window. When a spectral window is centered on each FFT bin across the entire frequency band, the sensitivity of the processor ripples across frequency, following the shape of the mainlobe of each spectral window. The loss in signal power associated with this reduced sensitivity is referred to as ripple loss, L_r. It depends on the shape of the mainlobe of the spectral window, i.e. the broader the mainlobe, the less will be the ripple loss.

In Figure 24 we examine the ripple loss (in dB) for both the rectangular window and the Hanning window. The loss is presented as a function of the relative displacement of the signal spectrum from the FFT bin center.[16] Curves are given for three values of signal bandwidth: $B_ST=0$, 0.5 and 1.0. For $B_ST>0$, the results are further divided between the two signal spectrum types. At $B_ST=0$, the loss is a direct measure of the spectral window sensitivity at each displacement; for example, the rectangular

---

[14] The two data windows considered in this report- the rectangular window and Hanning window- and their spectral windows are shown in Figure 2.

[15] For a discussion see Section 2.2.

[16] For relative displacements greater than 0.5, the signal is considered to lie in the adjacent bin.

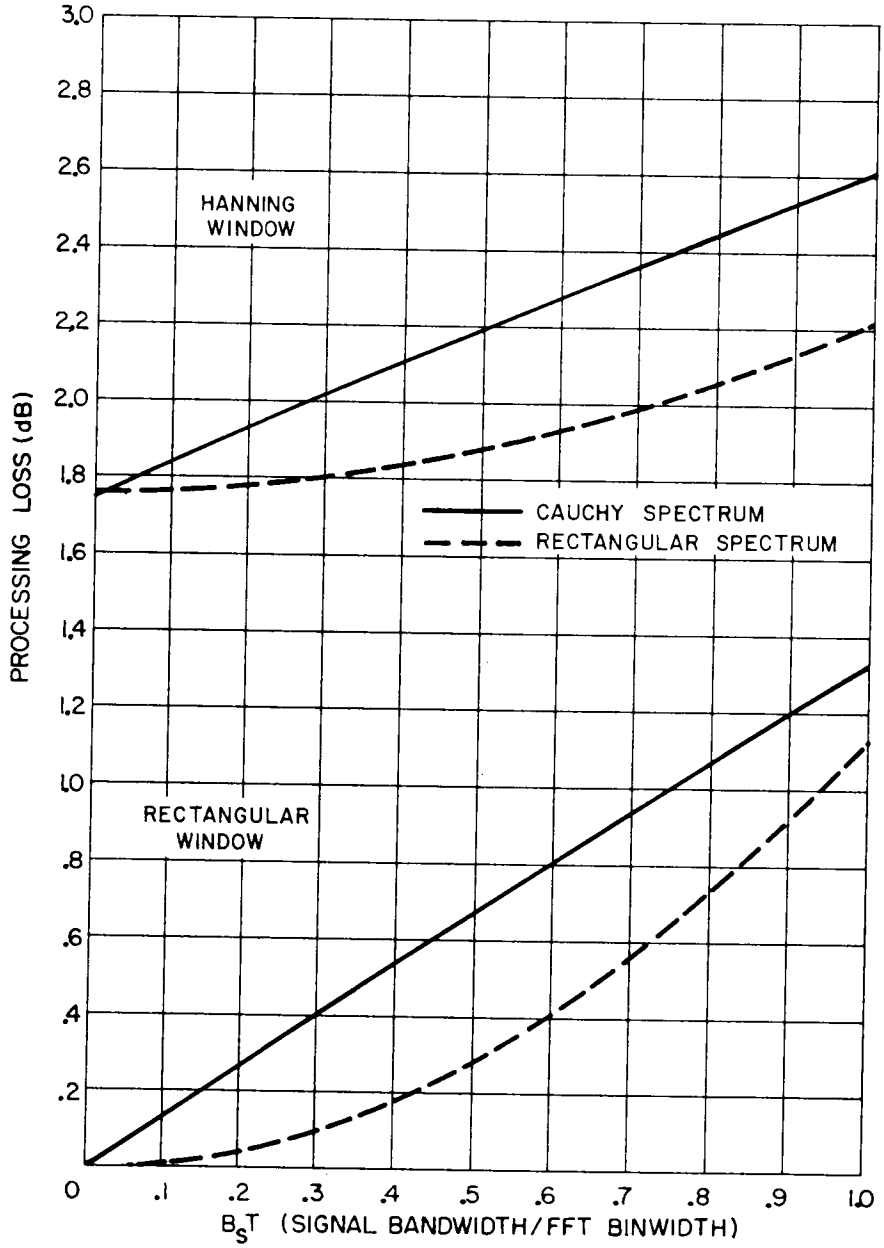

Figure 23. Processing loss vs. relative signal bandwidth for rectangular and Hanning windows.

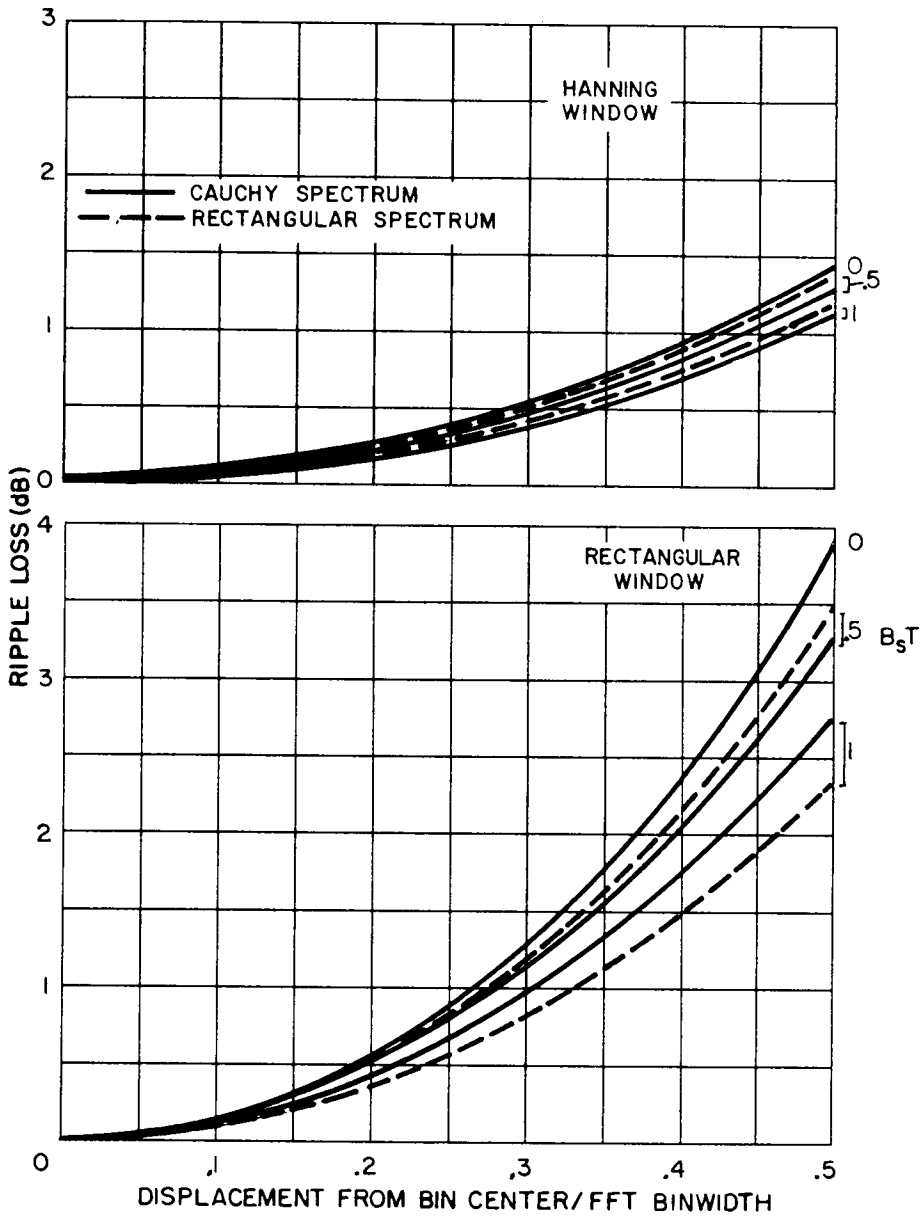

Figure 24. Ripple loss vs. displacement of signal frequency from bin center for rectangular and Hanning windows.

window is reduced by 3.9 dB in sensitivity at the bin edge. The loss is only 1.4 dB for the Hanning window, owing to its broader mainlobe. As B_ST increases from 0, the ripple loss is reduced.

The losses in Figure 24 are meaningful provided we know precisely the center frequency of the signal. Since this is usually not known, it is appropriate to define an average ripple loss across all possible displacements. This average ripple loss is shown in Figure 25 as a function of the signal bandwidth, B_ST. The results depend on window type and signal spectrum type. The loss decreases monotonically as signal bandwidth increases.

3.5 Zeroes Extension

The average ripple loss can be reduced by extending the length of the FFT segment with zeroes prior to Fourier transformation. Zeroes extension does not alter the shape of the spectral window. Hence, it does not change the resolution or stability of the spectral estimate. However, it does increase the number of frequency points at which the spectrum is estimated, thereby reducing the possibility of missing the signal peak.

The gain, G_z, in detection threshold due to zeroes extension is shown in Figure 26 versus the length of the segment extension. The gain represents the reduction in average ripple loss due to the closer spacing of spectral windows across frequency. The extension is normalized to units of the original segment length, e.g. a zeroes extension of 2 means the segment length has been doubled by adding zeroes. The gain depends on the data window, the signal bandwidth, B_ST, and the signal spectrum type. About 0.75 of the possible gain is achieved by doubling the segment length with zeroes. The maximum gain reduces as B_ST increases, since the average ripple loss reduces as well.

3.6 Segment Overlap

FFT segment overlap reduces the detection threshold since it effectively increases the amount of incoherent averaging, hence increasing the stability of the power estimate. The gain in detectability will depend on the correlation between noise samples from adjacent FFT segments - as the correlation increases, the effective increase in averaging is reduced. In Section 2 we showed that the correlation between adjacent samples depends on the shape of the data window. A more tapered window will produce less correlation between samples, and hence, the greater will be the gain due to overlap. This does not imply that further tapering of the data window is good, since for greater taper, the processing loss discussed in Section 3.3 increases. In effect, segment overlap is a means of recovering, at least in part, this processing loss. The detection gain due to overlap must be weighed against the accompanying increase in processor load.

In general, the detection gain due to overlap will include dependence on the signal type, its bandwidth and spectrum, the data window, time-bandwidth product, and detection and false-alarm probabilities. A common approximation to the effects of overlap is to define an effective number of averages, M_{eff}, that results from

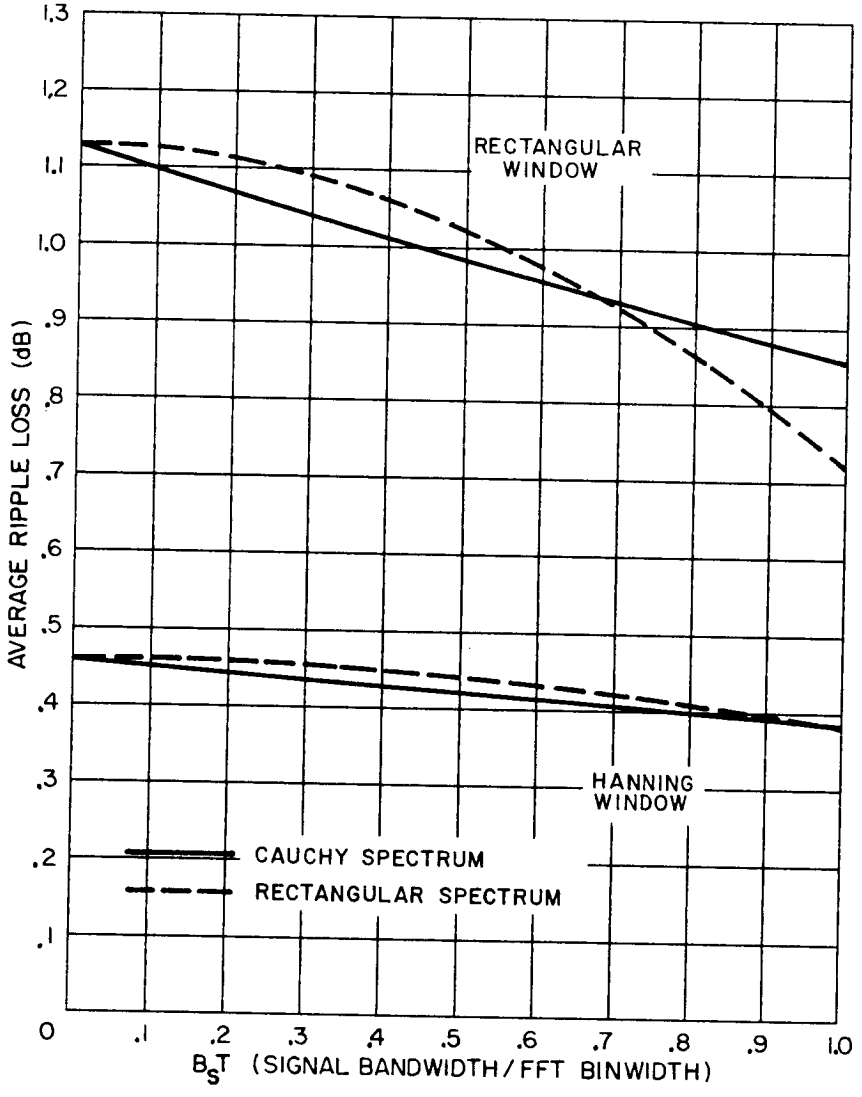

Figure 25. Average ripple loss vs. relative signal bandwidth for rectangular and Hanning windows.

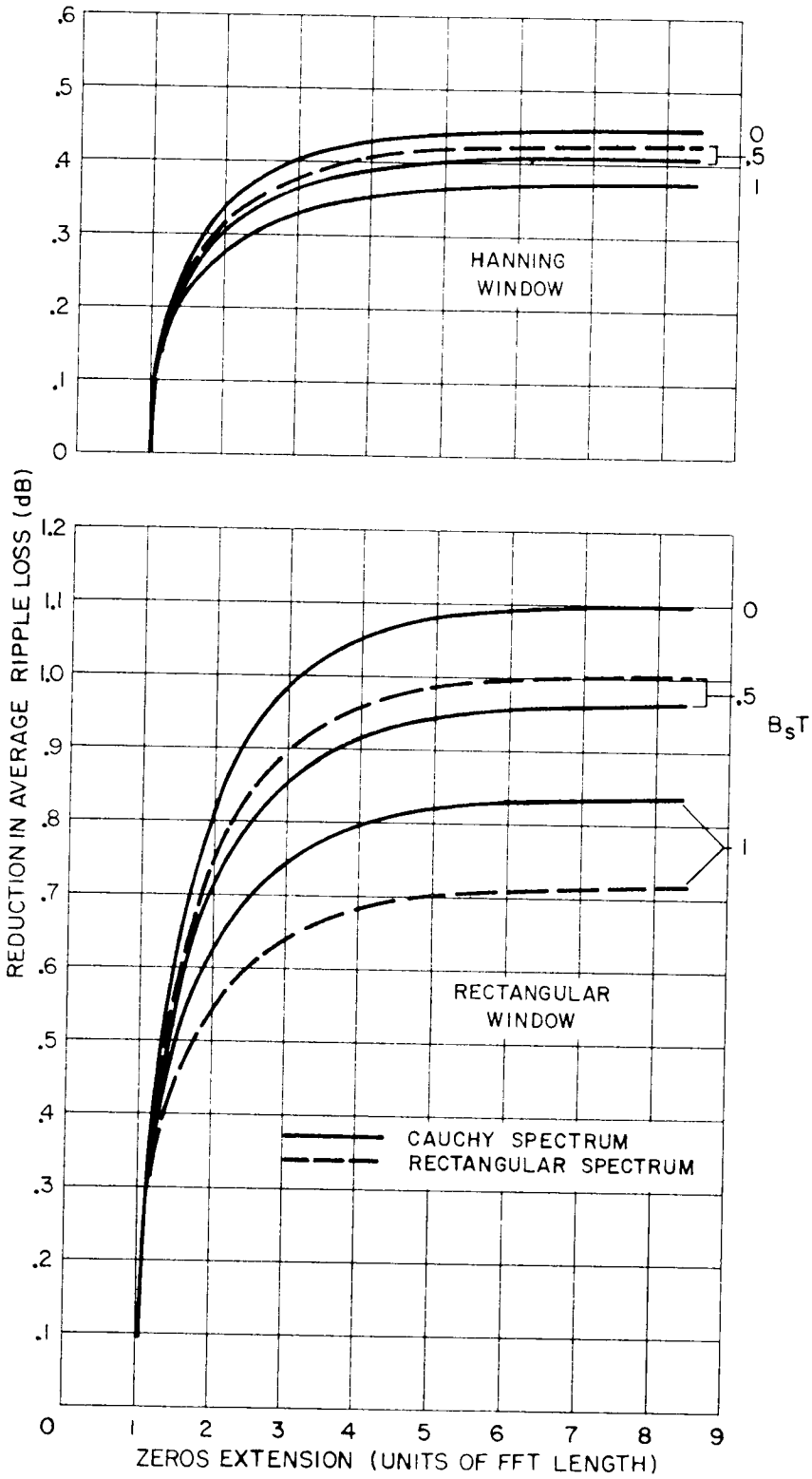

Figure 26. Reduction in average ripple loss due to zeroes extension.

overlap[11]. M_{eff} will exceed the time-bandwidth product, M, by an amount that depends on the extent of overlap and on the correlation between overlapped samples. As overlap increases, M_{eff} will approach a limiting value, since samples become highly correlated. In Appendix D.2, the ratio M/M_{eff} is derived on the assumption it equals the reduction in variance of the noise-only power samples. The ratio depends only on the data window and overlap. The detection gain due to overlap can be obtained from Figures 4-22 simply by increasing the time-bandwidth product by this ratio[11]. An alternative approximation assumes that the detection gain is proportional to the square-root of the increase in M, i.e.:

$$G_o = 5\log (M_{eff}/M). \qquad (45)$$

This is similar to the Gaussian approximation to G_M shown in Figures 5-7, where we see that G_M is proportional to $\sqrt{M}$. In Appendix D.2 we have compared the predictions of detection gain for the above two methods to those resulting from complete analysis over selected parameters. The method which uses a correction to Figures 4-22 is a better approximation for $20 < M < 100$; however, the maximum deviation we have observed using (45) is still only of the order of ±0.2 dB. Hence, considering its simple evaluation, the second approximation would seem adequate for our purposes.

Figure 27 shows the dependence of the detection gain on the fractional segment overlap, according to the approximation expressed by (45). Gains are presented for the rectangular and Hanning data windows, and for values of time-bandwidth products of: M=4, 8, 16, 32 and ∞. The gain to be made by segment overlap is significantly more for the Hanning window; however, its processing loss is likewise greater. For finite M, the maximum gain is achieved at a fractional overlap less than unity.

It is interesting that any gain results at all due to overlap for the rectangular window, since all data in the time record receives equal weight. Consider for the moment the inverse Fourier transform of the power spectral estimate, namely the autocorrelation estimate. The stability of the power estimate is related to the number of estimates of the autocorrelation available at each time lag. By segmenting the time record, we remove those autocorrelation estimates otherwise available across segment boundaries. Segment overlap attempts to return these estimates, thereby increasing the spectrum stability. This effect is realized regardless of the segment weighting.

While the curves presented in Figure 27 are continuous, only discrete values of the fractional overlap, γ , are possible for finite M. Otherwise, a non-integer number of overlapped segments results. For M' overlapped segments, γ must be chosen so that:

$$M' = (M-\gamma)/(1-\gamma) , \qquad (46)$$

where M' is an integer. The curves in Figure 27 interpolate gains between those at the allowed values of overlap.

3.7 Data Normalization

Threshold setting requires that we know the actual noise power in the frequency bin of interest. Since this is usually not known, the noise power must be estimated from the available data. One estimation method is to average the power in adjacent FFT bins, assuming that they contain only noise, and of the same mean level. The power estimate

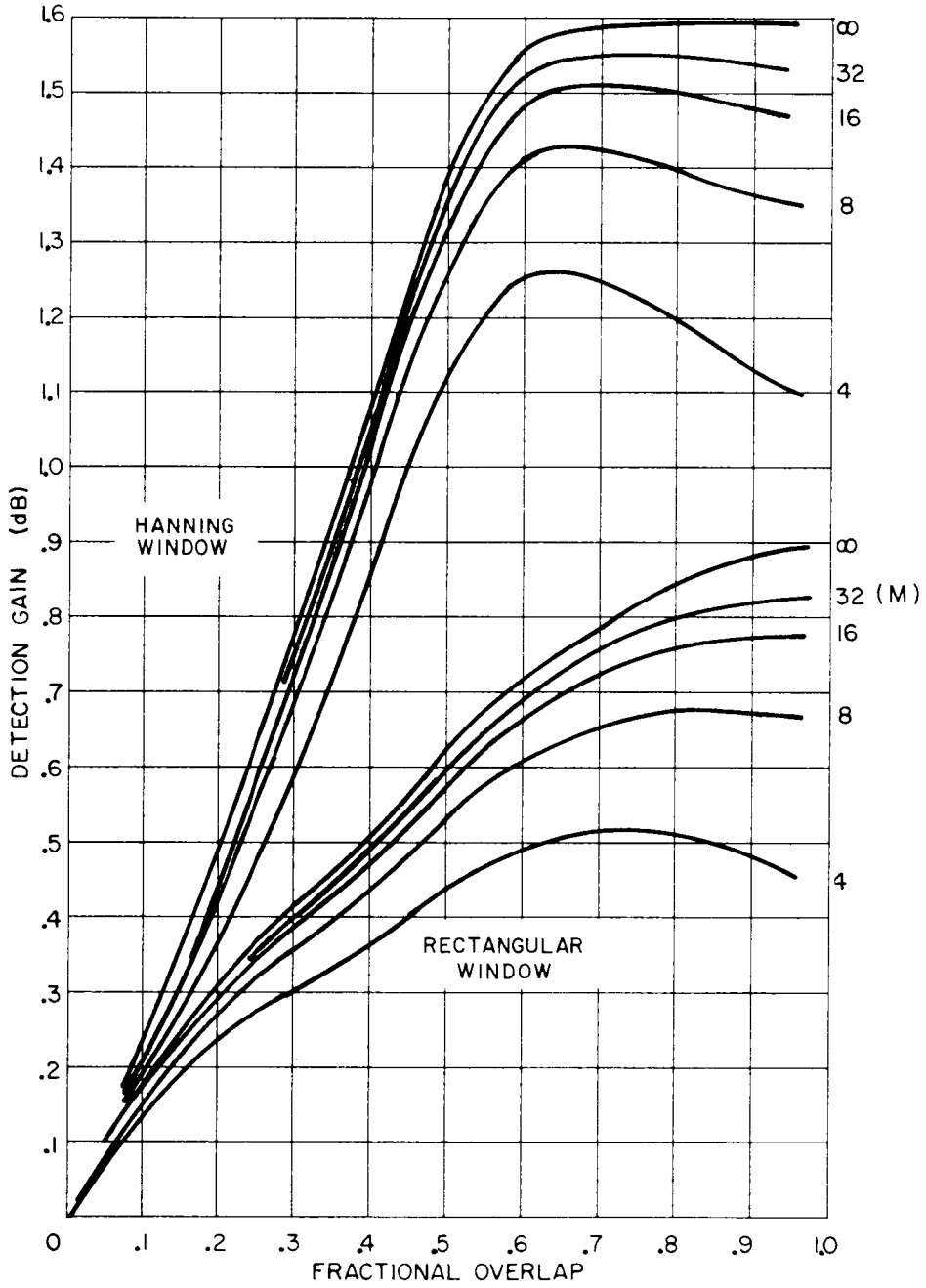

Figure 27. Reduction in Detection Threshold vs. fractional FFT segment overlap.

in the bin of interest may then be normalized by this estimated noise power; this removes the direct dependence of the threshold on the noise power.[17] When the normalizer uses some number of bins distributed about the bin of interest, the normalizer is referred to as a moving window normalizer. We consider its effect on detection performance below.

An increase in detection threshold is necessary when data normalization is required if we are to achieve the same P_D and P_{FA} had the noise power been known. We will assume that the noise is of uniform power across the bins to be averaged by the normalizer and that the power estimates in these bins are independent. Power estimates in adjacent bins will be correlated because of leakage through the spectral window. For typical spectral windows, and a reasonable number of bins in the average, the correlation can be ignored. One exception, of course, is when zeroes extension is used, since estimates in neighbouring bins will undoubtedly be correlated. One simple method of avoiding this correlation is to have the normalizer not use estimates from bins added by zeroes extension. The effect of leakage of signal power into bins included in the average is also neglected; it will influence the power estimates only at large signal-to-noise ratios, where the detection probability is high.

The detection threshold necessary when the normalizer is used depends on the time-bandwidth product, on the number of bins in the average, on the properties of the signal , as well as on P_D and P_{FA}. The threshold for the moving window normalizer, under the assumptions in the previous paragraph, is analyzed in Appendix F. Three signal types are considered: sinusoid, Swerling I and Swerling II. One important observation is that while the absolute detection threshold depends on the signal model and P_D, the *difference* in detection thresholds required with and without the data normalizer is only weakly dependent on these parameters. This has also been observed in **[24]**.

In Figures 28-30 we present the increase in threshold (in dB) required for the moving window normalizer. The increase is a function of the number of noise-only bins used by the normalizer; the range is from 5-55 bins. An odd number of bins is possible in the analysis, since no assumption of the distribution of bins around the bin of interest is necessary. Each figure is for one P_{FA}: 10^{-2} , 10^{-4} and 10^{-6}. The graphs depend on the time-bandwidth product, M, used in obtaining the spectral estimate. Values of M lie between 1 and 100. If segment overlap is used, the increases in DT will be somewhat less. The actual results pertain to the Swerling II signal at P_D=0.5; however, the results are essentially the same for the Swerling I and sinusoidal signals, and for $0.1 < P_D < 0.9$.

The detection losses shown in these figures are quite small for a reasonable number of bins in the normalizer average (greater than about 20). This loss is less a concern in practice than losses caused by a bias in the noise power estimate, i.e. the power estimate is different, on average, from the actual noise power. Such bias may be caused by non-uniformity, or non-whiteness, in the noise power spectrum over the normalizer window, or by the presence of narrowband signals within the window. Hence, the normalizer often contains design features to minimize these bias problems. For example, the normalizer may reject from the average the bin containing the largest power, so as to remove one narrowband signal. The median noise power**[25]** may be used rather than the mean, since it is less influenced by the presence of narrowband signals. Also, multiple passes of the window may be made for additional smoothing of non-uniform noise spectra.

---

[17] For a discussion, see Section 2.1.

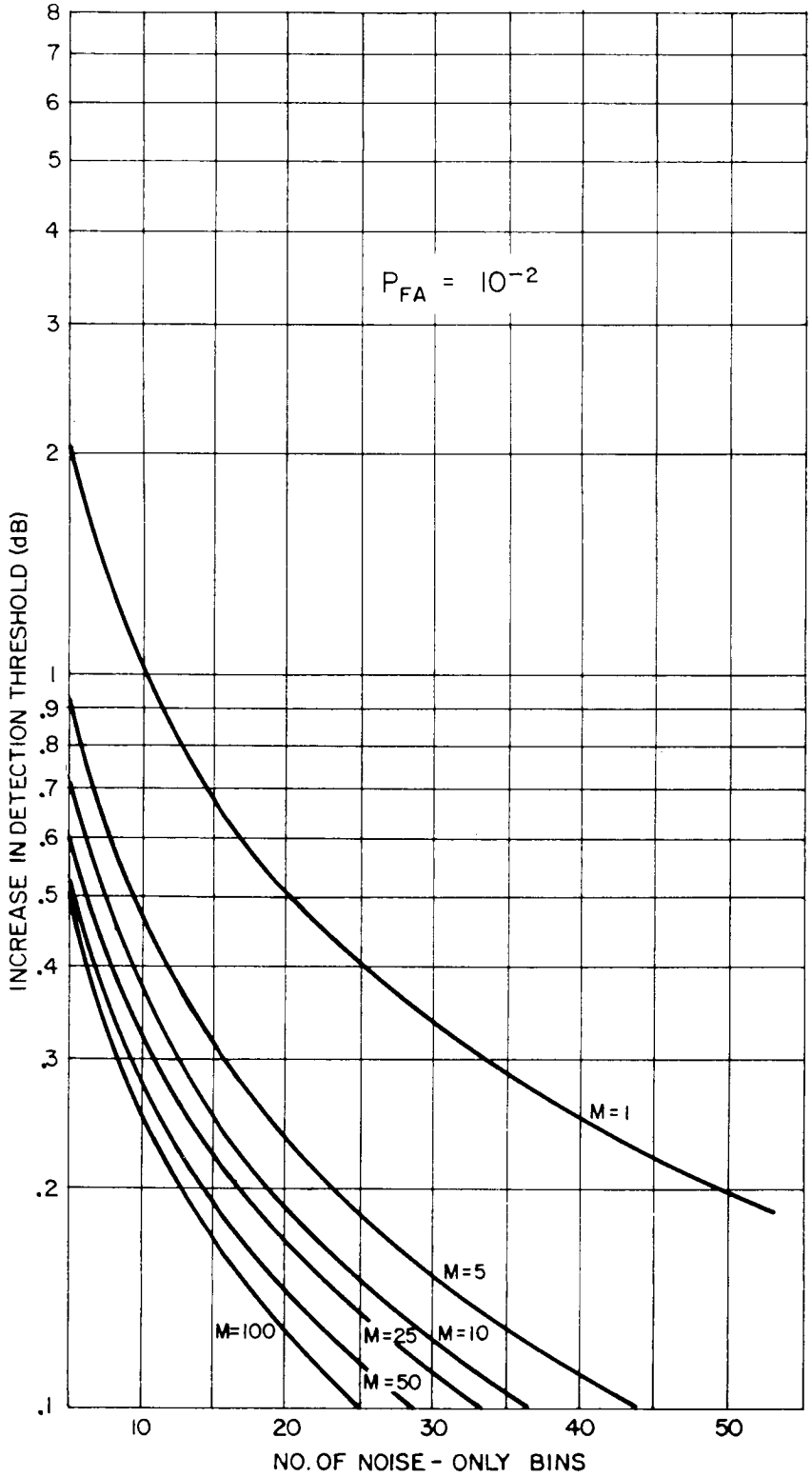

Figure 28. Loss in Detection Threshold vs. the number of noise-only FFT bins used in the data normalizer. $P_{FA}=10^{-2}$.

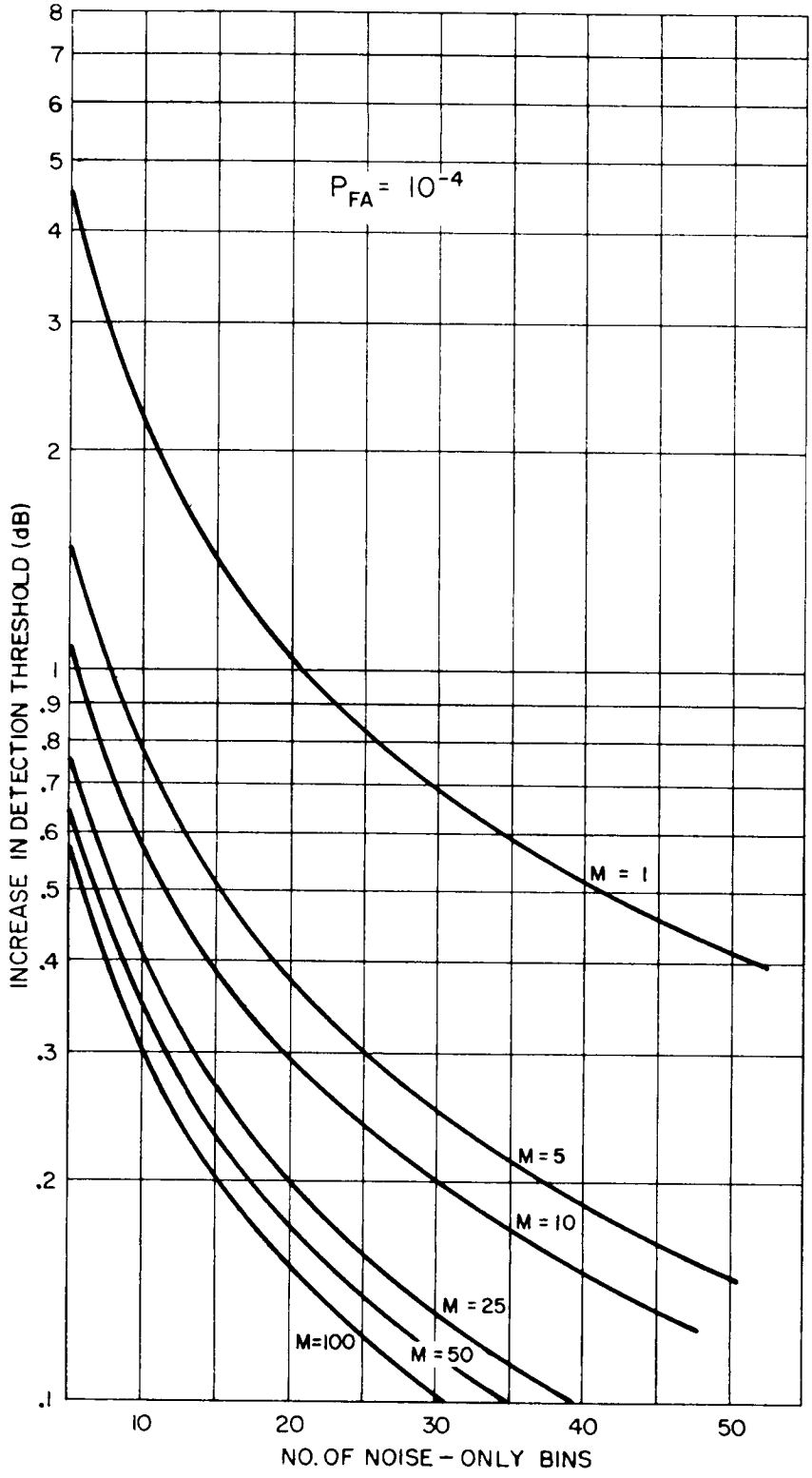

Figure 29. Loss in Detection Threshold vs. the number of noise-only FFT bins used in the data normalizer. $P_{FA}=10^{-4}$.

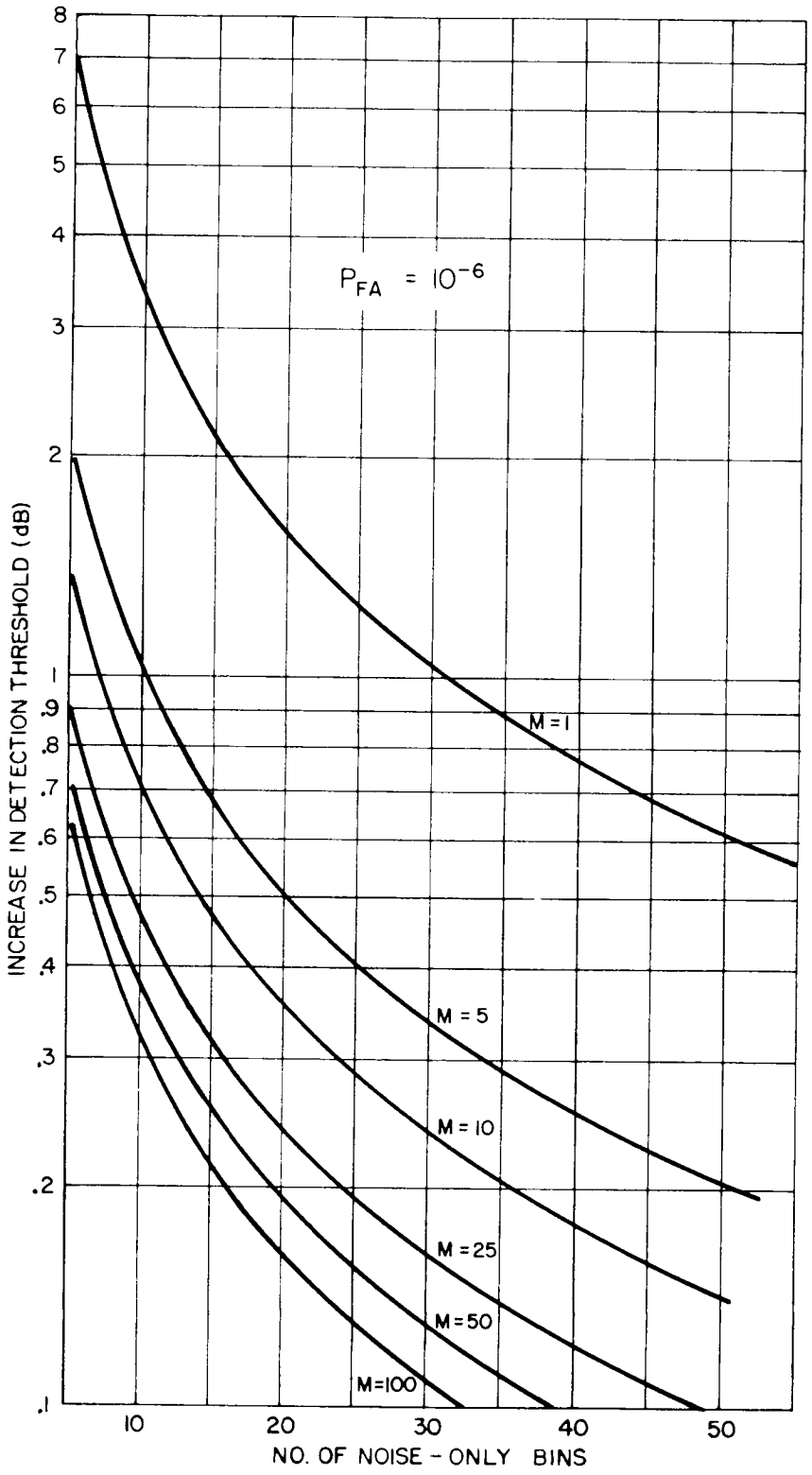

Figure 30. Loss in Detection Threshold vs. the number of noise-only FFT bins used in the data normalizer. $P_{FA}=10^{-6}$.

4 Examples of Use of the Results

In this section we present three examples of the use of the results of Section 3 to evaluate the detection threshold for a specific processor structure. The signal model for each example and the processor parameters are given in Table 1. The approach is to obtain from the graphs in Section 3 values for each of the terms in (43). Their summation will then yield the final detection threshold. Tables 2 - 4 tabulate each of these terms and the appropriate values for the above three examples. The tables include the source (Figure) of the value and comments to aid in its selection.

Table 1

Signal and processor parameters for example evaluation

PARAMETERS	EXAMPLE 1	EXAMPLE 2	EXAMPLE 3
1)signal type	Gaussian	Gaussian	sinusoid
2)Spectrum	rectangular	Cauchy	
3)bandwidth, B_S	0.1 Hz	0.001 Hz	0 Hz
4)record length, T_r	300 s.	150 s.	600 s.
5)segment length, T	10 s.	10 s.	2 s.
6)FFT binwidth, 1/T	0.1 Hz.	0.1 Hz.	0.5 Hz.
7)time-bandwidth product, M	30	15	300
8)relative signal bandwidth, B_ST	1	0.01	0
9)data window	Hanning	rectangular	Hanning
10)zeroes ext.	none	50%	none
11)fractional segment overlap	0.5	0.25	0.5
12)no. of bins in normalizer	20	20	20
13) P_D	0.5	0.9	0.2
14) P_{FA}	10^{-4}	10^{-2}	10^{-5}

Table 2

Performance evaluation for Example 1

TERM	VALUE(dB)	SOURCE	COMMENTS
G_M	-0.7	Fig. 6	P_D=0.5, $P_{FA}=10^{-4}$, narrowband Gaussian signal, rectangular spectrum, B_ST=1, M=30;
10logB	-10.0		B = 0.1 Hz;
SE	0		since P_D=0.5, not necessary;
L_w	2.2	Fig. 23	Hanning window, rectangular spectrum, B_ST = 1;
L_r	0.4	Fig. 25	Hanning window, rectangular spectrum, B_ST = 1;
$-G_z$	0		no zeroes extension;
$-G_o$	-1.4	Fig. 27	Hanning window, 0.5 fractional overlap, M = 30;
L_n	0.2	Fig. 29	$P_{FA}=10^{-4}$, M=30, 20 noise-only bins.

DT =	-9.3 dB		

Table 3

Performance evaluation for Example 2

TERM	VALUE(dB)	SOURCE	COMMENTS
G_M	-1.4	Figs.5,11	Fig.5: Gaussian signal, B_ST=0, P_D=.5, $P_{FA}=10^{-2}$, M=15: G_M = 0.0 dB; Fig.11: Cauchy spectrum, B_ST=0.01, P_D=0.9, $P_{FA}=10^{-2}$, M=15: correction to G_M = -1.4 dB;
10logB	-10.0		B = 0.1 Hz;
SE	8.7	Fig. 14	Swerling I (B_ST=0), P_D=0.9, $P_{FA}=10^{-2}$, NOTE:since Fig.11 is relative to Swerling I, we require SE for Swerling I;
L_w	0.0	Fig. 23	rectangular window, B_ST=0.01;
L_T	1.1	Fig. 25	rectangular window, B_ST=0.01;
$-G_z$	-0.6	Fig. 26	rectangular window, B_ST=0.01, zeroes extension=1.5;
$-G_0$	-0.4	Fig. 27	rectangular window, B_ST=0.01, 0.25 fractional overlap;
L_n	0.2	Fig. 28	$P_{FA}=10^{-2}$, M=15, 20 noise-only bins.

DT =	-2.4 dB		

Table 4

Performance evaluation for Example 3

TERM	VALUE(dB)	SOURCE	COMMENTS
G_M	-5.8	Figs.6,7	P_D=0.5, P_{FA}=10^{-5}, sinusoid, M=300 NOTE: interpolate in dB between results for 10^{-4} and 10^{-6};
10logB	-3.0		B = 0.5 Hz;
SE	-3.2	Figs.21,22	P_D=0.2, P_{FA}=10^{-5}, sinusoid, M=300 NOTE: interpolate between results for P_{FA}=10^{-4} and 10^{-6};
L_w	1.8	Fig. 23	Hanning window, B_ST=0;
L_r	0.6	Fig. 25	Hanning window, B_ST=0;
$-G_z$	0		no zeroes extension;
$-G_o$	-1.4	Fig. 27	Hanning window, .5 fractional overlap, M=300;
L_n	0.1	Figs.29,30	P_{FA}=10^{-5}, M=300, 20 noise-only bins NOTE: extrapolate results for P_{FA}=10^{-4} and 10^{-6}.

DT = -11.0 dB			

5 Summary

This report has presented an analysis of the detection performance of the FFT type processor for narrowband signals of unknown frequency in white Gaussian noise (of possibly unknown level). Detection of both narrowband Gaussian signals and sinusoidal signals has been treated. Various rates of amplitude fluctuation are considered in the case of Gaussian signals. The FFT processor returns an estimate of the power spectrum of the input process via the method of averaged short-time modified periodograms. The input may consist of the output of a single-channel receiver, or alternatively, a single beam as obtained by linearly beamforming the outputs of a multichannel receiver.

The detection performance analysis yields the detection threshold, DT, appropriate for a specified false-alarm probability,P_{FA}, and detection probability, P_D. We present results at P_{FA}'s of 10^{-2}, 10^{-4} and 10^{-6}, and at P_D's between 0.01 and 0.99. We examine the sensitivity of the DT to a variety of processor parameters, including: effects of integration time and processor bandwidth, the signal type, its bandwidth and spectrum, data windowing (rectangular and Hanning windows), FFT segment overlap, zeroes extension and data normalization. A *building-block* approach is taken whereby each processor parameter is isolated and its effect on the DT studied. Results are presented in graphical form so that for a particular processor design, the final DT can be readily obtained.

The Appendices contain the detailed mathematics necessary for the performance analysis.

Appendix A

The Characteristic Function Approach to Performance Evaluation

In the analysis of detection performance, we require the signal-to-noise ratio, ***SNR***, corresponding to a specified detection probability, P_D, and false alarm probability, P_{FA}. P_D and P_{FA} are obtained from the cumulative probability distribution, $F(y|H_1)$, of the FFT power estimate, $\hat{P}$, conditioned on the two hypotheses, H_0(signal absent) and H_1(signal present):

$$P_{FA} = 1 - F(y|H_0) = 1 - \int_0^y f(x|H_0)\, dx \tag{A.1}$$

and:

$$P_D = 1 - F(y|H_1) = 1 - \int_0^y f(x|H_1)\, dx$$

where $f(x|H_1)$ is the probability density function, or pdf, of $\hat{P}$, conditioned on H_1. The integration limit, y, is the power threshold setting; we discuss its selection in Appendix G. The integrations in (A.1) are lower bounded by zero, since negative powers are not possible.

Equation (A.1) can be solved, provided $f(x|H_1)$ is known. A common approach to obtaining f(x) - the conditional probability is implicit - uses the characteristic function, $\Phi(\xi)$, of $\hat{P}$, i.e.:

$$\Phi(\xi) = \int_0^\infty f(x)\, e^{j\xi x}\, dx, \tag{A.2}$$

where we see that the characteristic function and pdf are Fourier transform pairs. Provided $\Phi(\xi)$ is known, the pdf can be obtained as:

$$f(x) = \frac{1}{2\pi} \int_{-\infty}^{\infty} \Phi(\xi)\, e^{-j\xi x}\, d\xi. \tag{A.3}$$

The characteristic function is readily obtainable for the FFT power estimate under the signal and noise models treated in this report; they are derived in Appendix B. Still, the integration in (A.3) is often analytically intractable.[18] An approximate method of solving (A.3) has been developed by Bird[23]. He shows that f(x) can be expressed exactly out to some value, Y, by the following Fourier series:

[18] Several important cases which have analytic solutions are discussed in Appendix E.

$$f(x) = \sum_{n=-\infty}^{\infty} \Phi_n e^{-j2\pi nx/Y}, \quad 0 \le x \le Y \tag{A.4}$$

where:

$$\Phi_n = \frac{1}{Y} \int_0^Y f(x) e^{j2\pi nx/Y} dx. \tag{A.5}$$

The cumulative distribution, F(y), can be obtained from (A.4) as:

$$F(y) = \int_0^y f(x) dx \tag{A.6a}$$

$$= \sum_{n=-\infty}^{\infty} \Phi_n \int_0^y e^{-j2\pi nx/Y} dx, \qquad y<Y \tag{A.6b}$$

$$= y \sum_{n=-\infty}^{\infty} \Phi_n Sinc(\frac{\pi ny}{Y}) e^{-j\pi ny/Y}, \qquad y<Y \tag{A.6c}$$

where: $Sinc(z) = \sin(z)/z$.

The result in (A.6) is exact; however, we require the Φ_n. Comparing (A.2) and (A.5), we see that:

$$\Phi_n = \frac{1}{Y} \Phi(\frac{2\pi n}{Y}), \quad \text{provided } f(x)=0,\ x>Y \tag{A.7}$$

In which case, we can write (A.6c) as:

$$F(y) = \frac{y}{Y} \sum_{n=-\infty}^{\infty} \Phi(\frac{2\pi n}{Y}) Sinc(\frac{\pi ny}{Y}) e^{-j\pi ny/Y}, \tag{A.8}$$

for $y<Y$ and $f(x)=0$, $x>Y$.

Of course, the pdf is usually not zero for $x>Y$. If f(x) is so small for $x>Y$, so that the error in Φ_n from using (A.7) is negligible, then (A.8) may be used to approximate F(y). It is necessary to find Y, such that the error in F(y) is negligible, but so that the computational effort is reasonable. The value of Y appropriate for the signal and noise models considered in this report is, as given by Bird[23]:

$$Y = M'(1+SNR)\,ln(M'/\epsilon), \quad \text{narrowband Gaussian signal}$$
$$Y = M'(SNR+2(SNR\,ln(M'/\epsilon))^{1/2} + ln(M'/\epsilon)), \quad \text{sinusoidal signal,} \tag{A.9}$$

where: M' is the number of FFT averages,
SNR is the signal-to-noise ratio,
ϵ is the acceptable error in F(y).

When calculating P_{FA}, we have used $\epsilon=0.01P_{FA}$; when calculating P_D, we have used $\epsilon=10^{-5}$.

Besides the error in F(y) introduced by the fact that the pdf extends beyond Y, we must in practice truncate the infinite series in (A.8) after some finite number of terms, J. To examine this truncation error, we rewrite (A.8) as:

$$F(y) = \frac{y}{Y} + 2\sum_{n=1}^{J} Re\left[\frac{\Phi(2\pi n/Y)}{j2\pi n}(1 - e^{-j2\pi ny/Y})\right]. \tag{A.10}$$

Bird[23] has examined the truncation error in detail. He suggests the following practical rule of thumb for truncation:

$$\text{truncate at J=n if: } \frac{|\Phi(2\pi n/Y)|}{2\pi n} < 10^{-6}. \tag{A.11}$$

He has shown that the accuracy obtained using the above technique is usually of the order of 3 to 4 significant figures for *SNR*'s (in dB) of practical interest.

Appendix B

Relevant Characteristic Functions

B.1 Gaussian Noise

The FFT power estimate, $\hat{P}(f_k)$, in the FFT frequency bin centered at f_k, and due to noise only, is:

$$\hat{P}(f_k) = \frac{1}{M'} \sum_{i=1}^{M'} |X_{i,NG}(f_k)|^2, \tag{B.1}$$

which can be expressed as the scalar product:

$$\hat{P}(f_k) = \frac{1}{M'} X_{NG}^{\dagger} X_{NG}, \tag{B.2}$$

where:

$$X_{NG} = \begin{bmatrix} X_{1,NG} \\ X_{2,NG} \\ \cdot \\ \cdot \\ X_{M',NG} \end{bmatrix}, \tag{B.3}$$

and † is complex conjugate transposition. Under the assumption of Gaussian noise, X_{NG} is a vector of correlated complex Gaussian variates, where the real and imaginary parts are the in-phase and quadrature components. The second-order statistics of X_{NG} are defined by the M'xM' complex correlation matrix, K_N, given by:

$$K_N = E(X_{NG} X_{NG}^{\dagger}) \tag{B.4}$$

$E(\cdot)$ indicates expectation. The correlation matrix is Hermitian positive-definite:

$$K_{pq,N} = K_{qp,N}^{*}, \quad |K_N| > 0 \tag{B.5}$$

and also Toeplitz:

$$K_{pq,N} = K_{p-q,N}. \tag{B.6}$$

The Hermitian positive-definite property provides that K can be diagonalized:

$$K_N = R_N \Lambda_N R_N^{\dagger} = (R_N \Lambda_N^{1/2})(\Lambda_N^{1/2} R_N^{\dagger}), \tag{B.7}$$

where Λ_N is a diagonal matrix:

$$\Lambda_N = \begin{bmatrix} \lambda_{1,N} & 0 & 0 & \cdot \\ 0 & \lambda_{2,N} & 0 & \cdot \\ \cdot & \cdot & \cdot & \cdot \\ \cdot & \cdot & \cdot & \cdot \\ \cdot & \cdot & \cdot & \lambda_{M',N} \end{bmatrix}, \tag{B.8}$$

and $\lambda_{I,N}$ is the ith eigenvalue of K_N. R_N is an M'xM' real matrix, whose Ith column is the orthonormal eigenvector corresponding to $\lambda_{I,N}$. Hence, X_{NG} can be expressed as the transformation of uncorrelated Gaussian variates, according to:

$$X_{NG} = (R_N \Lambda_N^{1/2}) Y \tag{B.9}$$

where Y is a vector of complex uncorrelated Gaussian variates, having the identity correlation matrix, I. Equation (B.9) is seen to hold since:

$$\begin{aligned} E(X_{NG} X_{NG}^{\dagger}) &= E(R_N \Lambda_N^{1/2} Y Y^{\dagger} \Lambda_N^{1/2} R_N^{\dagger}) \\ &= R_N \Lambda_N^{1/2} I \Lambda_N^{1/2} R_N^{\dagger} \\ &= R_N \Lambda_N R_N^{\dagger} \\ &= K_N. \end{aligned} \tag{B.10}$$

Replacing X_{NG} in (B.2) by (B.9),we get:

$$\begin{aligned} \hat{P} &= \frac{1}{M'} Y^{\dagger} \Lambda_N^{1/2} R_N R_N^{\dagger} \Lambda_N^{1/2} Y \\ &= \frac{1}{M'} Y^{\dagger} \Lambda_N Y \\ &= \frac{1}{M'} \sum_{i=1}^{M'} \lambda_{I,N} |Y_I|^2 . \end{aligned} \tag{B.11}$$

Then $\hat{P}$ is the weighted sum of Chi-square variates, the $|Y_I|^2$'s, each having two degrees

of freedom, X_2^2, and unity mean but where the weights have possibly different values.[19]

The characteristic function, $\Phi(\xi)$, of $\hat{P}$ is:

$$\Phi(\xi) = \int_0^\infty f(x)\, e^{j\xi x}\, dx, \tag{B.12}$$

where f(x) is the probability density function, or pdf, of $\hat{P}$. Since according to (B.11), $\hat{P}$ is a sum of independent variables, $\Phi(\xi)$ becomes the product of the characteristic functions for each variable, i.e.:

$$\Phi(\xi) = \prod_{i=1}^{M'} \int_0^\infty f_i(x)\, e^{j\xi x}\, dx, \tag{B.13}$$

where $f_i(x)$ is the pdf for $\lambda_{i,N}|Y_i|^2/M'$, i.e.:

$$f_i(x) = \frac{M'}{\lambda_{i,N}}\, e^{-xM'/\lambda_{i,N}}, \quad x \geq 0. \tag{B.14}$$

Hence, $\Phi(\xi)$ becomes:

$$\Phi(\xi) = \prod_{i=1}^{M'} \int_0^\infty \frac{M'}{\lambda_{i,N}}\, e^{-xM'/\lambda_{i,N}}\, e^{j\xi x}\, dx, \tag{B.15a}$$

$$= \prod_{i=1}^{M'} \left[1 - \frac{j\xi\lambda_{i,N}}{M'}\right]^{-1}. \tag{B.15b}$$

[19] At $f_k=0$ or $f_k=\pm f_s/2$, the imaginary component of Y_i disappears. Hence, the $|Y_i|^2$'s are X_1^2 distributed with unity mean for these special bins.

B.2 Gaussian Signal in Gaussian Noise

The FFT power estimate, $\hat{P}(f_k)$, due to the narrowband Gaussian signal in Gaussian noise is:

$$\hat{P}(f_k) = \frac{1}{M'} \sum_{i=1}^{M'} |X_{I,SG}(f_k) + X_{I,NG}(f_k)|^2 = \frac{1}{M'} X_{SNG} X_{SNG}^{\dagger}, \tag{B.16}$$

where:

$$X_{SNG} = \begin{bmatrix} X_{1,SG}+X_{1,NG} \\ X_{2,SG}+X_{2,NG} \\ \cdot \\ \cdot \\ X_{M',SG}+X_{M',NG} \end{bmatrix}, \tag{B.17}$$

In a manner identical to that used for the noise-only case, we can express (B.16) as:

$$\hat{P}(f_k) = \frac{1}{M'} \sum_{i=1}^{M'} \lambda_{I,SN} |Y_I|^2, \tag{B.18}$$

where $\lambda_{I,SN}$ is the ith eigenvalue of the correlation matrix, K_{SN}, for the signal plus noise samples:

$$K_{SN} = E(X_{SNG} X_{SNG}^{\dagger}). \tag{B.19}$$

The matrix, K_{SN}, is evaluated in Appendix C.

As in Appendix B.1, the characteristic function, $\Phi(\xi)$, for Gaussian signal in Gaussian noise becomes:

$$\Phi(\xi) = \prod_{i=1}^{M'} \left[1 - \frac{j\xi\lambda_{I,SN}}{M'} \right]^{-1}. \tag{B.20}$$

B.3 Sinusoidal Signal in Gaussian Noise

The FFT power estimate, $\hat{P}(f_k)$, due to the sinusoidal signal in Gaussian noise is:

$$\hat{P}(f_k) = \frac{1}{M'} \sum_{i=1}^{M'} |X_{i,SS}(f_k) + X_{i,NG}(f_k)|^2 \tag{B.21a}$$

$$= \frac{1}{M'} \sum_{i=1}^{M'} |X_{i,SS}(f_k)|^2 + \frac{1}{M'} \sum_{i=1}^{M'} |X_{i,NG}(f_k)|^2 \tag{B.21b}$$

$$+ 2Re\left[\frac{1}{M'} \sum_{i=1}^{M'} X^*_{i,SS}(f_k) X_{i,NG}(f_k) \right] .$$

The summations in (B.21b) may be written as follows:

(1)
$$\frac{1}{M'} \sum_{i=1}^{M'} |X_{i,SS}(f_k)|^2 = C \frac{A^2}{4} . \tag{B.22}$$

A is the amplitude of the sinusoid, f_c is its frequency, and C is the value of the spectral window at $(f_k - f_c)$, i.e.:

$$C = |W(f_k - f_c)|^2, \tag{B.23}$$

and we have ignored the *edge-effect* term discussed with regard to (13) of the main text.

(2)
$$\frac{1}{M'} \sum_{i=1}^{M'} |X_{i,NG}|^2 = \frac{1}{M'} \sum_{i=1}^{M'} \lambda_{i,N} |Y_i|^2, \tag{B.24}$$

as in Appendix B.1.

(3)
$$\begin{aligned} \frac{1}{M'} \sum_{i=1}^{M'} (X^*_{i,SS} X_{i,NG}) &= \frac{1}{M'} \mathbf{X}^{\dagger}_{SS} \mathbf{X}_{NG} \\ &= \frac{1}{M'} \mathbf{X}^{\dagger}_{SS} R_N \Lambda_N^{1/2} \mathbf{Y} \quad \text{(see B9)} \\ &= \frac{1}{M'} \boldsymbol{\alpha}^{\dagger} \mathbf{Y} \\ &= \frac{1}{M'} \sum_{i=1}^{M'} \alpha^*_i Y_i , \end{aligned} \tag{B.25}$$

where we have defined a new vector, $\boldsymbol{\alpha}$, as:

$$\alpha = \Lambda_N^{1/2} R_N^{\dagger} X_{SS} . \tag{B.26}$$

Using the above summations, (B.21b) can be written as:

$$\hat{P} = \frac{CA^2}{4} + \frac{1}{M'} \sum_{i=1}^{M'} \lambda_{i,N} |Y_i|^2 + 2Re[\frac{1}{M'} \sum_{i=1}^{M'} \alpha_i^* Y_i] . \tag{B.27}$$

Since $\hat{P}$ is now expressed in terms of summations of independent variates, we can use the same technique as in (B.13) to obtain its characteristic function, $\Phi(\xi)$, as:

$$\begin{aligned} \Phi(\xi|H_1) &= \int_0^{\infty} f_y(y)\, e^{j\xi\hat{P}(y)}\, dy \\ &= e^{j\xi CA^2/4} \prod_{i=1}^{M'} [\int_0^{\infty} f_y(y)\, e^{j\xi(\lambda_{i,N}y^2+2\alpha_{i,R}y)/M'} dy] \\ &\quad \cdot [\int_0^{\infty} f_y(y)\, e^{j\xi(\lambda_{i,N}y^2+2\alpha_{i,I}y)/M'} dy] , \end{aligned} \tag{B.28}$$

where: $\alpha_i = \alpha_{i,R} + j\alpha_{i,I}$,

and f(y) is the pdf of the independent Gaussian variates comprising the real and imaginary parts of Y (each variate is zero-mean Gaussian with variance of 1/2):

$$f_y(y) = \pi^{-1/2}\, e^{-y^2} . \tag{B.29}$$

On substitution of (B.29) in (B.28), we have after some manipulation:

$$\Phi(\xi|H_1) = e^{j\xi CA^2/4} \prod_{i=1}^{M'} (1-\frac{j\xi\lambda_{i,N}}{M'})^{-1} \exp[-\frac{|\alpha_i|^2\xi^2/M'^2}{1-j\xi\lambda_{i,N}/M'}] . \tag{B.30}$$

To obtain $|\alpha_i|^2$ in (B.30), we observe that:

$$\alpha\alpha^{\dagger} = \Lambda_N^{1/2} R_N^{\dagger} X_{SS} X_{SS}^{\dagger} R_N \Lambda_N^{1/2} , \tag{B.31}$$

and $$|\alpha_l|^2 = (\boldsymbol{\alpha}\boldsymbol{\alpha}^{\dagger})_{ll} = \lambda_{l,N} \sum_{p=1}^{M'} \sum_{q=1}^{M'} X^*_{p,SS} X_{q,SS}\, R_{pl} R_{ql}$$

$$= \lambda_{l,N} \frac{CA^2}{4} \sum_{p=1}^{M'} \sum_{q=1}^{M'} e^{-j2\pi(p-q)(1-\gamma)Nf_c/f_s}\, R_{pl} R_{ql}\,, \tag{B.32}$$

$$= \lambda_{l,N} \frac{CA^2}{4} \sum_{p=1}^{M'} \sum_{q=1}^{M'} e^{j2\pi(p-q)(1-\gamma)N(f_k-f_c)/f_s}\, |R_{pl}||R_{ql}|\,,$$

$$= \lambda_{l,N} \frac{CA^2}{4} K_l\,.$$

where the parameter, K_l, simplifies to:

$$K_l = 1\,.$$

when there is no segment overlap, and to:

$$K_l = \sum_{p=1}^{M'} \sum_{q=1}^{M'} |R_{pl}||R_{ql}|\,.$$

when there *is* overlap but the signal is centered on the bin.

By inserting (B.32) for $|\alpha_l|^2$ in (B.30), we can reduce the expression to:

$$\Phi(\xi|H_1) = \prod_{i=1}^{M'} \left(1 - \frac{j\xi\lambda_{l,N}}{M'}\right)^{-1} \exp\left[\frac{j\xi CA^2/4M' + \xi^2 CA^2\lambda_{l,N}(1-K_l)/4M'^2}{1 - j\xi\lambda_{l,N}/M'}\right]. \tag{B.33}$$

It is useful to have the signal-to-noise ratio, ***SNR***, appear explicitly in the above, since ultimately it is the ***SNR*** which we must obtain. Hence, we can normalize the signal power, $A^2/4$, by the noise power in the FFT bin, then proceed by assuming the noise power per bin is unity. This normalization does not alter the analysis in any way, beyond its advantage in having the ***SNR*** appear. The noise power in the bin is obtained from (C.13) as:

$$P_N = \sigma_N^2 f_s R_W(0)\,,$$

where the terms in the above are defined in Appendix C. Noting now that ***SNR*** is:

$$\boldsymbol{SNR} = \frac{A^2}{4\sigma_N^2 B}\,,$$

and that the binwidth, B, is related to the sampling frequency, f_s, by $f_s = B \cdot N$, where N is the transform size, we obtain for (B.33):

$$\Phi(\xi|H_1) = \prod_{i=1}^{M'} \left(1 - \frac{j\xi\lambda_{i,N}}{M'}\right)^{-1} \exp\left[\frac{j\xi SNR \cdot C_1/M' + \xi^2 SNR \cdot C_1\lambda_{i,N}(1-K_i)/M'^2}{1 - j\xi\lambda_{i,N}/M'}\right]. \quad \text{(B.34)}$$

where the new constant, C_1, is:

$$C_1 = C/NR_W(0).$$

Appendix C

Correlation Between FFT Samples

To solve for the detection performance of the FFT processor, we require the correlation, K_{pq}, between the FFT outputs at f_k from the pth and qth FFT's, where (see Figure 1):

$$X_p(f_k) = \sum_{n=0}^{N-1} w(n)\, x_p(n)\, e^{-j2\pi n f_k/f_s}, \tag{C.1}$$

and:

$$K_{pq} = E(X_p(f_k)X_q^*(f_k)) . \tag{C.2}$$

N is the number of discrete time samples per FFT segment and f_s is the sampling frequency. The $x_p(n)$ is the *real* input time sequence for the pth segment, i.e.:

$$x_p(n) = x[n+(p-1)(1-\gamma)N] \qquad n=0,.....,N-1 . \tag{C.3}$$

γ is the fractional segment overlap. The w(n) is the data window, n=0,....., N-1. We consider only real data windows here.

Then we have:

$$X_p(f_k)X_q^*(f_k) = \sum_{n=0}^{N-1}\sum_{m=0}^{N-1} w(n)w(m)\, x_p(n)x_q(m)\, e^{-j2\pi(n-m)f_k/f_s} . \tag{C.4}$$

On taking expectations, we obtain:

$$\begin{aligned} E[X_p(f_k)X_q^*(f_k)] &= K_{pq} \\ &= \sum_{n=0}^{N-1}\sum_{m=0}^{N-1} w(n)w(m)\, R(n-m+\aleph)\, e^{-j2\pi(n-m)f_k/f_s}, \end{aligned} \tag{C.5}$$

where: $\aleph = (p-q)(1-\gamma)N$,

and R(n) is the autocorrelation between samples of the input sequence separated by n time units:

$$R(n) = E[x(i+n)x(i)] . \tag{C.6}$$

Equation (C.5) can be shown to reduce to:

$$K_{pq} = \sum_{n=-N+1}^{N-1} R_W(n)\, R(n+\aleph)\, e^{-j2\pi n f_k/f_s} . \tag{C.7}$$

$R_W(n)$ is the autocorrelation function of the data window:

$$R_W(n) = \sum_{i=0}^{N-|n|-1} w(i+|n|)w(i) , \qquad 0 \le |n| \le N-1 ,$$
$$= 0 \qquad \text{elsewhere} . \tag{C.8}$$

Equation (C.7) is recognized as the Fourier transform of the discrete sequence $R_W(n)R(n+\tilde{n})$, which, on performing the transform, yields:

$$K_{pq} = \int_{-f_s/2}^{f_s/2} |W(f_k-f)|^2 \, S(f) \, e^{j2\pi\tilde{n}f/f_s} \, df , \tag{C.9}$$

where $|W(f)|^2$ is the spectral window, and S(f) is the power spectrum of the input sequence at f. The convolution of the spectral window and spectrum in (C.9) is equivalent to the multiplication of the window autocorrelation function and that for the signal in the lag domain. The phase term in (C.9) performs the same function as the time shift operator, $\tilde{n}$, in (C.7). Since both $|W(f)|^2$ and S(f) relate to discrete sequences, they are cyclic in frequency, with period, f_s.

Special Cases

(1) p = q:

$$K_{pp} = E|X_p(f_k)|^2$$
$$= E(\hat{P}(f_k)) \tag{C.10}$$
$$= \int_{-f_s/2}^{f_s/2} |W(f_k-f)|^2 \, S(f) \, df .$$

Hence, the mean of the power estimate is the convolution of the true spectrum and the spectral window.

(2) white Gaussian noise:

For white Gaussian noise of power, σ_N^2, per unit bandwidth, the noise autocorrelation becomes:

$$R(n) = \sigma_N^2 f_s \delta(n) , \tag{C.11}$$

where $\delta(n)$ is the delta function. In this case, the correlation, $K_{pq,N}$, due to the noise is:

$$K_{pq,N} = \sigma_N^2 f_s R_W(\tilde{n})\, e^{j2\pi \tilde{n} f_k/f_s} \qquad |\tilde{n}| \le N-1 , \qquad (C.12)$$

$$= 0 \qquad \text{elsewhere} .$$

where we have used the property that $R_W(n) = R_W(-n)$. Hence, the noise power, P_N, in the FFT bin is:

$$P_N = K_{pp,N} = \sigma_N^2 f_s R_W(0) . \qquad (C.13)$$

This may be rewritten as:

$$P_N = \frac{\sigma_N^2 f_s}{N} \left[N \sum_{n=0}^{N-1} w^2(n) \right]$$

$$= \sigma_N^2 B \left[N \sum_{n=0}^{N-1} w^2(n) \right] , \qquad (C.14)$$

to observe directly the dependence on the FFT binwidth, $B = 1/T$.

For no segment overlap, the correlation reduces to:

$$K_{pq,N} = \sigma_N^2 f_s R_W(0) \delta(p-q) . \qquad (C.15)$$

It is convenient to normalize the correlation, such that $K_{pp,N}=1$, implying that the noise power in the bin has been normalized to unity. We shall see shortly that this normalization has the advantage that the correlation between samples of signal and noise explicity contains the signal-to-noise ratio. Beyond this convenience, the normalization in no way alters the analysis. Hence, (C.12) becomes:

$$K_{pq,N} = \frac{R_W(\tilde{n})}{R_W(0)}\, e^{j2\pi \tilde{n} f_k/f_s} \qquad |\tilde{n}| \le N-1 , \qquad (C.16)$$

$$= 0 \qquad \text{elsewhere} .$$

(3) narrowband Gaussian signal in white Gaussian noise:

In this case the autocorrelation of the input sequence is:

$$R(n) = R_S(n) + \sigma_N^2 f_S \delta(n) , \qquad (C.17)$$

and:

$$K_{pq,SN} = \sum_{n=-N+1}^{N-1} R_W(n) R_S(n+\tilde{n})\, e^{-j2\pi n f_k/f_s} + \sigma_N^2 f_S R_W(\tilde{n})\, e^{j2\pi \tilde{n} f_k/f_s} \qquad (C.18)$$

The autocorrelation of the narrowband signal has the complex representation:

$$R_S(n) = \frac{1}{2}\, Re[\bar{R}_S(n)\, e^{j2\pi n f_c/f_s}] \qquad \text{(C.19a)}$$

$$= \frac{1}{4}\, \bar{R}_S(n)\, e^{j2\pi n f_c/f_s} + \frac{1}{4}\, \bar{R}_S^*(n)\, e^{-j2\pi n f_c/f_s}, \qquad \text{(C.19b)}$$

where f_c is the center frequency of the signal spectrum and $\bar{R}_S(n)$ is the autocorrelation of the complex signal envelope. Since the signal spectra we shall consider are symmetric about f_c, $\bar{R}_S(n)$ will be purely real.

Inserting (C.19b) in (C.18) we obtain:

$$K_{pq,SN} = \frac{1}{4} \sum_{n=-N+1}^{N-1} R_W(n)\bar{R}_S(n+\tilde{n})\, e^{-j2\pi n(f_k-f_c)/f_s} + \sigma_N^2 f_S R_W(\tilde{n})\, e^{j2\pi \tilde{n} f_k/f_s}, \qquad \text{(C.20)}$$

where we have omitted the *edge-effect* term that results in (C.20) due to the the second term in (C.19b). It will be negligible provided f_k is not near 0 or $\pm f_s/2$.

If the bandwidth of the signal spectrum is narrow compared to the bandwidth of the spectral window, and if the signal is centered on the FFT bin, the first term on the RHS of (C.20) defines the signal power, P_S, in the bin (when p=q):

$$P_S \approx \frac{\bar{R}_S(0)}{4} \sum_{n=-N+1}^{N-1} R_W(n) = \frac{\sigma_S^2}{2} \left[\sum_{n=0}^{N-1} w(n)\right]^2 . \qquad \text{(C.21)}$$

The term, $[\Sigma w(n)]^2$, is the coherent power gain, P_c, of the data window. The ratio of signal power, (C.21), to noise power, (C.14), at the FFT output is:

$$P_S/P_N = \boldsymbol{SNR}\, \left[\, \frac{(\Sigma w(n))^2}{N\, \Sigma w^2(n)}\, \right] . \qquad \text{(C.22)}$$

where ***SNR*** is the ratio of narrowband signal power to the noise power in the FFT bin. The term in [•] is the processing gain, PG, of the data window. Its reciprocal is referred to as the equivalent noise bandwidth, B_{EN}, of the window; it defines the bandwidth of an ideal (rectangular) filter, in units of FFT binwidth, which would have the same noise power as obtained from the spectral window. Without a loss in generality, we can normalize the correlation, (C.20), so that the noise power in the FFT bin is unity, and:

$$K_{pq,SN} = \frac{SNR}{N} \sum_{n=-N+1}^{N-1} \frac{R_W(n)}{R_W(0)} \frac{\bar{R}_S(n+\tilde{n})}{2\sigma_S^2} e^{-j2\pi n(f_k-f_c)/f_s}$$

$$+ \frac{R_W(\tilde{n})}{R_W(0)} e^{j2\pi \tilde{n} f_k/f_s} . \qquad (C.23)$$

(4) Sinusoidal signal in white Gaussian noise:

The correlation between FFT samples of a sinusoid in white Gaussian noise is not needed for our analysis (see Appendix B.3). However, the result is given here for the sake of completeness. The correlation can be obtained easily from (C.20) by realizing that the autocorrelation of the signal envelope for the sinusoid is simply:

$$\bar{R}_S(n) = A^2 , \qquad (C.24)$$

where A is the sinusoid amplitude. On substituting (C.24) in (C.20) we find:

$$K_{pq,SN} = \frac{A^2}{4} \sum_{n=-N+1}^{N-1} R_W(n) e^{-j2\pi n(f_k-f_c)/f_s}$$

$$+ \sigma_N^2 f_S R_W(\tilde{n}) e^{j2\pi \tilde{n} f_k/f_s} , \qquad (C.25a)$$

$$= \frac{A^2}{4} |W(f_k-f_c)|^2 + \sigma_N^2 f_S R_W(\tilde{n}) e^{j2\pi \tilde{n} f_k/f_s} . \qquad (C.25b)$$

The correlation can be normalized as was (C.23), in which case:

$$K_{pq,SN} = \frac{SNR}{N} \frac{|W(f_k-f_c)|^2}{R_W(0)} + \frac{R_W(\tilde{n})}{R_W(0)} e^{j2\pi \tilde{n} f_k/f_s} .$$

where now: $SNR = \frac{A^2}{4\sigma_N^2 B}$.

(5) Properties of the data windows used in this report:

(5a) rectangular window

$w(n) = 1$ $\qquad n=0,\ldots\ldots\ldots,N-1$,

$R_W(n) = N-|n|$ $\qquad -N+1 \le n \le N-1$,

$$|W(f)|^2 = N^2 \frac{\sin^2(N\pi f/f_s)}{\sin^2(\pi f/f_s)} ,$$

$P_C = N^2$,

$PG = 1$,

$B_{EN} = 1$.

(5b) Hanning window

$$w(n) = 0.5\,[1 - \cos(2\pi n/N)] \qquad n=0,.....,N-1\ ,$$

$$R_W(n) = \frac{1}{4}\,[\,(n+N)(1+0.5\cos(\frac{2\pi n}{N})) - \frac{3}{4}N\sin(\frac{2\pi n}{N})/\pi\,]$$

$$-N+1 \le n \le N-1\ ,$$

$$|W(f)|^2 = \frac{N^2}{4}\ [.5D(f) + .25(D(f-f_s/N) + D(f+f_s/N))]^2,$$

where: $D(f) = \dfrac{\sin(N\pi f/f_s)}{\sin(\pi f/f_s)}$

$$P_C = \frac{N^2}{4}\ ,$$

$$PG = 2/3,$$

$$B_{EN} = 1.5\ .$$

Appendix D

Gaussian Approximations

D.1 Large time-bandwidth product

We will obtain asymptotic expressions for the basic detection threshold, G_M, at large time-bandwidth products (see Sec.3.1). Three signal types will be considered: sinusoidal, Swerling I and Swerling II.

For time-bandwidth product, M, large, and for no segment overlap, the probability density function, or pdf, of the noise power estimate, approaches a Gaussian, with mean, P_N , and variance, $\sigma_N^2=P_N^2/M$ (Chi-Square with 2M degrees of freedom)[8]. Similarly, the pdf of the power estimates for either the sinusoidal signal or Swerling II signal in noise approaches the Gaussian, with mean, P_{S+N}, and variance, $\sigma_{S+N}^2=P_{S+N}^2/M$[8]. Then the false alarm probability, P_{FA}, and detection probability, P_d, become:

$$P_{FA} = \text{erfc}\left(\frac{P_T-P_N}{\sigma_N}\right) = \text{erfc}\left(\sqrt{M}\left(\frac{P_T}{P_N}-1\right)\right), \tag{D.1a}$$

$$P_D = \text{erfc}\left(\frac{P_T-P_{S+N}}{\sigma_{S+N}}\right) = \text{erfc}\left(\sqrt{M}\left(\frac{P_T}{P_{S+N}}-1\right)\right), \tag{D.1b}$$

where erfc(y) is the complementary error function:

$$\text{erfc}(y) = (2\pi)^{-1/2}\int_y^\infty e^{-x^2/2}\,dx, \tag{D.2}$$

and P_T is the power threshold.

We want to know what value of $SNR=P_S/P_N$ is necessary when P_D and P_{FA} are specified values. Solving both (D.1a) and (D.1b) for P_T, and equating the results, we have:

$$P_N + \frac{P_N}{\sqrt{M}}\,\text{erfc}^{-1}(P_{FA}) = P_{S+N} + \frac{P_{S+N}}{\sqrt{M}}\,\text{erfc}^{-1}(P_D), \tag{D.3}$$

where $\text{erfc}^{-1}(x)$ is that value of y such that erfc(y) = x. Since $P_{S+N}=P_S+P_N$, (D.3) becomes:

$$\frac{P_N}{\sqrt{M}}\left[\text{erfc}^{-1}(P_{FA}) - \text{erfc}^{-1}(P_D)\right] = \frac{P_S}{\sqrt{M}}\left[\sqrt{M} + \text{erfc}^{-1}(P_D)\right] \tag{D.4a}$$

or:

$$\frac{P_S}{P_N} = SNR = \frac{\text{erfc}^{-1}(P_{FA}) - \text{erfc}^{-1}(P_D)}{\sqrt{M} + \text{erfc}^{-1}(P_D)}. \tag{D.4b}$$

Since $\sqrt{M} >> |\text{erfc}^{-1}(P_D)|$ for large M, we have:

$$SNR = \frac{\text{erfc}^{-1}(P_{FA}) - \text{erfc}^{-1}(P_D)}{\sqrt{M}} . \tag{D.5}$$

It is usual to define a detection index, d, as[5]:

$$d = \frac{(P_{S+N}-P_N)^2}{\sigma_N^2} = \frac{P_S^2}{P_N^2/M} = M \cdot SNR^2 . \tag{D.6}$$

Comparing (D.5) and (D.6) we see that:

$$SNR = (d/M)^{1/2} , \tag{D.7a}$$

or:

$$DT = 10 \log SNR \cdot B = 5 \log B^2 d/M , \tag{D.7b}$$

where:

$$d = [\text{erfc}^{-1}(P_{FA}) - \text{erfc}^{-1}(P_D)]^2 . \tag{D.7c}$$

In Figures 5-7, we require d for $P_D = 0.5$ and for $P_{FA} = 10^{-2}$, 10^{-4}, and 10^{-6}. Since $\text{erfc}^{-1}(0.5) = 0$, we have for d:

$$\begin{aligned} d &= [\text{erfc}^{-1}(P_{FA})]^2 \\ &= 5.4 \qquad (P_{FA}=10^{-2}) , \\ &= 13.8 \qquad (P_{FA}=10^{-4}) , \\ &= 22.6 \qquad (P_{FA}=10^{-6}) . \end{aligned} \tag{D.8}$$

For Swerling I signals at large M, the pdf for signal plus noise approaches a constant plus an exponential, i.e.:

$$f_{S+N}(x) = P_N + \frac{1}{P_S} e^{-x/P_S} U(P_S) , \tag{D.9}$$

since the pdf for noise-only approaches a delta function relative to that for signal-only. In this case, P_D becomes:

$$P_D = \int_{P_T-P_N}^{\infty} \frac{1}{P_S} e^{-x/P_S} dx = e^{-(P_T-P_N)/P_S} . \tag{D.10}$$

Solving both (D.1a) and (D.10) for P_T, and equating the results, we obtain:

$$P_N + \frac{P_N}{\sqrt{M}}\ \mathrm{erfc}^{-1}(P_{FA}) = P_N + P_S\, ln\,(\frac{1}{P_D}) \qquad (D.11a)$$

or:

$$SNR = \frac{P_S}{P_N} = \frac{\mathrm{erfc}^{-1}(P_{FA})}{\sqrt{M}\, ln(1/P_D)}\ . \qquad (D.11b)$$

If we compare the above result with that in (D.5), we find that at P_D=0.5, the detection threshold for the Swerling I signal will be greater than that for the sinusoidal or Swerling II signals by:

$$-10\ log[ln(1/P_D)] = -10 \log 0.693 = 1.6\ \mathrm{dB}\ . \qquad (D.12)$$

D.2 Segment Overlap

In general, the gain in signal detectability due to the use of FFT segment overlap depends on many parameters. These include the signal type, its bandwidth and spectrum, the data window, time-bandwidth product and the detection and false-alarm probabilities. At large time-bandwidth products, the probability density function, $f(x|H_0)$, of the noise power estimate approaches a Gaussian distribution(see Appendix D.1). Hence, a commonly used approximation to the effects of overlap considers only the reduction in the variance of $f(x|H_0)$ when overlap is introduced[11].

The variance of the noise power estimate can be calculated as follows:

$$\mathrm{Var}[\hat{P}(f_k)] = E[\hat{P}^2(f_k)] - E^2[\hat{P}(f_K)] \qquad (D.13a)$$

$$= E\,[\frac{1}{M'^2}\sum_{p=1}^{M'}\sum_{q=1}^{M'} |X_{p,NG}(f_k)|^2\, |X_{q,NG}(f_k)|^2\,] \qquad (D.13b)$$

$$- E^2\,[\frac{1}{M'}\sum_{p=1}^{M'} |X_{p,NG}(f_k)|^2]\ .$$

For simplicity, we drop the subscripts NG (noise, Gaussian) and the frequency variable. Then we have:

$$\mathrm{Var}(\hat{P}) = \frac{1}{M'^2}\sum_{p=1}^{M'}\sum_{q=1}^{M'} E(X_p X_p^* X_q X_q^*) - \frac{1}{M'^2}\,[\sum_{p=1}^{M'} E(X_p X_p^*)]^2 \qquad (D.14a)$$

$$= \frac{1}{M'^2}\sum_{p=1}^{M'}\sum_{q=1}^{M'} E(X_p X_q^*)\, E(X_p^* X_q) \qquad (D.14b)$$

$$= \frac{1}{M'^2}\sum_{p=1}^{M'}\sum_{q=1}^{M'} |K_{pq}|^2\ , \qquad (D.14c)$$

where $K_{pq}=E(X_pX_q^*)$, and is the correlation between the pth and qth noise samples. From (25) in the main text, we can express the correlation as:

$$K_{pq} = \sigma_N^2 f_s R_W[(p-q)(1-\gamma)N]\, e^{j2\pi(p-q)(1-\gamma)Nf_k/f_s}, \qquad (D.15)$$

where σ_N^2 is the noise power per unit bandwidth, f_s is the sampling frequency, γ is the fractional overlap, N is the number of samples in the segment, and R_W is the autocorrelation function of the data window:

$$R_W(n) = \sum_{i=0}^{N-|n|-1} w(i+|n|)w(i) \qquad 0 \le |n| \le N-1$$

$$= 0 \qquad |n| > N-1 , \qquad (D.16)$$

and w(n) is the actual data window. Since R_W depends only on the difference in the indices, p and q, we can write (D.14) as:

$$\mathrm{Var}[\hat{P}] = \frac{(\sigma_N^2 f_s)^2}{M'^2} \sum_{n=-M'+1}^{M'-1} (M'-|n|)\, R_W^2\,[n(1-\gamma)N] . \qquad (D.17)$$

When no segment overlap is used, (D.17) reduces to:

$$\mathrm{Var}[\hat{P}] = \frac{(\sigma_N^2 f_s)^2}{M^2}\,[M\, R_W^2(o)] = \frac{[\sigma_N^2 f_s R_W(0)]^2}{M} \qquad (D.18)$$

where M' and M are related by:

$$M' = \frac{M-\gamma}{1-\gamma} . \qquad (D.19)$$

We can define an effective number of independent averages when overlap is used as M_{eff}, where:

$$M_{eff} = M \cdot \frac{\mathrm{Var}(\hat{P})|_{\text{no overlap}}}{\mathrm{Var}(\hat{P})|_{\text{overlap}}} \qquad (D.20a)$$

$$= M'^2 \left[\sum_{n=-M'+1}^{M'-1} (M'-|n|)\, \frac{R_W^2[n(1-\gamma)N]}{R_W^2(0)} \right]^{-1} \qquad (D.20b)$$

$$= M'^2 \left[M' + 2 \sum_{n=1}^{M'-1} (M'-n) \frac{R_W^2[n(1-\gamma)N]}{R_W^2(0)} \right]^{-1} \qquad (D.20c)$$

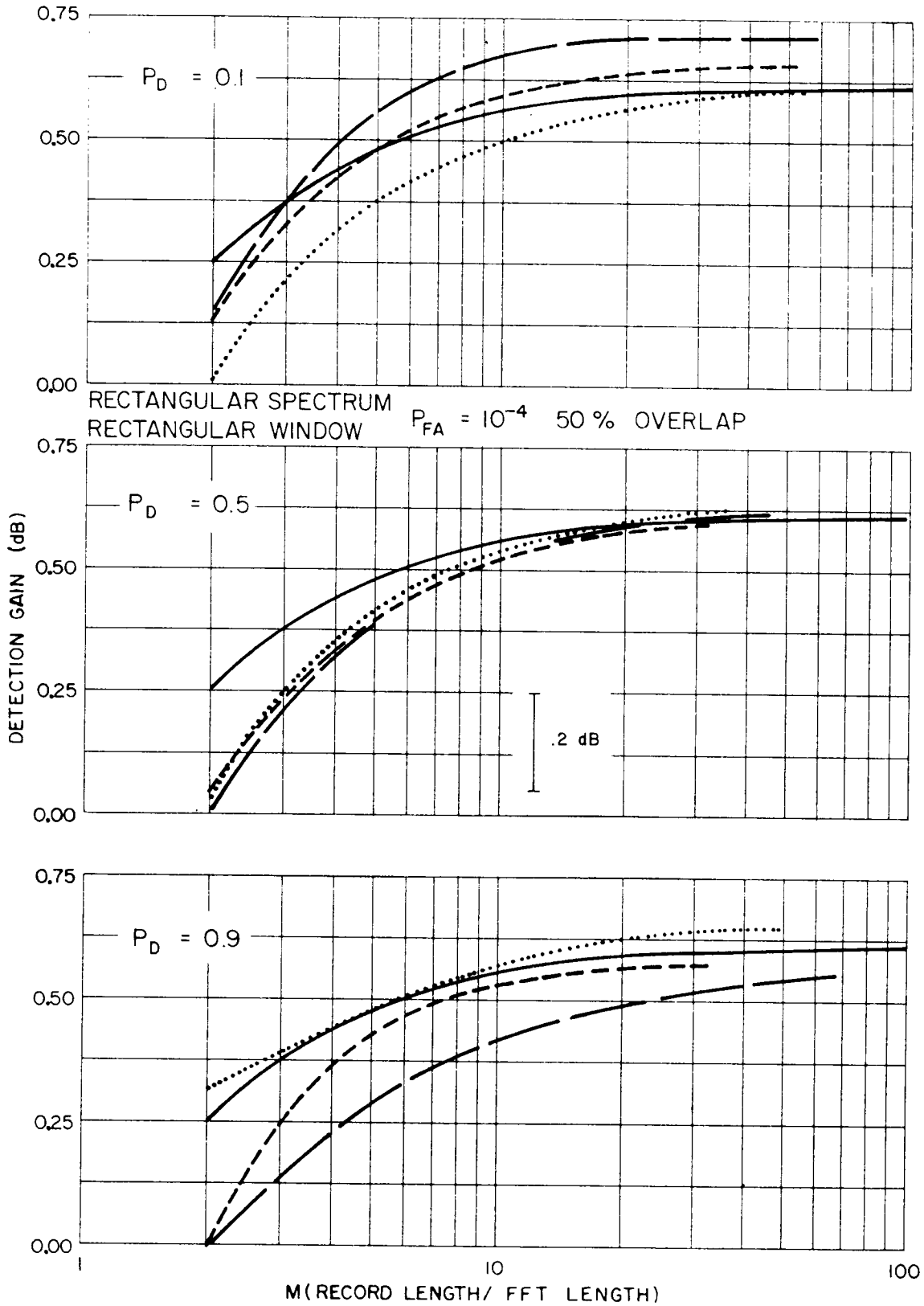

Figure D.1. Comparison of methods for calculating detection improvement due to FFT segment overlap. Rectangular window. Solid line - Equation (D.21), small dashed line - Swerling I signal, medium dashed line - Swerling II signal, heavy dashed line - sinusoidal signal.

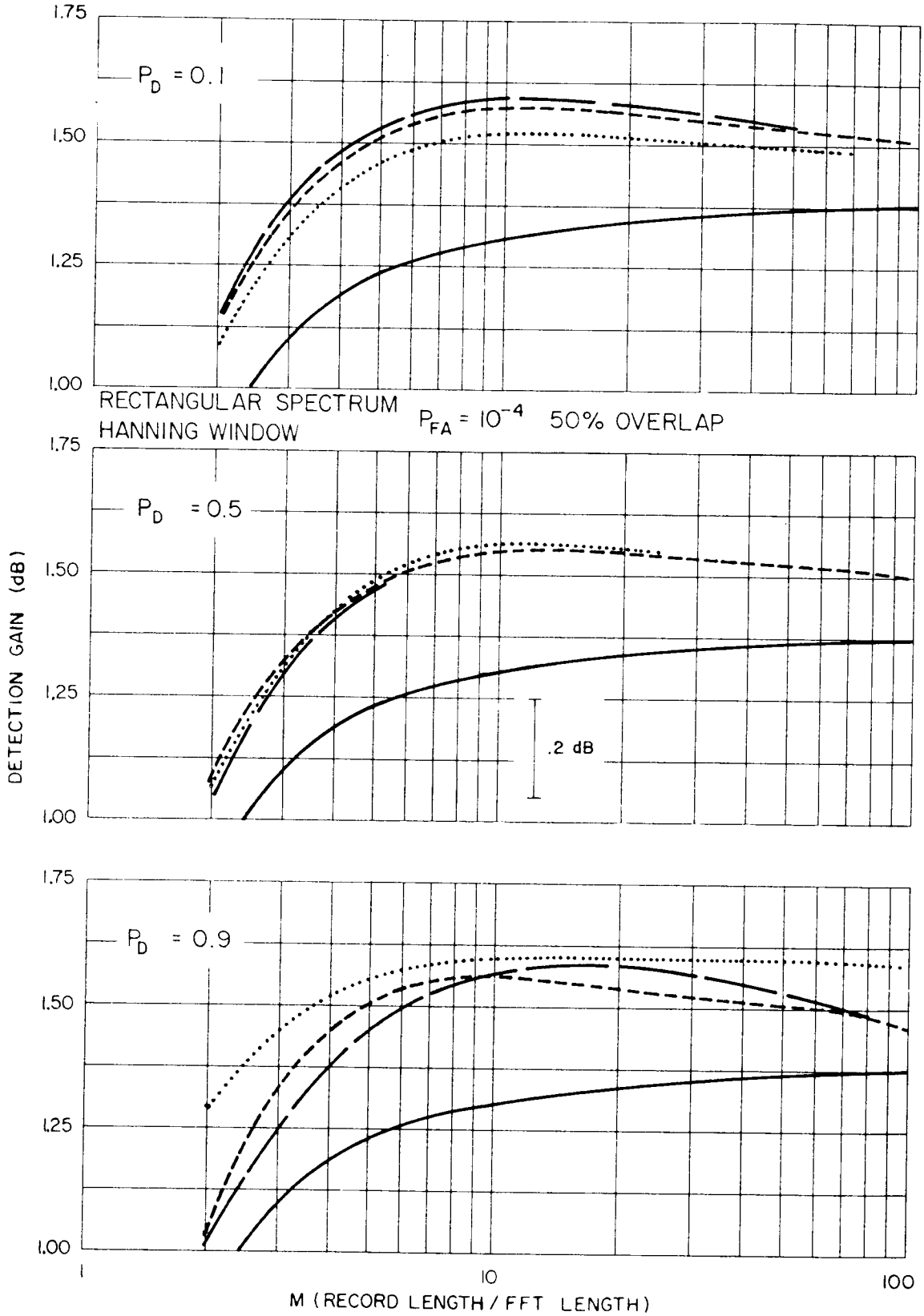

Figure D.2. Comparison of methods for calculating detection improvement due to FFT segment overlap. Hanning window. Solid line - Equation (D.21), small dashed line - Swerling I signal, medium dashed line - Swerling II signal, heavy dashed line - sinusoidal signal.

Since the term in [•] is always greater than M' whenever there is overlap, M_{eff} will always be less than M'. When no overlap is used, $M_{eff} \rightarrow M' = M$.

Given the effective number of averages associated with a selected data window and segment overlap, we can approximate the signal detection performance in one of two ways. First, we can proceed through the analysis discussed in Section 3 but using a time-bandwidth product of M_{eff}[11]. Secondly, we can assume that the increase in detection performance due to overlap obeys the relationship:

$$G_o = 5 \log[\frac{M_{eff}}{M}] . \qquad (D.21)$$

This follows from the Gaussian approximation to the detection threshold developed in Appendix D.1 (see (D.7)).

In Figures D.1 and D.2 we have compared the approximation given by (D.21) with an analysis of the effects of overlap using the more accurate characteristic function technique of Appendix A. We present results for a $P_{FA}=10^{-4}$, and at P_D's of 0.1, 0.5 and 0.9. The fractional segment overlap is 0.5 in all cases. Figure D.1 treats the rectangular data window and Figure D.2 the Hanning window. The solid line in each graph is (D.21) as a function of M, for $1<M<100$. The results are independent of P_D and P_{FA}. The various dashed lines refer to three cases treated using the characteristic function approach: the sinusoidal signal, the Gaussian signal having $B_ST=0$, and the Gaussian signal having $B_ST=1$ (and rectangular spectrum). We estimate the accuracy of these results to be of the order of ±0.05 dB. In all cases, the dashed lines and solid line converge as M increases. This is expected since as M increases, the Gaussian assumption becomes increasingly valid. For $M<100$, the maximum difference between any of the dashed lines and that due to (D.21) is about ±0.2 dB.

If we use the first of the methods to measure the effects due to overlap (that is, proceed through Section 3 using a time-bandwidth product of M_{eff}) we obtain good agreement with the dashed lines of Figures D.1 and D.2 for $M \geq 10$. We have not shown these results here. At small M, this method overestimates the gain in detectability by up to 0.2 dB.

Appendix E

Special Cases

In this appendix we consider the detection problem for some important special cases of signal and noise for which there is a ready analytic solution. The general problem is solution of the integral (see Appendix A):

$$f(x|H_1) = \frac{1}{2\pi} \int_{-\infty}^{\infty} \Phi(\xi|H_1)\, e^{-j\xi x}\, d\xi \,, \tag{E.1}$$

where $f(x|H_1)$ is the probability density function, or pdf, of the FFT power estimate, conditioned on hypothesis, H_1. The $\Phi(\xi|H_1)$ is the characteristic function of the random variable,under the same hypothesis. In Appendix A, we developed an approximate solution to (E.1) for arbitrary $\Phi(\xi|H_1)$. In the following, we will examine some special cases for which (E.1) can be solved analytically:

(1) Case 1: white Gaussian noise, no segment overlap

$\Phi(\xi|H_0)$, as given by (B.15b) reduces in this case to:

$$\Phi(\xi|H_0) = (1 - \frac{j\xi}{M})^{-M} \,, \tag{E.2}$$

where we have chosen to normalize the noise power in the FFT bin to unity, and M is the time-bandwidth product (or number of FFT segments in the power average).

On substituting (E.2) in (E.1), we have:

$$f(x|H_0) = \frac{1}{2\pi} \int_{-\infty}^{\infty} (1 - \frac{j\xi}{M})^{-M} e^{-j\xi x}\, d\xi \tag{E.3a}$$

$$= \frac{M^M}{(M-1)!} x^{M-1} e^{-Mx} \qquad x \geq 0$$

$$= 0 \qquad \text{elsewhere} \,, \tag{E.3b}$$

which is a scaled Chi-square distribution with 2M degrees of freedom, X^2_{2M}. The false alarm probability, P_{FA}, is given by:

$$P_{FA} = \int_{P_T}^{\infty} f(x|H_0)\, dx = e^{-MP_T} \sum_{n=0}^{M-1} \frac{(MP_T)^n}{n!} \,, \tag{E.4}$$

where P_T is the threshold power (normalized by the noise power).

(2) Case 2: Narrowband Gaussian signal in white Gaussian noise, no segment overlap, $B_sT = 1$, rectangular signal spectrum, signal centered on bin

This case closely approximates the Swerling II signal model.

$\Phi(\xi|H_1)$ as given by (B.20) becomes:

$$\Phi(\xi|H_1) \approx [1 - \frac{j\xi}{M}(1+\frac{SNR}{B_{EN}})]^{-M}, \qquad (E.5)$$

SNR is the signal-to-noise ratio (the noise power has been normalized to unity), and B_{EN} is the equivalent noise bandwidth of the spectral window. The result is approximate since it assumes that the signal spectrum is narrowband relative to the spectral window. This is a weak assumption for $B_ST=1$. Nevertheless, we have found the error introduced in the ***SNR*** by this assumption to be less than 0.1 dB in most cases examined. The solution to (E.1) is similar to that found in Case 1, i.e.:

$$P_D = \int_{P_T}^{\infty} f(x|H_1)\,dx \qquad (E.6a)$$

$$= e^{-MP_T/(1+SNR/B_{EN})} \sum_{n=0}^{M-1} \frac{(MP_T)^n}{n!(1+SNR/B_{EN})^n} . \qquad (E.6b)$$

(3) Case 3: Swerling I signal in white Gaussian noise, no segment overlap, signal centered on bin

In this case, $\Phi(\xi|H_1)$ as given by (B.20) becomes:

$$\Phi(\xi|H_1) = (1 - \frac{j\xi}{M})^{-(M-1)}[1 - \frac{j\xi}{M}(1+\frac{SNR}{B_{EN}})]^{-1}, \qquad (E.7)$$

The result is exact, since the signal spectrum is indeed narrowband relative to the spectral window. Using straightforward mathematics, we find P_D to be:

$$P_D = (1 + \frac{B_{EN}}{M \cdot SNR})^{M-1} e^{-MP_T/(1+M\cdot SNR/B_{EN})}$$

$$+ e^{-MP_T} \sum_{n=0}^{M-2} \frac{(MP_T)^n}{n!} [1 - (1+\frac{B_{EN}}{M\cdot SNR})^{M-n-1}], \qquad M>1 . \qquad (E.8)$$

(4) Case 4: Sinusoidal signal in white Gaussian noise, no segment overlap, signal centered on bin

$\Phi(\xi|H_1)$ as given by (B.34) becomes:

$$\Phi(\xi|H_1) = (1 - \frac{j\xi}{M})^{-M} e^{j\xi(1-j\xi/M)^{-1}SNR/B_{EN}} . \quad (E.9)$$

This function does not yield a convenient analytic solution for P_D. For the result see [14].

Appendix F

Data Normalization

Provided the mean noise level, P_N, in the frequency bin of interest is known, the false-alarm and detection probabilities are given by:

$$P_{FA} = \int_{(1+r)P_N}^{\infty} f(x|H_0)\, dx\,, \tag{F.1a}$$

$$P_D = \int_{(1+r)P_N}^{\infty} f(x|H_1)\, dx\,, \tag{F.1b}$$

where $f(x|H_1)$ is the probability density function of the power estimate, conditioned on hypothesis, H_1. The lower integration limit is the power threshold. We observe it is proportional to P_N (for a discussion, see Sec.2.1). Suppose instead that the mean noise power is not known, but is estimated in some manner. Then we must replace P_N in (F.1) by a random variable, say z, corresponding to this estimate. The average P_{FA} and P_D are obtained by averaging this result over the distribution of possible values for z, i.e.:

$$P_{FA} = \int_0^{\infty} \left[\int_{(1+r)z}^{\infty} f(x|H_0)\, dx \right] f_z(z)\, dz\,, \tag{F.2a}$$

$$P_D = \int_0^{\infty} \left[\int_{(1+r)z}^{\infty} f(x|H_1)\, dx \right] f_z(z)\, dz\,, \tag{F.2b}$$

where $f_z(z)$ is the probability density function of z.

Bird[26] has shown that the characteristic function method of solving (F.1), as described in Appendix A, can be extended to solve (F.2). From (A.10) we have the following approximate expression for the cumulative distribution of f(x):

$$F(y) = \int_0^{y} f(x)\, dx \approx \frac{y}{Y} + 2Re \sum_{n=1}^{J} \frac{\Phi(2\pi n/Y)}{j2\pi n} \left(1 - e^{-j2\pi ny/Y}\right), \tag{F.3}$$

where $\Phi(\xi)$ is the characteristic function corresponding to f(x), and Y is chosen so that $f(x) \approx 0$, $x > Y$. Hence we can write (F.2) as:

$$1 - \int_0^\infty F[(1+r)z]\, f_z(z)\, dz \tag{F.4a}$$

$$= 1 - \frac{(1+r)}{Y} \int_0^\infty z\, f_z(z)\, dz$$

$$- 2Re \sum_{n=1}^{J} \frac{\Phi(2\pi n/Y)}{j2\pi n} \left(1 - \int_0^\infty f_z(z)\, e^{-j2\pi n(1+r)z/Y}\, dz\right), \tag{F.4b}$$

where we have used the fact that:

$$\int_0^\infty f_z(z)\, dz = 1 . \tag{F.5}$$

(F.4b) can be simplified to:

$$1 - \frac{(1+r)\bar{P}_N}{Y} - 2Re \sum_{n=1}^{J} \frac{\Phi(2\pi n/Y)}{j2\pi n} \left(1 - \Phi_z[-\frac{2\pi n(1+r)}{Y}]\right), \tag{F.6}$$

where $\Phi_z(\xi)$ is the characteristic function of z, and we have assumed that the mean of $f_z(z)$ is $\bar{P}_N$.

The data normalizer we shall examine averages the power in a selected number, K, of frequency bins surrounding the bin of interest. The split window normalizer is a special case of this method. We will assume that the power estimates are independent across frequency, contain no contribution due to the signal, and have the same mean noise level. Hence, z becomes:

$$z = \frac{1}{KM'} \sum_{i=1}^{M'} \lambda_{i,N} \sum_{j=1}^{K} |Y_{i+j}|^2 , \tag{F.7}$$

where, as in Section 2.2, $\lambda_{i,N}$ is the ith eigenvalue of the noise correlation matrix, and Y_i is an independent, complex Gaussian variate of unity variance. Then z is proportional to a weighted sum over KM' Chi-Square variates, each having 2 degrees of freedom.

Equation (F.2) has an analytic solution for some important special cases. For example, if there is no segment overlap, then M'→M and the $\lambda_{i,N}$ become identical. Hence, z is a scaled Chi-Square variate with 2KM degrees of freedom. In this case, we have the following solutions to (F.2) under the indicated signal and noise conditions[24],[27]:

(a) *Gaussian noise only*:

$$P_{FA} = [1 + \frac{1+r}{K}]^{-KM} \sum_{n=0}^{M-1} \binom{KM+n-1}{n} [1 + \frac{K}{1+r}]^{-n} . \qquad (F.8)$$

(b) *Swerling II signal in Gaussian noise*:

$$P_D = [1 + \frac{1+r}{K(1+SNR/B_{EN})}]^{-KM} \sum_{n=0}^{M-1} \binom{KM+n-1}{n} [1 + \frac{K(1+SNR/B_{EN})}{1+r}]^{-n} . \qquad (F.9)$$

(c) *Swerling I signal in Gaussian noise, M>1*:

$$P_D = [1 + \frac{1}{M \cdot SNR/B_{EN}}]^{M-1} [1 + \frac{1+r}{K(1+M \cdot SNR/B_{EN})}]^{-KM}$$
$$+ [1 + \frac{1+r}{K}]^{-KM} \sum_{n=0}^{M-2} \binom{KM-n-1}{n} [1 - (1 + \frac{1}{M \cdot SNR/B_{EN}})^{M-n-1}] [1 + \frac{K}{1+r}]^{-n} \qquad (F.10)$$

(d) *Sinusoidal signal in Gaussian noise*:

$$P_D = 1 - [1 + \frac{K}{1+r}]^{-KM} e^{-SNR/B_{EN}/[1+(1+r)/K]}$$
$$\cdot \sum_{n=0}^{M-1} \binom{MK+n-1}{n} [1 + \frac{1+r}{K}]^{-n} {}_1F_1(-n; MK; \frac{-SNR/B_{EN}}{[1+K/(1+r)]}) , \qquad (F.11)$$

where ${}_1F_1$ is the confluent hypergeometric function.

In **[28]** an iterative numerical solution to the above four cases is presented, which is simpler to implement than the above analytic expressions.

Appendix G

Threshold Setting

In this Appendix, we discuss the problem of setting the power threshold in order to achieve a particular P_{FA}. We shall briefly examine those processor parameters which affect the setting.

We will express the power threshold, P_T, as:

$$P_T = (1+r)P_N \,, \tag{G.1}$$

where r is a constant power ratio and P_N is the mean noise power (or an estimate of P_N, should data normalization be used). Our aim is to obtain that value of r which will provide a specified P_{FA}.

In a manner similar to that used in Section 3 to determine the detection threshold, we can express r in terms of the following decibel summation:

$$10\log r = 10\log r_0 - G_o + L_n \,, \tag{G.2}$$

where:

$10\log r_0$ is the basic power ratio associated with M non-overlapped FFT segments;

G_o is the reduction in threshold due to the introduction of segment overlap;

L_n is the increase in threshold necessary when data normalization is used.

The basic power ratio, $10\log r_0$, is obtained by finding that value of r_0 in (E.4) which gives the selected P_{FA} (in (E.4), $P_T=(1+r_0)$). We have plotted $10\log r_0$ in Figure G.1 for $1 \le M \le 1000$, and for P_{FA}'s of 10^{-2}, 10^{-4} and 10^{-6}. At large M, these results become identical to the detection thresholds presented in Figures 5-7 for sinusoidal and narrowband Gaussian signals ($B_ST=1$) at $P_D=0.5$. This occurs since at large M, the density functions of signal and noise become Gaussian, and hence symmetric. Then the power ratio, r_0, equals the signal-to-noise ratio, ***SNR***, necessary for the same P_{FA} and for a $P_D=0.5$.

G_o and L_n in (G.2) can be obtained using the results presented in Sections 3.6 and 3.7.

We conclude with an example calculation. Table G.1 outlines a particular set of processor parameters. Table G.2 presents values for each of the terms in (G.2) and a brief description of how they are obtained.

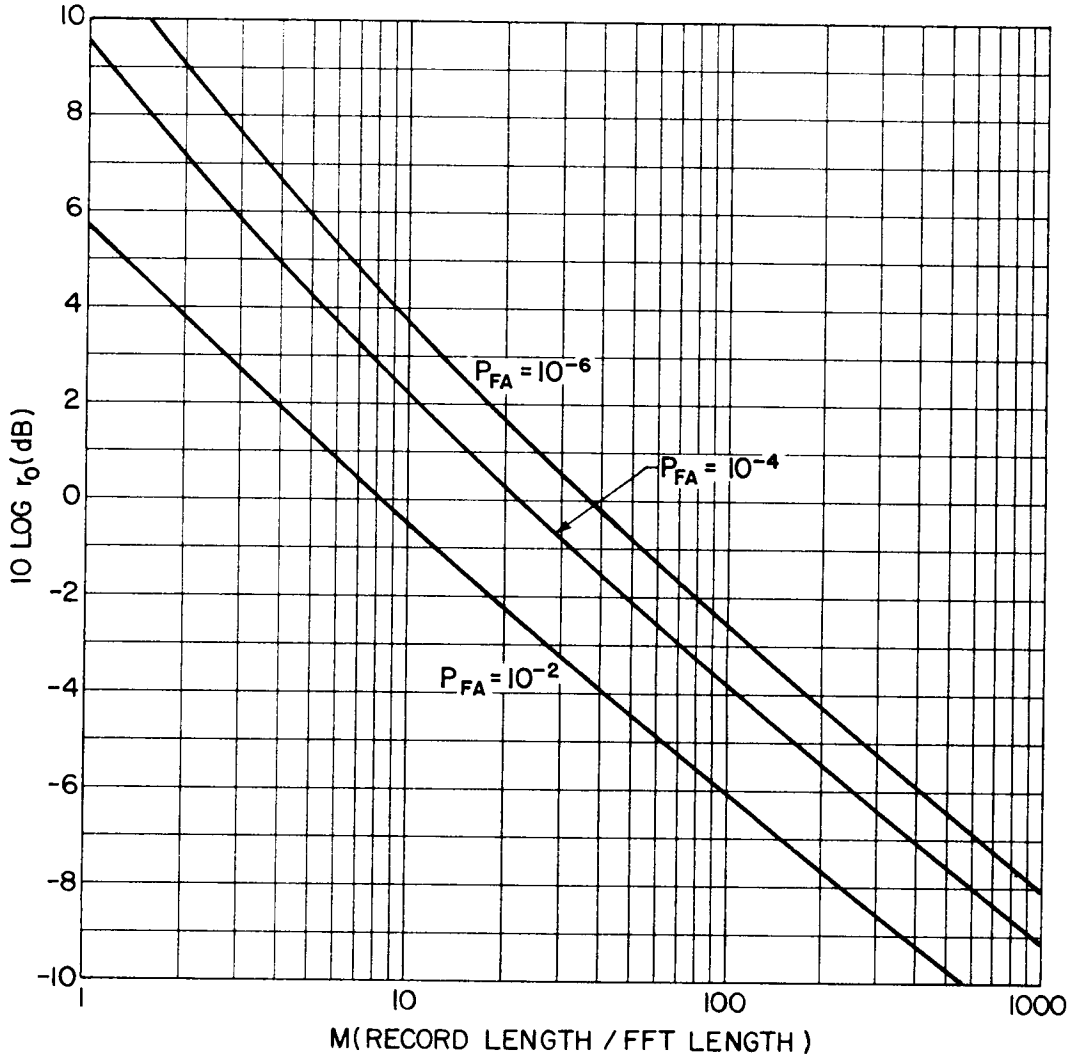

Figure G.1. Basic power ratio vs. M for P_{FA}'s of 10^{-2}, 10^{-4} and 10^{-6}.

Table G.1

Processor parameters for threshold setting example

PARAMETER	VALUE
record length, T_r	300 sec.
segment length, T	10 sec.
time-bandwidth product, M	30
data window	Hanning
segment overlap	0.5
no.of bins in normalizer	20
P_{FA}	10^{-4}

Table G.2

Evaluation of threshold setting for parameters in Table G.1

TERM	VALUE(dB)	SOURCE	COMMENTS
$10log r_0$	-0.8	Figure G.1	$P_{FA}=10^{-4}$;
$-G_o$	-1.4	Figure 7	Hanning window, 0.5 overlap, M=30;
L_n	0.2	Figure 29	$P_{FA}=10^{-4}$, M=30, 20 noise-only bins;

$10log r$ =	-2.0 dB		

Hence (1+r)=1.63 and:
$10log(1+r)$=2.1 dB.
Then the power threshold should be set 2.1 dB above the estimate of the mean noise power.

References

1. J.R.Williams and G.G.Ricker,"Signal detectability performance of optimum Fourier receivers",*IEEE Trans. Audio Electroacoust.*, Vol.AU-20, pp.264-270 (1972).

2. R.C.Trider,"A Fast Fourier Transform (FFT) based sonar signal processor", *IEEE Trans. Acoustics, Speech, Signal Processing*, Vol.ASSP-26, No.1, pp.15-20 (1978).

3. R.J.Urick, "Models for the amplitude fluctuations of narrow-band signals and noise in the sea", *J. Acoust. Soc. Am.*, Vol.62, No.4, pp.878-887 (1977).

4. W.J.Jobst and S.L.Adams, "Statistical analysis of ambient noise", *J. Acoust. Soc. Am.*, Vol.62, No.1, pp.63-71 (1977).

5. R.J.Urick, *Principles of Underwater Sound* (McGraw-Hill: New York, 1967).

6. C.P.Hastell and L.W.Nolte, "On transient and periodic signal detection in time-varying noise power", *IEEE Trans. Aerosp. Electron. Syst.*, Vol.AES-7, No.6, pp.1100-1112 (1971).

7. G.G.Ricker and J.R.Williams, "Redundant Processing Sensitivity", *IEEE Trans. Audio Electroacoust.*, Vol.AU-21, No.4, pp.348-354 (1973).

8. A.Papoulis, *Probability, Random Variables, and Stochastic Processes* (McGraw-Hill: New York, 1965).

9. C.N.Prior, "Calculation of the minimum detectable signal for practical spectrum analyzers", *Naval Ordnance Lab Rept.* NOLTR 71-92, Silver Spring, Md. (2 August 1971).

10. A.H.Nuttall, "Spectral estimation by means of overlapped FFT processing of windowed data", *NUSC Rept.* 4169, New London (13 October 1971).

11. J.R.Williams and G.G.Ricker, "Spectrum analyzer overlap requirements and detectability using discrete Fourier transform and composite digital filters", *J. Acoust. Soc. Am.*, Vol.64, No.3, pp.815-822 (1978).

12. R.S.Walker, "On the detection of fluctuating signals", in *Proc. NATO Advanced Study Institute on Underwater Acoustics and Signal Processing*, L.Bjorno, ed., pp.559-562 (Reidel:Holland, 1980).

13. P.D.Welch, "The use of fast Fourier transform for the estimation of power spectra: a method based on time-averaging over short, modified periodograms", *IEEE Trans. Audio Electroacoust.*, Vol.AU-15, No.2, pp.70-73 (1967).

14. J.V.DiFranco and W.L.Rubin, *Radar Detection* (Prentice-Hall: Englewood Cliffs, N.J., 1968).

15. G.M.Jenkins and D.G.Watts, *Spectral Analysis and its Applications* (Holden-Day: San Francisco, 1968).

16. C.W.Helstrom, *Statistical Theory of Signal Detection* (Pergamon: New York, 1968).

17. I.S.Reed and G.P.Dinneen, "An analysis of signal detection and location by digital methods", *IRE Trans. Information Theory*, Vol.IT-2, pp.29-38 (1956).

18. H.M.Finn and R.S.Johnson, "Adaptive detection mode with threshold control as a function of spatially sampled clutter-level estimates", *RCA Rec.*, Vol.29, pp.414-464 (Sept. 1968).

19. F.J.Harris, "On the use of windows for harmonic analysis with the discrete Fourier transform", *Proc. IEEE*, Vol.66, No.1, pp.51-83 (1978).

20. G.H.Robertson, "Influence of data window shape on detectability of small cw signals in white noise", *J. Acoust. Soc. Am.*, Vol.67, No.4, pp.1274-1276 (1980).

21. G.E.Stanford, "Low-frequency fluctuations of a CW signal in the ocean", *J. Acoust. Soc. Am.*, Vol.55, No.5, pp.968-977 (1974).

22. R.J.Urick, "Solving the sonar equations with fluctuating signals in noise", *Proc. IEEE Int. Conf. Acoust., Speech, Signal Processing*, pp.272-275 (1977).

23. J.S.Bird, "Calculating detection probabilities for radar and sonar systems that employ non-coherent integration", *IEEE Trans. Aerosp. Electron. Syst.*, accepted for publication.

24. A.H.Nuttall and P.G. Cable, "Operating characteristics for maximum likelihood detection of signals in Gaussian noise of unknown level, III Random signals of unknown level", *NUSC Rept.* TR-4783, New London (31 July 1974).

25. J.A.Shooter and S.L.Watkins, "Estimation of background ambient noise levels from the spectral analysis of time series with application to cw propagation-loss measurements", *J. Acoust. Soc. Am.*, Vol.62, No.1, pp.84-90 (1977)

26. J.S.Bird, "Calculating detection probabilities for adaptive thresholds with correlated and uncorrelated noise", *IEEE Trans. Aerosp. Electron. Syst.*, in review.

27. P.G.Cable and A.H.Nuttall, "Operating characteristics for maximum likelihood detection of signals in Gaussian noise of unknown level, II Phase-incoherent signals of unknown level", *NUSC Rept.* TR-4683 (22 April 1974).

28. R.L.Mitchell and J.F.Walker, "Recursive methods for computing detection probabilities", *IEEE Trans. Aerosp. Electron. Syst.*, Vol.AES-7, No.4, pp.671-676 (1971).

UNCLASSIFIED

Security Classification

DOCUMENT CONTROL DATA - R & D

(Security classification of title, body of abstract and indexing annotation must be entered when the overall document is classified)

1. ORIGINATING ACTIVITY

2a. DOCUMENT SECURITY CLASSIFICATION: UNCLASSIFIED

2b. GROUP

3. DOCUMENT TITLE

THE DETECTION PERFORMANCE OF FFT PROCESSORS FOR NARROWBAND SIGNALS

4. DESCRIPTIVE NOTES (Type of report and inclusive dates)

5. AUTHOR(S) (Last name, first name, middle initial)

R. S. WALKER

6. DOCUMENT DATE: FEBRUARY 1982

7a. TOTAL NO. OF PAGES: 107

7b. NO. OF REFS: 28

8a. PROJECT OR GRANT NO.

8b. CONTRACT NO.

9a. ORIGINATOR'S DOCUMENT NUMBER(S)

DREA Technical Memorandum 82/A

9b. OTHER DOCUMENT NO.(S) (Any other numbers that may be assigned this document)

10. DISTRIBUTION STATEMENT

11. SUPPLEMENTARY NOTES

12. SPONSORING ACTIVITY

13. ABSTRACT

The report analyses the detection performance of the Fast Fourier Transform (FFT) type signal processor for narrowband signals in white Gaussian noise. Sinusoidal and narrowband Gaussian signals are considered. The signal processor structure is based on the short-time averaged periodogram approach to spectral estimation. Processor parameters considered in the study include time-bandwidth product, data windowing, periodogram overlap, FFT zeroes extension and data normalization. A building-block approach is adopted, whereby the effects of each parameter on the detection threshold can be determined. Results are presented in graphical form. Hence, for a selected set of processor parameters, the appropriate detection threshold can be readily obtained. A thorough mathematical treatment of the problem is presented in the Appendices.

DSIS
78-070

KEY WORDS

SIGNAL PROCESSING
DETECTION THRESHOLD
NARROWBAND SIGNAL
FAST FOURIER TRANSFORM
PERIODOGRAM
SPECTRAL ESTIMATION
CHARACTERISTIC FUNCTION
GAUSSIAN NOISE
PASSIVE SONAR

INSTRUCTIONS

1. ORIGINATING ACTIVITY: Enter the name and address of the organization issuing the document.

2a. DOCUMENT SECURITY CLASSIFICATION: Enter the overall security classification of the document including special warning terms whenever applicable.

2b. GROUP: Enter security reclassification group number. The three groups are defined in Appendix 'M' of the DRB Security Regulations.

3. DOCUMENT TITLE: Enter the complete document title in all capital letters. Titles in all cases should be unclassified. If a sufficiently descriptive title cannot be selected without classification, show title classification with the usual one-capital-letter abbreviation in parentheses immediately following the title.

4. DESCRIPTIVE NOTES: Enter the category of document, e.g. technical report, technical note or technical letter. If appropriate, enter the type of document, e.g. interim, progress, summary, annual or final. Give the inclusive dates when a specific reporting period is covered.

5. AUTHOR(S): Enter the name(s) of author(s) as shown on or in the document. Enter last name, first name, middle initial. If military, show rank. The name of the principal author is an absolute minimum requirement.

6. DOCUMENT DATE: Enter the date (month, year) of Establishment approval for publication of the document.

7a. TOTAL NUMBER OF PAGES: The total page count should follow normal pagination procedures, i.e., enter the number of pages containing information.

7b. NUMBER OF REFERENCES: Enter the total number of references cited in the document.

8a. PROJECT OR GRANT NUMBER: If appropriate, enter the applicable research and development project or grant number under which the document was written.

8b. CONTRACT NUMBER: If appropriate, enter the applicable number under which the document was written.

9a. ORIGINATOR'S DOCUMENT NUMBER(S): Enter the official document number by which the document will be identified and controlled by the originating activity. This number must be unique to this document.

9b. OTHER DOCUMENT NUMBER(S): If the document has been assigned any other document numbers (either by the originator or by the sponsor), also enter this number(s).

10. DISTRIBUTION STATEMENT: Enter any limitations on further dissemination of the document, other than those imposed by security classification, using standard statements such as:

(1) "Qualified requesters may obtain copies of this document from their defence documentation center."

(2) "Announcement and dissemination of this document is not authorized without prior approval from originating activity."

11. SUPPLEMENTARY NOTES: Use for additional explanatory notes.

12. SPONSORING ACTIVITY: Enter the name of the departmental project office or laboratory sponsoring the research and development. Include address.

13. ABSTRACT: Enter an abstract giving a brief and factual summary of the document, even though it may also appear elsewhere in the body of the document itself. It is highly desirable that the abstract of classified documents be unclassified. Each paragraph of the abstract shall end with an indication of the security classification of the information in the paragraph (unless the document itself is unclassified) represented as (TS), (S), (C), (R), or (U).

The length of the abstract should be limited to 20 single-spaced standard typewritten lines; 7½ inches long.

14. KEY WORDS: Key words are technically meaningful terms or short phrases that characterize a document and could be helpful in cataloging the document. Key words should be selected so that no security classification is required. Identifiers, such as equipment model designation, trade name, military project code name, geographic location, may be used as key words but will be followed by an indication of technical context.